



Workshop On Chaotic And Nonlinear Dynamics In Circuits And Systems

Sponsored by IEEE Circuits and Systems Society (CASS)
Through Outreach Initiative 2015

Instituto Potosino de Investigación científica y Tecnológica A. C.
IPICYT

December 7-8, 2015
San Luis Potosí, México



2015 WORKSHOP ON CHAOTIC AND NONLINEAR DYNAMICS IN CIRCUITS AND SYSTEMS

SPONSORED BY IEEE CASS OUTREACH INITIATIVE

DECEMBER 7 AND 8, 2015

Instituto Potosino de Investigación Científica y Tecnológica
San Luis Potosí, Mexico

THE TARGET OF THIS WORKSHOP IS TO MEET RESEARCHES AND POSTGRADUATE STUDENTS IN THE AREA OF CHAOTIC AND NONLINEAR DYNAMICS

Integrated multi-scroll chaotic systems
Esteban Tlelo Cuatle
Instituto Nacional de Astrofísica, Óptica y Electrónica

Chaotic oscillator derived from a fractional order dynamic system
Ernesto Zambrano Serrano
Instituto Potosino de Investigación Científica y Tecnológica

Electronic implementation of chaotic systems
Jesús Manuel Muñoz Pacheco
Benemérita Universidad Autónoma de Puebla

Two-input logic function implementation
Isaac Campos Cantón
Universidad Autónoma de San Luis Potosí

Brief History of Fractional Order Calculus and its main lines of Application
Manuel Guía Calderón
Universidad de Guanajuato

The participation ratio as a signature of chaos in an interacting radiation-atoms quantum systems
Sergio Adrián Llerma Hernández
Universidad Veracruzana

Prediction of periodic solutions by means the First Harmonic Method
Baltazar Aguirre Hernández
Universidad Autónoma Metropolitana

Parallel phase-shifting digital holography by use of Fractional Talbot Effect
María Auxiliadora Araiza
Universidad Autónoma de Zacatecas

Bio-inspired chaotic systems and their application
Luis Javier Ontañón García
Universidad Autónoma de San Luis Potosí

Monoestabilidad selectiva en sistemas multiestables
Guillermo Huerta Cuellar
Universidad de Guadalajara

New Lyapunov functions for fractional order systems
Guillermo Fernández Anaya
Universidad Iberoamericana

Deterministic coherence resonance in coupled chaotic oscillators with frequency mismatch
Jaimes R. Rider
Universidad de Guadalajara

Wings generation from chaotic attractors
Salvador González Salas
Universidad Politécnica de San Luis Potosí

Sensorial stimulation effects on a neural dynamic system
Luis Martín Torres Treviño
Universidad Autónoma de Nuevo León

Multistable structure via chaotic synchronization and preservation of scrolls
Eduardo Jiménez López
El Colegio Mexiquense A.C.

Brain regions organization in epileptic seizure
Gualberto Solís Perales
Universidad de Guadalajara

Polynomial Trajectories To Provoke Chaos and Bifurcations
Jorge Antonio López Rentería
Universidad Iberoamericana

Simulation of the growth of the kidneys
Francisco Cruz Ordaz
Universidad Politécnica de San Luis Potosí

Chaotic dynamics applied to cryptography
Moisés García Martínez
El Colegio de la Frontera Sur

Opening remarks and Closing remarks on chaotic and nonlinear dynamics in circuits and systems
Gonzalo Barajas Ramírez and Eric Campos Cantón
Instituto Potosino de Investigación Científica y Tecnológica

Committee program: Esteban Tlelo Cuatle; Baltazar Aguirre Hernandez,
Juan Gonzalo Barajas Ramírez, Eric Campos Cantón.

There are scholarships for students.
Please contact Ms. Elizabeth Ruiz (eruiz@ipicyt.edu.mx)

www.ipicyt.edu.mx

Workshop On Chaotic And Nonlinear Dynamics In Circuits And Systems

J. G. Barajas-Ramírez and Eric Campos Cantón
IPICYT, División de Matemáticas Aplicadas,
Camino a la Presa San José 2055
Lomas 4a Secc. C.P. 78216,
San Luis Potosí, S.L.P., México.
Emails: {jgbarajas, eric.campos}@ipicyt.edu.mx

Abstract—The IEEE Circuits and Systems Society (CASS) established the Outreach Initiative 2015 as a fund to provide financial support to projects that benefit CASS and the circuits and systems community in general. As part of this program, the 2015 Workshop on Chaotic and Nonlinear Dynamics in Circuits and Systems aims to provide a meeting place for researchers and postgraduate students in the area of chaotic and nonlinear dynamics. A particularly significant aspect of this Workshop is that it takes place in San Luis Potosí, México, at the Institute for Scientific and Technological Research of San Luis Potosí (IPICYT) which highlights the significant development of contribution on topics of chaotic and nonlinear dynamics that are generated by Mexican nationals and allows one to recognize the impact of chaotic and nonlinear circuits in the IEEE R9-Latin-America region. The main objective of the 2015 Workshop on Chaotic and Nonlinear Dynamics in Circuits and Systems is to provide the possibility to start of further the scientific collaboration between the different research groups that participate with the aim of forming a network of interchange and mutual work.

I. OVERVIEW

The 2015 Workshop on Chaotic and Nonlinear Dynamics in Circuits and Systems includes contributions in three main research lines: Chaotic Circuits, Bio-inspired Systems and Fractional Dynamics.

A. Chaotic Circuits:

Chaotic behavior has passed from an undesirable feature of nonlinear systems to a design objective in many cases. This is due in part to the dynamical richness of chaotic trajectories, which allow for variety alternative goals not available to systems with stable fixed-points or periodic orbits. Chaotic dynamics have potential applications in secure communications, pseudo-random number generation, mixing patterns, persistent excitation of systems, and information processing, to mention but a few. Over the past few years, the scientific community has placed increasing attention on the design of chaotic circuits and systems with simple algebraic structure and direct electronic realizations, yet with fully complex and elegant chaotic dynamics and their application. In this topic the contributions presented are:

1. “Wings generation from chaotic attractors” By Javier Salvador González Salas.
2. “Prediction of periodic solutions by means of the first harmonic method” By Baltazar Aguirre Hernández.

3. “Chaotic dynamics applied to cryptography” By M. García-Martínez.
4. “Selective monostability in multi-stable systems: experimental results” By R. Sevilla-Escoboza, R. Jaimes-Reátegui, G. Huerta-Cuellar, J.H. García-López, A. N. Pisarchik.
5. “Deterministic coherence resonance in two unidirectionally coupled Rössler oscillators” By R. Jaimes-Reátegui, G. Huerta-Cuellar, Carlos E. Castañeda, R. Chiu-Zarate, A. N. Pisarchik.
6. “Multistable structure via chaotic synchronization and preservation of scrolls” By E. Jiménez-López.
7. “The participation ratio as a signature of chaos in an interacting radiation-atoms system” By S. Lerma-Hernández, B. López-del-Carpio, M. A. Bastarrachea-Magnani, J. Chávez-Carlos, J. G. Hirsch.
8. “Polynomial Trajectories To Provoke Chaos and Bifurcations” By Jorge A. López-Rentería.
9. “Electronic Implementation of Chaotic Systems” By J.M. Muñoz-Pacheco.
10. “Integrated Multi-Scroll Chaotic Systems” By Esteban Tlelo-Cuautle

B. Bio-inspired Systems:

One of the most significant sources of inspiration to design efficient and effective systems is the living world. As the modeling process begins the intricate nonlinear and possibly not stationary relations between the forces and elements that conform a biological entity need to be removed from consideration, resulting in very simplified mathematical representations, that although very adequate for analysis, at most can capture only very basic features of the original system. In this sense, drawing on the biological inspiration, nonlinear features and structural conditions can be included in the simplified models to generate refined mathematical models, that sometimes we call bio-inspired. In this topic, the following contributions were presented in our workshop:

1. “Bio-inspired chaotic systems and their application” By L.J. Ontañón-García.

2. "Simulation model of renal arterial tree growth in 3D" By Francisco C. Ordaz-Salazar, Ricardo Femat, Aurora Espinoza-Valdez.
3. "Brain regions organization in epileptic seizure" By G. Solís Perales, A. Espinosa, H. Vélez, R. Romo, A. González-Garrido.
4. "Sensorial stimulation effects on a neural dynamic systems" By Luis M. Torres-Treviño.

C. Fractional Dynamics:

In the theory of dynamical systems and that of Ordinary Differential Equations are in many senses identical, under the assumptions of existence and uniqueness the solutions of a set of ODE is a description of the systems dynamics. The extension of these features and tools of analysis when the equations that represent the system are defined on fractional derivatives, a large set of questions and opportunities arise. In this particular topic the contributions presented in our workshop were:

1. "Parallel Phase-Shifting Digital Holography by Use of the Fractional Talbot Effect" By Ma. Araiza-Esquivel, Enrique Tajahuerce Romera, Lluís Martínez-León, Jesús Lancis, Pedro Andrés.
2. "New Lyapunov Functions for Fractional Order Systems" By Guillermo Fernández-Anaya, Guillermo Nava-Antonio, Jack Jamous-Galante, Rodrigo Muñoz-Vega.
3. "Chaotic oscillator derived from a fractional order dynamic system" By E. Zambrano-Serrano.

We thank to all authors who submitted their papers and express our deepest gratitude to the committee program members for their effort in providing valuable feedback to realize this Workshop On Chaotic And Nonlinear Dynamics In Circuits And Systems. We also express our sincere appreciation to IEEE Circuits and Systems Society (CASS): the Outreach Initiative 2015 for financial support for conducting this workshop.

Prediction of periodic solutions by means of the first harmonic method

Baltazar Aguirre Hernández

Departamento de Matemáticas

UAM Iztapalapa

México, D.F.

Email: bahe@xanum.uam.mx

Abstract—It is Known that the question of finding the periodic solutions of a system of differential equations is a difficult problem. For this reason it is convenient to use approximation methods. In this talk we explain the First Harmonic Method, which is based in the idea of using a Truncated Fourier Serie.

I. INTRODUCTION

The first researches about the Harmonic Balance Method for the study of control systems were reported in the 40's [6], [7], [10], [11] and [12].

In [8, cap. IX, p. 583] it is explained a method for the research of periodic orbits of some systems and such method is similar to the harmonic balance method. The harmonic balance method can be consulted in the books: [9], [13] and [14].

In this work we will consider systems of the form

$$\begin{aligned} \begin{pmatrix} \dot{x}_1 \\ \dot{x}_2 \\ \dot{x}_3 \end{pmatrix} &= \begin{pmatrix} 0 & 1 & 0 \\ 0 & 0 & 1 \\ -a_3 & -a_2 & -a_1 \end{pmatrix} \begin{pmatrix} x_1 \\ x_2 \\ x_3 \end{pmatrix} \\ &+ \begin{pmatrix} 0 \\ 0 \\ 1 \end{pmatrix} \times \\ &\mathcal{S} \left((a_3 - k_3 \delta^3, a_2 - k_2 \delta^2 d_2, a_1 - k_1 \delta) \begin{pmatrix} x_1 \\ x_2 \\ x_3 \end{pmatrix} \right) \end{aligned}$$

with a_1, a_2, a_3 satisfying $a_1, a_3, a_1 a_2 - a_3 < 0$, ($\sigma(A) \subseteq \mathbb{C}^+$) and k_1, k_2, k_3 satisfying $k_1, k_3, k_1 k_2 - k_3 > 0$ y $\delta > 0$

$$\mathcal{S}(v) = \begin{cases} -1 & \text{if } -1 > v \\ v & \text{if } -1 \leq v \leq 1 \\ 1 & \text{if } v > 1. \end{cases} \quad (1)$$

If we define
 $A = \begin{pmatrix} 0 & 1 & 0 \\ 0 & 0 & 1 \\ -a_3 & -a_2 & -a_1 \end{pmatrix}$, $b = \begin{pmatrix} 0 \\ 0 \\ 1 \end{pmatrix}$,

$K^T = (a_3 - k_3 \delta^3, a_2 - k_2 \delta^2 d_2, a_1 - k_1 \delta)$
 then the system can be written as

$$\dot{x} = \begin{cases} Ax - b & \text{si } -1 > K^T x \\ (A + bK^T)x & \text{si } -1 \leq K^T x \leq 1 \\ Ax + b & \text{si } K^T x > 1. \end{cases} \quad (2)$$

Around the origin the system is defined as

$\dot{x} = (A + bK^T)x$ that is

$$\begin{pmatrix} \dot{x}_1 \\ \dot{x}_2 \\ \dot{x}_3 \end{pmatrix} = \begin{pmatrix} 0 & 1 & 0 \\ 0 & 0 & 1 \\ -k_3 \delta^3 & -k_2 \delta^2 & -k_1 \delta \end{pmatrix} \begin{pmatrix} x_1 \\ x_2 \\ x_3 \end{pmatrix}$$

$$p(t) = t^3 + k_1 \delta t^2 + k_2 \delta^2 t + k_3 \delta^3.$$

Where $p(t)$ is the characteristic polynomial and its roots are $\delta \lambda_i$, $i = 1, 2, 3$ and the λ_i are the roots of the polynomial

$$g(t) = t^3 + k_1 t^2 + k_2 t + k_3.$$

Since $k_1, k_3, k_1 k_2 - k_3 > 0$, $\lambda_i \in \mathbb{C}^-$ and then

$$\delta \lambda_i \rightarrow -\infty, \quad \delta \rightarrow \infty.$$

A. The harmonic balance method

The harmonic balance method is based en the following ideas:

Consider the system

$$\dot{x} = Ax + b\eta(u), \quad u = c^T x \quad (3)$$

where

$$A = \begin{bmatrix} 0 & 1 & 0 & \cdots & 0 \\ 0 & 0 & 1 & \cdots & 0 \\ \vdots & \vdots & \vdots & \ddots & \vdots \\ 0 & 0 & 0 & \cdots & 1 \\ -a_n & -a_{n-1} & -a_{n-2} & \cdots & -a_1 \end{bmatrix}, \quad b = \begin{bmatrix} 0 \\ 0 \\ \vdots \\ 0 \\ 1 \end{bmatrix}$$

$u = u(t)$ is a real function named control and $\eta : R \rightarrow R$ is a nonlinear continuous function.

Denote $p = \frac{d}{dt}$. Given $u(t) = c^T x(t)$ and writing the system $\dot{x} = Ax + b\eta(u)$ in the form

$$(A - pI)x(t) = -b\eta(u(t))$$

it follows the equality:

$$\det(A - pI)u(t) = -c^T \text{adj}(A - pI)b\eta(u(t)).$$

The last equation is a differential equation that governs the dynamical behavior of $u(t)$. This equation is frequently written as:

$$u(t) = -W(p)\eta(u(t)) \quad (4)$$

where $W(p) = c^T(A - pI)^{-1}b$.

Suppose that the system (4) has a periodic solution $u(t) = \sum_{-\infty}^{\infty} \alpha_m \exp(im\omega t)$, con $\alpha_m = \overline{\alpha}_{-m}$.

Consider the Fourier series of the nonlinear function $\eta(u)$: $\eta(u(t)) = \sum_{-\infty}^{\infty} \beta_m \exp(im\omega t)$ con $\beta_m = \overline{\beta}_{-m}$.

Replacing these series in (4) we can get

$$\sum_{-\infty}^{\infty} \alpha_m \exp(im\omega t) = - \sum_{-\infty}^{\infty} W(im\omega) \beta_m \exp(im\omega t). \quad (5)$$

Then we obtain the system of equations

$$\alpha_m + W(im\omega) \beta_m = 0, \quad m = 0, \pm 1, \pm 2, \dots \quad (6)$$

Solving this system we find a periodic solution of the system (4).

On the other hand, it is known that

$$1 + W(s) = \frac{\det(A + bc^T - sI)}{\det(A - sI)} [5].$$

It implies that $W(s)$ is a rational function with degree of numerator < degree of denominator. Consequently $W(i\omega) \rightarrow 0$ when $\omega \rightarrow \infty$.

Based in this ideas the method propose to suppose that the equation (4) has an approximated solution in the form:

$$u_0(t) = \alpha_0 + a \sin \omega t, \quad a, \omega > 0$$

and we write $\eta(u_0(t))$ as a Fourier series

$\eta(u_0(t)) = \sum_{l=0}^{\infty} \beta_l \sin l\omega t$ [13]. Taking into account only two terms (first harmonic approximation), we obtain the following equations:

$$\alpha_0 + W(0)F_{\eta}(a, \alpha_0) = 0 \quad (7)$$

$$1 + W(iw)G_{\eta}(a, \alpha_0) = 0 \quad (8)$$

where

$$F_{\eta}(a, \alpha_0) = \beta_0 = \frac{1}{2\pi} \int_0^{2\pi} \eta(\alpha_0 + a \sin \theta) d\theta \quad (9)$$

$$G_{\eta}(a, \alpha_0) = \frac{\beta_1}{a} = \frac{1}{\pi a} \int_0^{2\pi} \eta(\alpha_0 + a \sin \theta) \sin \theta d\theta. \quad (10)$$

For studying the symmetric periodic orbits we must write $\alpha_0 = 0$. Observe that

$$\beta_0 = F_{\eta}(a, 0) = 0.$$

Then we should solve only the following equation

$$1 + W(j\omega)N_{\eta}(a) = 0 \quad (11)$$

where

$$N_{\eta}(a) = \frac{\beta_1}{a} = \frac{1}{\pi a} \int_0^{2\pi} \eta(a \sin \theta) \sin \theta d\theta. \quad (12)$$

The first harmonic method consists in finding the solutions α_0 and $a, \omega > 0$ to (7)-(8) ((11) if $\alpha_0 = 0$). The obtained solutions $u_0(t) = \alpha_0 + a \sin \omega t$ are named *first harmonic periodic orbits* of (4). If $\alpha_0 = 0$ ($\alpha_0 \neq 0$) the corresponding periodic orbit is *symmetric* (*non-symmetric*). The real coefficient $N_{\eta}(a)$ is named the *describing function* associated to the nonlinear function $\eta(\cdot)$ and in this case the method of harmonic balance is also known as *Method of the describing function* [13], [14].

II. MAIN RESULTS

The proofs of the theorems of this section can be consulted in [1], [2], [3] and [4].

A. First harmonic non-symmetric periodic orbits

Consider the system

$$\begin{pmatrix} \dot{x}_1 \\ \dot{x}_2 \\ \dot{x}_3 \end{pmatrix} = \begin{pmatrix} 0 & 1 & 0 \\ 0 & 0 & 1 \\ -a_3 & -a_2 & -a_1 \end{pmatrix} \begin{pmatrix} x_1 \\ x_2 \\ x_3 \end{pmatrix} + \begin{pmatrix} 0 \\ 0 \\ 1 \end{pmatrix} \mathcal{S} \left((a_3 - d_3, a_2 - d_2, a_3 - d_3) \begin{pmatrix} x_1 \\ x_2 \\ x_3 \end{pmatrix} \right)$$

where $d_1 = k_1\delta, d_2 = k_2\delta^2, d_3 = k_3\delta^3$ y $k_1, k_3, k_1k_2 - k_3 > 0$.

Theorem 1. Let A totally unstable. Then, there are 2 first harmonic non-symmetric periodic orbits **for every positive** δ . Besides there is α_0^* such that α_0 , as a function of δ , satisfies $\alpha_0 > \alpha_0^* > 0$.

Here $u(t) = \alpha_0 + a \sin \omega t$ and $u(t) = -\alpha_0 + a \sin \omega t$ determine the periodic orbits.

B. A Hopf bifurcation

The theorem 1 suggests the existence of a Hopf bifurcation.

Consider the system

$$\begin{pmatrix} \dot{x}_1 \\ \dot{x}_2 \\ \dot{x}_3 \end{pmatrix} = \begin{pmatrix} 0 & 1 & 0 \\ 0 & 0 & 1 \\ -a_3 & -a_2 & -a_1 \end{pmatrix} \begin{pmatrix} x_1 \\ x_2 \\ x_3 \end{pmatrix} + \begin{pmatrix} 0 \\ 0 \\ 1 \end{pmatrix} \mathcal{S} \left((a_3 - d_3, a_2 - d_2, a_3 - d_3) \begin{pmatrix} x_1 \\ x_2 \\ x_3 \end{pmatrix} \right)$$

where $a_1 = -\nu - 2\mu, a_2 = 2\mu\nu + \mu^2 + \gamma^2, a_3 = -\nu(\mu^2 + \gamma^2)$ where ν, γ are fixed and μ is a parameter.

The Jacobian matrix in the points $(\pm \frac{1}{a_3}, 0, 0)$ is the following

$$\begin{pmatrix} 0 & 1 & 0 \\ 0 & 0 & 1 \\ \nu(\mu^2 + \gamma^2) & -2\mu\nu - \mu^2 - \gamma^2 & \nu + 2\mu \end{pmatrix}.$$

Observe that $\lambda_1 = \nu > 0$ is an eigenvalue of A and the other two eigenvalues are given by $\lambda(\mu) = \mu \pm i\gamma$. So $\Re(\lambda(0)) = 0$ and $\frac{d}{d\mu}\Re(\lambda(\mu)) = 1$. Consequently for each one of the equilibrium points $(\pm \frac{1}{a_3}, 0, 0)$ a Hopf bifurcation appears [15].

C. Additional periodic orbits

Theorem 2. Let A be a totally unstable matrix that is $a_1, a_3, a_1a_2 - a_3 < 0$ then there is only a first harmonic symmetric periodic orbit.

Theorem 3. If A is totally unstable (all of its eigenvalues have positive real part) then there exists a set R satisfying the following:

- a) For every $\delta \in R$ there are at least two first harmonic non-symmetric periodic orbits.
- b) For δ small enough or large enough there is not first harmonic non-symmetric periodic orbits.

III. CONCLUSION

Results on the existence of symmetric periodic orbits have been presented. Such results must be seen only as an evidence of the existence of real periodic orbits since the first harmonic method is an approximated method. Besides, such results must be seen as a motivation to do a study using rigorous methods (Hopf bifurcation, Poincaré maps).

REFERENCES

- [1] R. Suárez, J. Alvarez-Ramírez and B. Aguirre, *First harmonic analysis of planar linear systems with singled saturated feedback*, International Journal of Bifurcation and Chaos, Vol. 6, No. 12B, 2605-2610, 1996.
- [2] B. Aguirre, J. Alvarez-Ramírez, G. Fernández and R. Suárez, *First harmonic analysis of linear control systems with high-gain saturating feedback*, International Journal of Bifurcation and Chaos, Vol. 7, No. 11, 2501-2510, 1997.
- [3] B. Aguirre, J. Alvarez-Ramírez and R. Suárez, *Symmetry breaking of periodic orbits in control systems: a harmonic balance approach*, International Journal of Bifurcation and Chaos, Vol. 8, No. 12, 2439-2448, 1998.
- [4] B. Aguirre, J. Alvarez-Ramírez and R. Suárez, *Estimation of the region of attraction of the origin of closed-loop linear systems with saturated linear controllers: A first harmonic approach*, Boletín de la Sociedad Matemática Mexicana, 6 (1), pp. 111-150, 2001.
- [5] S. Barnett and R.G. Cameron, *Introduction to Mathematical Control Theory*, Oxford, Clarendon Press, 1985.
- [6] L. C. Goldbarb, *On some nonlinear phenomena in regulatory systems*, Auto. Telemekh. 8, 349-383, 1947.
- [7] J. Dutilh, *Théorie des servomechanismes à relais*, Onde Electr., 438-445, 1950.
- [8] A. A. Andronov, S. E. Khaikin and A. A. Vitt, *Theory of Oscillations*, Princeton N. J.: Princeton Press, 1949.
- [9] M. A. Aizerman, *Theory of Automatic Control*, Massachusetts, U.S.A.: Addison-Wesley, 1963.
- [10] R. J. Kuchenburger, *A frequency response method for analysing and synthesizing contactor servomechanisms*, Trans. Am. Inst. Electr. Eng. Part 2, 69, 270-283, 1950.
- [11] W. Oppelt, *Locus curve method for regulators with friction*, VDI Z 90, 179-183, 1948.
- [12] A. Tustin, *The effects of backlash and of speed dependent friction on the stability of closed loop control systems*, J. Inst. Electr. Eng. Part 2, 94, 143-151, 1947.
- [13] A. I. Mees, *Dynamics of Feedback Systems*, New York: J. Wiley and Sons, 1981.
- [14] M. Vidyasagar, *Nonlinear Systems Analysis*, New Jersey: Prentice-Hall, 1993.
- [15] J. Marsden and M. McCracken, *The Hopf bifurcation and its applications*, Springer-Verlag: Applied Mathematical Sciences, 19, 1976.

Parallel Phase-Shifting Digital Holography by Use of the Fractional Talbot Effect

Ma. Araiza-Esquivel
 Doctorado en Ciencias de la Ingeniería
 Unidad Académica de Ingeniería Eléctrica
 Universidad Autónoma de Zacatecas
 López Velarde 801, Col. Centro, Zacatecas, México.
 Email: araizamae@yahoo.com

Enrique Tajahuerce Romera,
 Lluís Martínez-León,
 Jesús Lancis
 Universitat Jaume I
 Departamento de Física
 12071 Castelló, Spain
 Email: etajahuerce—@uji.es

Pedro Andrés
 Universitat de València,
 Departamento de Óptica
 46100 Burjassol, Spain

Abstract—We present a method for recording on-axis digital color holograms of 2D objects in a single shot. The system performs parallel phase-shifting techniques by using the fractional Talbot effect for each chromatic channel. A simple two-dimensional periodic binary grating is used to codify the reference beam. The interference patterns are recorded at once at different axial distances, generating a Talbot periodic phase distribution over each sensor plane. The images of the object are reconstructed numerically from digital holograms. The color image reconstructed is shown in the experimental results.

I. INTRODUCTION

Thanks to advances in the digital sensor (CCD CMOS) and the improvement in the computational resources, the holography developed toward digital recording and processing procedures. The digital holography has a variety of applications such as interferometry, three-dimensional (3D) images, microscopy, encryption and pattern recognition.

In terms of spatial resolution, Yamaguchi and Zhang, developed an efficient method to record digital holograms [1]. However, the method as its name says, required sequential interference patterns with different phase retardation.

On the other hand, several techniques have been developed, so that with one-shot capture can acquire all the interference patterns, but limited by the sensor capabilities [2]–[4]. In addition, there are procedures for color parallel phase-shifting techniques which were proposed using digital holography off-axis or phase-shifting interferometry [5]. Digital holography techniques have also been developed using polychromatic illumination to color object and in one-shot capture digital holograms.

We propose a method for recording single-shot digital color holograms based on the fractional Talbot effect and using polychromatic illumination [6]. A two-dimensional binary grating is illuminated and a self-imaging phenomenon is observed (Talbot effect). At the Talbot distance of the grating, it is possible to generate a periodic phase distribution with uniform irradiance. The properties of the Talbot effect ensure that the axial distance of each spectral component is obtained at a suitable phase shifting. Thereby, the sensor of each spectral component records different phase shifting over the different

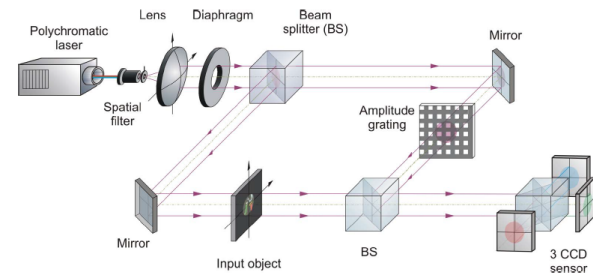


Fig. 1. Optical setup for recording digital color holograms using polychromatic laser beam and binary amplitude grating.

pixels of the interferogram. Digital images of the object are calculated numerically and digitally reconstructed.

In Section 2, we discuss a simple parallel phase-shifting technique to digital holography base in the fractional Talbot effect. In Section 3, we show the experimental results on the implementation. And in Section 4, we comment on the merits and limitations of our proposal.

II. TALBOT DIGITAL HOLOGRAPHY

Figure 1 shows the experimental setup to perform Talbot digital color holography using a 2D binary amplitude grating in the reference arm of the Mach-Zehnder interferometer. A polychromatic laser beam is spatially filtered, collimated, and split into an object path and a reference path. The object beam illuminates the test object, and the light scattered travels through the second beam splitter, and later to the 3-CCD detector.

The fractional Talbot effect works in the reference arm when the reference beam is diffracted by a 2D binary amplitude grating providing a three-step phase distribution and traveling to three sensors, one by each spatial component of the polychromatic laser beam. Each Sensor has to be shifted axially by a small amount with respect to the others, in such a way that they record the same Fresnel image in each

interference pattern of the three chromatic components. The Fresnel images are a superposition of a certain number of copies of the input grating in each transversal dimensional. These copies have different weight phase factors. The Fresnel images are obtained at distance

$$z' = \frac{2d^2}{\lambda} \left(q + \frac{n}{m} \right) = z_t \left(q + \frac{n}{m} \right) \quad (1)$$

where z_t is the Talbot distance, $\lambda = \lambda_R, \lambda_G \lambda_B$ is associated with red (R), green (G) and blue (B) spectral components of the beam, q is an integer, and n and m are natural numbers where $n < m$. The ration n/m determines the amplitude distribution at the unit cell of a particular Fresnel image. In our case, we restrict our analysis to the particular case $n/m = 1/4$ or $3/4$ to obtain the weighting phase factor 0, $\pi/2$ and π . Thus the phase-only modulation is carried out in the reference arm using the fraction Talbot effect

The complex field generated by interference of the object beam and the reference beam at the output plane, our digital hologram, it obeys the following relation:

$$O(x, y, 0) = \frac{1}{4} \{ I(x, y; 0) - I(x, y; \pi) \\ + i[2I(x, y; \pi/2) - I(x, y; 0) - I(x, y; \pi)] \} \quad (2)$$

The final hologram is half the size of each interferometer pattern ($I_0, I_{\pi/2}, I_\pi$) in each transversal dimension. The image can be reconstructed numerically by computing a discrete Fresnel integral of complex digital hologram $O(x, y, 0)$. The complex amplitude distribution, $O(x, y, z)$ is generated by the 3D object at any plane located at a distance z from the camera sensor:

$$O(m, n, z) = F^{-1} \{ F[O(m, n, 0)] \\ \times \exp \left[-i\pi\lambda z \left(\frac{u^2}{(\Delta x N_x)^2} + \frac{v^2}{(\Delta y N_y)^2} \right) \right] \}, \quad (3)$$

where F denotes the fast Fourier transform, (m, n) are discrete transversal spatial coordinates in both CCD planes and the output plane, (u, v) are discrete spatial frequency variables, and N_x and N_y are the numbers of samples in the x and y directions.

III. EXPERIMENTAL RESULTS

Each one of the three sensors records the interference pattern between the object beam and the reference beam. The pixelated phase-shifting interferogram is processed to measure the amplitude and the phase of the object light field. Figure 2 shows the constructed image applied to the Fresnel diffraction integral in a computer.

IV. CONCLUSION

For recording and reconstructing color holograms with one-shot of the camera, we propose a method base in the fractional Talbot effect. Using a 2D amplitude grating, it was



Fig. 2. Image reconstructed of the three chromatic channels.

possible to record the phase-shifting interferometry patterns simultaneously.

We propose a dynamic operation with an in-line configuration, which does not need any special phase diffractive elements to make several copies of the object and the reference beams. Moreover, We do not need complex pixelated polarization devices, which are difficult to build and hard to integrate with the CCD sensor.

The 2D amplitude grating is not sensitive to the wavelength. By shifting the grating, we get the same phase shifts for different wavelengths. The limitations of the method are: decrease of the spatial resolution and increase of the sensor acquisition time and the numerical processing.

ACKNOWLEDGMENT

One of the authors (MAE) wishes to thank CONACYT (Mexico) for providing partial financial support for this work with the project INFRA-23015-01-254438.

REFERENCES

- [1] I. Yamaguchi and T. Zhang, "Phase-shifting digital holography," Opt. Lett. 22, 1268-1270 (1997).
- [2] Y. Awatsuji, T. Tahar, A. Kaneko, T. Koyama, K. Nishio, S. Ura, T. Kubota, and O. Motoba, "Parallel two step phase-shifting digital holography", Appl. Opt. 47, D183-D189 (2008).
- [3] M. Imbe, and Talampro Nomura, "Single-exposure Phase-shifting digital holography using a random-complex-amplitude encoded reference wave". Appl. Opt. 52, A161- A166 (2013).
- [4] Ll. Martnez-Len, M. Araiza-Esquivel, Bahram Javidi, Pedro Andrs, Vicent Climent, Jess Lancis, and Enrique Tajahuerce, "Single-shot digital holography by use of the fractional Talbot effect", Opt. Express 17, 12900-129009 (2009).
- [5] T. Kakue, T. Tahara, K. Ito, Y. Shimozato, Y. Awatsuji, K. Nishio, S. Ura, Toshihiro Kubota, and Osamu Matoba , "Parallel phase-shifting color digital holography using two phase shifts", Appl. Opt. 48, H244-H250 (2009).
- [6] M. Araiza-Esquivel, Llus Martnez-Len, Bahram Javidi, Pedro Andrs, Jess Lancis, and Enrique Tajahuerce, "Single-shot color digital holography based on the fractional Talbot effect", Appl. Opt. 50, pp. B96-B101 (2011).

New Lyapunov Functions for Fractional Order Systems

Guillermo Fernández-Anaya

Universidad Iberoamericana

Departamento de Física y Matemáticas

01219 Ciudad de México, D.F.

Email: guillermo.fernandez@ibero.mx

Guillermo Nava-Antonio

Universidad Iberoamericana

Departamento de Física y Matemáticas

01219 Ciudad de México, D.F.

Email: gnava95@hotmail.com

Jack Jamous-Galante

Universidad Iberoamericana

Departamento de Física y Matemáticas

01219 Ciudad de México, D.F.

Email: jackjamousg@gmail.com

Rodrigo Muñoz-Vega

Universidad Autónoma de la Ciudad de México

Departamento de Física

06720 Ciudad de México, D.F.

Email: rodrigo.munoz@uacm.edu.mx

Abstract—In this conference, we present new methods to construct Lyapunov functions of fractional order systems. As a consequence, we extend recent results for Lyapunov stability and asymptotic stability of nonlinear fractional order systems.

I. INTRODUCTION

In recent years, there have been several results for nonlinear fractional order systems stability based on direct Lyapunov method (see [1], [2], [3], [4], [5]).

A problem that usually appears in these methods is the construction of Lyapunov functions appropriate to test this system's stability, since the product rule (Leibniz's rule) is no longer valid for Caputo derivative, nor the chain rule as we know it for integer order.

In the interesting paper [5], it is proved a lemma with several potential applications. We generalize this lemma, and give new lemmas for nonlinear fractional order systems stability results via direct Lyapunov method.

II. PRELIMINARY CONCEPTS

A. Caputo fractional derivative [5]

The Caputo fractional derivative of order $\alpha \in \mathbb{R}^+$ on the half axis \mathbb{R}^+ is defined as follows

$${}_{t_0}^C D_t^\alpha f(t) = \frac{1}{\Gamma(m-\alpha)} \int_{t_0}^t \frac{f^{(m)}(\tau)}{(t-\tau)^{\alpha-n+1}} d\tau, \quad t > t_0, \quad (1)$$

with $m = \min \{k \in \mathbb{N} / k > \alpha\}$, $\alpha > 0$.

B. Hadamard product [6]

Hadamard product of two matrices A , B of the same dimension is a matrix $A \odot B$ of the same dimension as the operands, with elements given by

$$(A \odot B)_{i,j} = (A_{i,j}) \cdot (B_{i,j}). \quad (2)$$

For matrices of different dimensions the Hadamard product is undefined.

III. A NEW LEMMA FOR CAPUTO FRACTIONAL DERIVATIVE

A. Lemma

Let $x(t); \mathbb{R} \rightarrow \mathbb{R}$ be any derivable function. Then the following relationships hold:

$$\frac{1}{n} {}_{t_0}^C D_t^\alpha x^n(t) \leq x^{n-1}(t) {}_{t_0}^C D_t^\alpha x^{n-1}(t) \quad (3)$$

$$\frac{1}{2m} {}_{t_0}^C D_t^\alpha x^{2m}(t) \leq x^m(t) {}_{t_0}^C D_t^\alpha x^m(t) \quad (4)$$

$$\forall \alpha \in (0, 1), \quad n \in \{2k, k \in \mathbb{N} - \{0\}\}, \quad m \in \{N - \{0\}\}.$$

1) *Remark:* Note that if $x(t)$ is non-negative, then (3) is also valid for odd n . This is

$$\frac{1}{n} {}_{t_0}^C D_t^\alpha x^n(t) \leq x^{n-1}(t) {}_{t_0}^C D_t^\alpha x^{n-1}(t) \quad (5)$$

where $n \in \{k, k \in \mathbb{N} - \{0\}\}$.

2) *Corollary:* In the case where $x(t) \in \mathbb{R}^p$, (3) and (4) are still valid. That is, considering $\forall \alpha \in (0, 1)$ and $t \geq t_0$

$$\frac{1}{n} {}_{t_0}^C D_t^\alpha x^{[n]}(t) \leq x^{[n-1]}(t) \odot {}_{t_0}^C D_t^\alpha x^{[n-1]}(t) \quad (6)$$

$$\frac{1}{2m} {}_{t_0}^C D_t^\alpha x^{[2m]}(t) \leq x^{[m]}(t) \odot {}_{t_0}^C D_t^\alpha x^{[m]}(t), \quad (7)$$

for (3) and (4) respectively, where the notation $x^{[n]} = x \odot x \odot \dots \odot x$ is the Hadamard product of a n amount of x vectors as in Definition II-B and the inequality of vectors denotes p inequalities for each scalar component. In both cases, the proves are straightforward, analyzing the expressions (6) and (7) entrywise, and using (3) and (4) respectively in each escalar component.

B. Corollary

Let $x(t)$ be defined as in Lemma III-A. Then, for any time instant $t \geq t_0$ the following relationships hold:

$$\frac{1}{n!} {}_{t_0}^C D_t^\alpha x^n(t) \leq x^{n(n+1)/2}(t) {}_{t_0}^C D_t^\alpha x(t) \quad (8)$$

$${}_{t_0}^C D_t^\alpha x^{2^m+1}(t) \leq 2^{m(m+1)/2} x^{(2^m-1)}(t) {}_{t_0}^C D_t^\alpha x(t) \quad (9)$$

$$\forall \alpha \in (0, 1), \quad n = 2\gamma, \quad \gamma \in \mathbb{N}, \quad m \in \mathbb{N}.$$

C. Corollary

In the case where $x(t) \in \mathbb{R}^p$, (8) and (9) are still valid. That is, considering $\forall \alpha \in (0, 1)$ and $t \geq t_0$:

$$\frac{1}{n!} {}_{t_0}^C D_t^\alpha x^{[n]}(t) \leq x^{[n(n+1)/2]}(t) \odot {}_{t_0}^C D_t^\alpha x(t) \quad (10)$$

$${}_{t_0}^C D_t^\alpha x^{[2^m+1]}(t) \leq 2^{m(m+1)/2} x^{[(2^m-1)]}(t) \odot {}_{t_0}^C D_t^\alpha x(t), \quad (11)$$

for (8) and (9), respectively.

In both cases, the proves are straightforward, analyzing the expressions (10) and (11) entrywise, and using (8) and (9), respectively in each escalar component.

IV. NEW RESULTS FOR NON-LINEAR FRACTIONAL ORDER SYSTEM STABILITY

A. Theorem

Consider the fractional order system

$${}_{t_0}^C D_t^\alpha x = f(x(t)), \quad (12)$$

where $\alpha \in (0, 1)$, $x = 0$ is the equilibrium point and $x(t)$ as defined in Lemma III-A. Then, the following statements are satisfied:

- If $x^{n(n+1)/2} f(x(t)) \leq 0$, the origin of the system is stable. If $x^{n(n+1)/2} f(x(t)) < 0$, the origin of the system is asymptotically stable, where $n = 2\gamma$, $\gamma \in \mathbb{N}$.
- If $x^{(2^m-1)}(t) f(x(t)) \leq 0$, the origin of the system is stable. If $x^{(2^m-1)}(t) f(x(t)) < 0$, the origin of the system is asymptotically stable, where $m \in \mathbb{N}$.

1) *Corollary:* Theorem IV-A is still valid when $x(t) \in \mathbb{R}^p$. That is, for the fractional order system

$${}_{t_0}^C D_t^\alpha x = f(x(t)),$$

where $\alpha \in (0, 1)$, $x = 0$ is the equilibrium point and each scalar component of $x(t)$ is defined as in Lemma III-A, the following statements are satisfied:

- If $x^{[n(n+1)/2]} \odot f(x(t)) \leq 0$, then the origin of the system is stable. If $x^{[n(n+1)/2]} \odot f(x(t)) < 0$ then, the origin of the system is asymptotically stable, where $n = 2\gamma$, $\gamma \in \mathbb{N}$.

- If $x^{[(2^m-1)]}(t) \odot f(x(t)) \leq 0$ then, the origin of the system is stable. If $x^{[(2^m-1)]}(t) \odot f(x(t)) < 0$ then, the origin of the system is asymptotically stable, where $m \in \mathbb{N}$.

2) *Remark:* Note that the second statement in Theorem IV-A has been recently proved with other techniques for asymptotical stability case in [2].

V. EXAMPLE

Let us consider the following fractional order nonlinear system, with $\alpha \in (0, 1)$, and $x_2(t) \geq 0$:

$${}_{t_0}^C D_t^\alpha x_1(t) = -x_1(t) + x_2^{15}(t)$$

$${}_{t_0}^C D_t^\alpha x_2(t) = -x_2(t) - \frac{2}{6!} x_1(t),$$

and a Lyapunov candidate function, which is positive definite.

$$V(x_1(t), x_2(t)) = x_1^2(t) + x_2^6(t). \quad (13)$$

Now, applying (3), it can be found that

$${}_{t_0}^C D_t^\alpha V(x_1(t), x_2(t)) \leq 2x_1 {}_{t_0}^C D_t^\alpha x_1 + 6x_2^5 {}_{t_0}^C D_t^\alpha x_2^5.$$

Since $x_2(t) > 0$, we can use (5) 4 times to obtain

$${}_{t_0}^C D_t^\alpha V(x_1(t), x_2(t)) \leq -2x_1^2 - 6!x_2^{16} < 0.$$

Considering that the fractional derivative of the Lyapunov function is negative definite, it can be concluded, by using Theorem IV-A, that the origin of the system is asymptotically stable.

Note that Lemma 1 in [5] cannot be applied, thus, Corollary 1 in [5] and Proposition 5 in [2], either.

VI. CONCLUSION

Based on a series of lemmas derived from generalizations of Lemma 1 in [5] and using the Lyapunov direct method, we obtain new results for Lyapunov stability and asymptotic stability of nonlinear systems of fractional order.

REFERENCES

- [1] Y. Li, Y. Chen, and I. Podlubny, "Stability of fractional-order nonlinear dynamic systems: Lyapunov direct method and generalized mittag-leffler stability," *Comput. Math. Appl.*, vol. 59, no. 5, pp. 1810–1821, Mar. 2010.
- [2] J. Baranowski, M. Zagorowska, W. Bauer, T. Dziwinski, and P. Piatek, "Applications of direct lyapunov method in caputo non-integer order systems," *Elektronika ir Elektrotechnika*, vol. 21, no. 2, pp. 10–13, 2015.
- [3] J.-B. Hu, G.-P. Lu, S.-B. Zhang, and L.-D. Zhao, "Lyapunov stability theorem about fractional system without and with delay," *Communications in Nonlinear Science and Numerical Simulation*, vol. 20, no. 3, pp. 905–913, 2015.
- [4] Z. Wang, D. Yang, T. Ma, and N. Sun, "Stability analysis for nonlinear fractional-order systems based on comparison principle," *Nonlinear Dynamics*, vol. 75, no. 1-2, pp. 387–402, 2014.
- [5] J. A. G. Norelys Aguilera-Camacho, Manuel A. Duarte-Mermoud, "Lyapunov functions for fractional order systems," *Commun. Nonlinear Sci. Numer. Simul.*, vol. 19, pp. 2951–2957, February 2014.
- [6] D. S. Bernstein, *Matrix mathematics : theory, facts, and formulas with application to linear systems theory*. Woodstock: Princeton University Press, 2005.

Chaotic dynamics applied to cryptography

M. García-Martínez
 El Colegio de la Frontera Sur
 Chetumal, Quintana Roo
 Email: mogarciam@ecosur.mx

Abstract—In this work we present a Pseudo-Random Bit Generator via unidimensional discrete dynamical systems called multi-modal maps. These systems are based on the logistic map, the sequences generated via multi-modal maps are the result of mix multiple maps, in concrete we mix k time series from k -modal map.

I. INTRODUCTION

There exist a close relationship between chaos and cryptography, for example in [1] authors made a comparison between the properties of these areas and show that the ergodicity, sensitivity to initial conditions and the control parameter, mixing property, deterministic dynamics and complex structure are analogous to confusion, sensitivity to key, diffusion, deterministic pseudo-randomness and algorithm complexity, respectively.

Symmetric ciphers are classified into two: block ciphers and stream ciphers, the block ciphers work with permutations generally are called S-Box, on the other hand the stream ciphers require a pseudo-random sequence generally referred as keystream, this sequence has certain requirements one of them is the randomness.

There have been proposals of generators based on unimodals chaotic maps, for example in [2] a pseudo-random bit generator is proposed which employs the logistic map as a perturbation and a piecewise linear chaotic map as the main generator. Other works such as [3], [4] used two chaotic maps and combined to obtain a complex sequence of bits.

In this work we show how the use of one multi-modal chaotic map may replaced multiple uni-modal chaotic maps and produce a complex sequence that can be used like a keystream.

II. MULTI-MODAL MAPS

A discrete-time dynamical system is given as follows:

$$x_{n+1} = f(x_n), \quad n = 0, 1, 2, \dots, N,$$

where $x_n \in \mathbb{R}$ and x_0 is the initial condition, this kind of dynamical system is usually referred to as map. The simplest maps are the so-called uni-modal maps like the tent and logistic maps, while their generalization, the so-called multi-modal or k -modal maps may present even more rich dynamical behaviors, [5], [6].

We denote the interval $\mathcal{I} := [0, 1]$ and note that the **critical point** c of the continuous piecewise smooth map $f(x) : \mathcal{I} \mapsto \mathcal{I}$ is $c \in \mathcal{I}$ where f is differentiable and

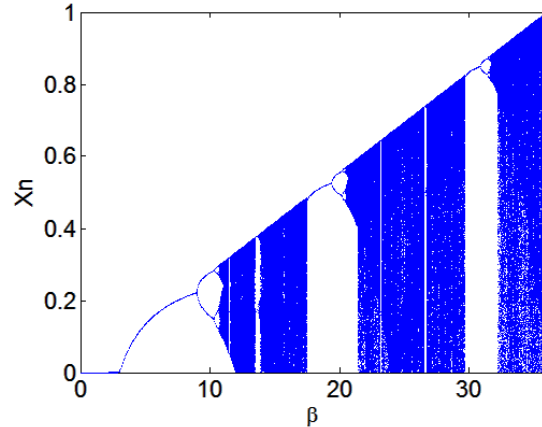


Fig. 1. Bifurcation diagram for the tri-modal map given by Eq. 2.

$f'(c) = 0$. The critical point c occurs for $f'(c) = 0$ or $f'(c)$ does not exist. But continuous smooth maps always present $f'(c) = 0$.

Definition 1 The map $f : \mathcal{I} \mapsto \mathcal{I}$ is called as the k -modal one, if it is continuous on \mathcal{I} and it has k critical points denoted by $c_0, c_1 \dots c_{k-1}$ in \mathcal{I} . Moreover, there exist intervals \mathcal{I}_i , $i = 0, \dots, k - 1$, $\cup_{i=1}^k \mathcal{I}_{i-1} = \mathcal{I}$, such that $\forall i = 0, \dots, k - 1$ it holds $c_i \in \mathcal{I}_i$ and $f(c_i) > f(\beta, x)$, $\forall x \in \mathcal{I}_i$ and $x \neq c_i$, where β is a parameter. The case $k = 1$ will be further simply referred as to the so-called **uni-modal** map.

Note that only considered those critical points that are local maximum on a subinterval.

This means that the number k defines the maximal numbers of modals in a family \mathcal{F} and the interval $\mathcal{I} = [a, b]$ is divided between k subintervals $\mathcal{I}_0 = [d_1, d_2], \mathcal{I}_1 = [d_2, d_3], \dots, \mathcal{I}_{k-2} = [d_{k-2}, d_{k-1}], \mathcal{I}_{k-1} = [d_{k-1}, d_k]$ so the system f_β is a piecewise function by k uni-modals maps.

The parameterized family \mathcal{F} of maps f_β is defined by the following piecewise function

$$f_\beta = \beta(d_{r+1} - x)(x - d_r), \quad x \in \mathcal{I}_r \quad (1)$$

where $d_r = r/k$, ($r = 0, 1, 2, \dots, k - 1$), k is the number of modals, $\beta = \beta(k, \gamma)$ is the bifurcation parameter, $\gamma = 1/k$ is the carrying on capacity. To obtain the maximum value of β with k -modals there is a direct relationship, $\beta_{max} = (4/k)/(1/\gamma)$ for more detail information see ref. [5].

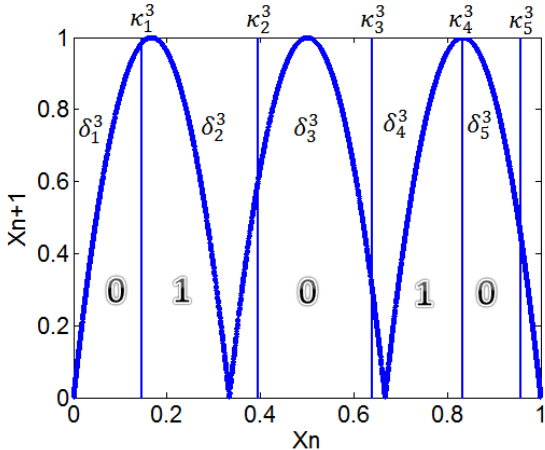


Fig. 2. Plot of the phase space of the tri-modal map with $\beta = \beta_3$.

Lets make an example of k -modal map with $k = 3$, to construct the function of the monoparametric family we use the equation (1) and we will have 3 subintervals \mathcal{I}_r , ($r = 0, 1, 2$), so the function f_β which is given by the equation (2) is expressed as follows

$$f_\beta(x) = \begin{cases} \beta(1/3 - x)(x), & \text{for } x \in [0, 1/3]; \\ \beta(2/3 - x)(x - 1/3), & \text{for } x \in [1/3, 2/3]; \\ \beta(1 - x)(x - 2/3), & \text{for } x \in [2/3, 1]; \end{cases} \quad (2)$$

where $\beta \in [0, 36]$ is the bifurcation parameter, depending on the value of β the system may be uni-modal, bi-modal or tri-modal.

Figure 1 shows a bifurcation diagram of the tri-modal map $f_B(x)$.

III. PROPOSED PSEUDO-RANDOM BIT GENERATOR

In this section we show the algorithm to produce pseudo-random sequences using one k -modal map and a combination of its k -time series.

Step 1: Set the value of $k \in \mathbb{N}^+$.

Step 2: Compute the values of β_j , for $j = 1, \dots, k$, by means of the following equations.

$$\beta_1 = (4)(k) \quad (3)$$

$$\beta_j = j * \beta_1; \quad \text{for } j \geq 2. \quad (4)$$

Taking these values of β_j we are avoiding periodic windows and guarantee chaotic orbits.

Step 3: Take the values of β_j and split the space into $2 * j$ regions $\delta_1^j, \dots, \delta_{2*j}^j$ which are determined by values $\kappa_1^j, \dots, \kappa_{(2*j)-1}^j$, see figure 2. Iterating the system $x_n^j = f(\beta_j, x_n)$ and depending on which region evolves i.e. δ_1^j, δ_2^j represent the value of 0 or 1 with this a binary sequence ζ_j is generated, see figure 3. Note that the generation of the number of 0's is approximately equal to the number of 1's in all the generated sequences with a tolerance of 1%.

Step 4: A k number of chaotic time series are generated by

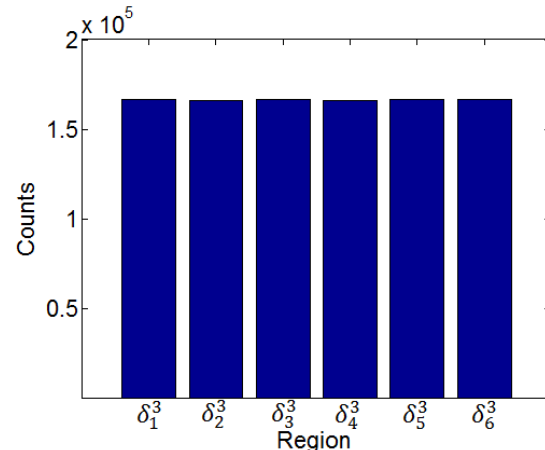


Fig. 3. Distribution of the tri-modal map with $\beta = \beta_3$.

$x_n^j = f(\beta_j, x_n)$ and each one produces a binary sequence ζ_j . These sequences are mixed and the final sequence Z is gotten as follows:

$$Z = \zeta_1 \oplus \zeta_2 \oplus \dots \oplus \zeta_k \quad (5)$$

IV. CONCLUSION

In this work we present a Pseudo-random Bit Generator based on discrete dynamical system of 1-Dimension and multi-modal or k -modal map, we construct the key stream by the combination of k time series we obtained satisfactory results which show that this sequences possess statistical properties like truly random sequences also the k -modal map is highly sensitive to initial conditions.

ACKNOWLEDGMENT

M. García-Martínez is CONACYT Research Fellow El Colegio de la Frontera Sur, Unidad Chetumal.

REFERENCES

- [1] G. Alvarez, S. Li. Some Cryptographic requirements for Chaos-Based cryptosystems, Int J Bifurc Chaos, **16**(8), 2129-2151, 2006.
- [2] Wang Xing-Yuan, Yang Lei. Design of pseudo-random bit generator based on chaotic maps, Int J Modern Phys B, **26**(32), 1250208, 2012.
- [3] Ali Kanso, Nejib Smaoui. Logistic chaotic maps for binary numbers generations, Chaos Solitons Fractals, **40**(5), 2557-2568, 2009.
- [4] M. García-Martínez, E. Campos-Cantón. Pseudo-Random Bit Generator Based on Lag Time Series, Int J Modern Phys C, **25**(4), 1350105, 2014.
- [5] E. Campos-Cantón, R. Femat and A.N. Pisarchik. A family of multimodal dynamic maps, Commun Nonlinear Sci Numer Simulat, **16**(9), 3457-3462, 2011.
- [6] M. García-Martínez, I. Campos-Cantón, E. Campos-Cantón, S. Cejkovský. Difference map and its electronic circuit realization, Nonlinear Dyn, **74**(3), 819-830, 2013.

Wings generation from chaotic attractors

Javier Salvador González Salas
 Universidad Politécnica de San Luis Potosí
 Academia de Matemáticas
 Urbano Villalón No. 500,
 San Luis Potosí, S.L.P.
 email: salvador.gonzalez@upslp.edu.mx

Abstract—In this work a review of some of the mainly methodologies used to generate multi-wins from chaotic attractors is briefly described. Numerical examples that illustrate each one of these methodologies are shown.

I. INTRODUCTION

In the last decades, the nonlinear dynamical system have been an object study. Lastly, a research topic is to generate construct atractors with a more complex dynamic but with low dimension. One form that have been developed is the wings generation in these atractors. In this work are shown methodologies which generate wings like:

- By adding a Controller signal.
- Substituting a hysteresis function in the nonlinear terms.
- By making heteroclinic loops.
- By using a multi-segment quadratic function.

All these methods have the in commun that as they increase the wings number in the oscillators, they increase the number of equilibrium points where the number of equilibrium points its at least greater than one in comparison with the number of wings generated from the chatoic oscillators. Nevertheless, it has been possilble to generate attractors with a greater number of wings than equilibrium points. To ilustrate this kind of generation, it is shown a chotic attractor with four wings but just only one equilibrium point.

II. MULTI-SEGMENT CUADRATIC FUNCTION

This method generates from chaotic systems where the nonlinear part is a cross-product or square terms, and they have the following characteristics [1]:

- Each system has two equilibrium oints, correspondig to the double-wing structure of their attractors.
- These systems are invariant under the transformation $(x, y, z) \rightarrow (-x, -y, -z)$
- The locations of the equililibrium points are closely related to one of the square or cross product of the terms in the systems.
- The non-linear term dynamics are governed by the square and/or the cross product terms of the states.

The achievement is based on replacing the nonlinear part of the aforementioned system with the multi-segment quadratic function of the next form [1]:

$$f(x) = F_0 x^2 - \sum_{i=1}^N F_i [1 + 0.5 \operatorname{sgn}(x - E_i)] - 0.5 \operatorname{sgn}(x + E_i)$$

where N , $F_0 = k/P$, $F_i = 2AP/k_i$, $E_i = (i + 1)AP/(2k)$ with some constants A , P and k_i and the sign function

$$\operatorname{sgn}(x) = \begin{cases} 1, & x > 0 \\ 0, & x = 0 \\ -1, & x < 0 \end{cases}$$

As a numerical example, the chen system is modified by substituying the $f(u)$ in the xy product [1]:

$$\begin{aligned} \dot{x} &= -ax + ay \\ \dot{y} &= (c-a)x + cy - 1/P)xz \\ \dot{z} &= f(x) - bz \end{aligned} \quad (1)$$

In Fig. 1 is shown the graph for the case $N = 4$ [1]. The System (1) has $(2N + 2)$ equilibrium points, which can be derived as $(u_{\pm n}, u_{\pm n}, P(2c - a))$, where $n = 0, 1, 2, 3, 4$ and

$$u_{\pm} = \begin{cases} \pm\sqrt{\varepsilon/F_0}, & n = 0, \\ \pm\sqrt{\frac{\varepsilon + \sum_{i=1}^n F_i}{F_0}}, & i \leq n \leq N, \end{cases}$$

with $\varepsilon = bP(2c - a)$.

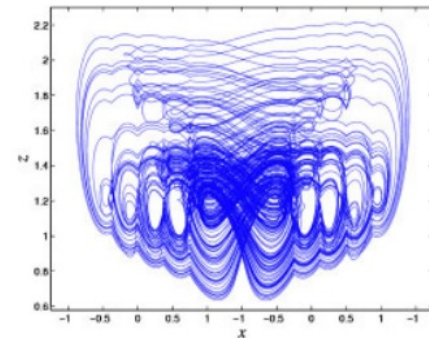


Fig. 1. Multi-wing attractor from Chen modified system.

III. HYSTERESIS FUNCTION

This method changes a two-wing butterfly chaotic system in a grid multiwing butterfly chaotic system by replacing state variables of the system by two piecewise hysteresis

functions [2]. The modified system generates $2(N_1+M_1+2) \times (N_2+M_2+2)$ -wing butterfly chaotic attractors. The hysteresis function (HF) are defined as follows [2]:

$$\begin{aligned} g_{xm} &= \sum_{-M_1}^{N_1} h_{xm}(x), \\ g_{zm} &= \sum_{-M_2}^{N_2} h_{zm}(z), \end{aligned}$$

where

$$h_{xm} = \begin{cases} -2m & x > 2m - 1 - A, \\ -2(m-1) & x < 2m - 1 + A, \end{cases}$$

$$h_{zm} = \begin{cases} -2m & x > 2m - 0.5 - A, \\ -2(m-1) & x < 2m + 0.5 + A, \end{cases}$$

As an example, it is used the Lorenz system. By modifying with HF the system appropriately, a novel system modified is obtained

$$\begin{aligned} \dot{x} &= a(y - f_{xm}(x)) \\ \dot{y} &= c f_{xm}(x) - y - \beta f_{xm}(x) f_{zm}(z) \\ \dot{z} &= \gamma f_{xm}(x) - b f_{zm}(z) \end{aligned} \quad (2)$$

where a, b, c, β and γ are system parameters, $f_{xm} = x + g_{xm}(x)$, and $f_{zm}(z) = z + g_{zm}(z)$. The equilibrium points of the system (2) are the following:

$$\begin{aligned} s_{1m} &= (E_{xm}, 0, 0); \\ s_{2m} &= \left(\sqrt{\frac{b(c-1)}{\beta\gamma}} + E_{xm}, \sqrt{\frac{b(c-1)}{\beta\gamma}}, \frac{c-1}{\beta} + E_{zm} \right) \\ s_{3m} &= \left(-\sqrt{\frac{b(c-1)}{\beta\gamma}} + E_{xm}, -\sqrt{\frac{b(c-1)}{\beta\gamma}}, \frac{c-1}{\beta} + E_{zm} \right) \end{aligned}$$

where $E_{xm} = 2m$, $m = -M_1, \dots, -1, 0, 1, \dots, M_1$ and $E_{zm} = 2m$, $m = -M_2, \dots, -1, 0, 1, \dots, M_2$.

Figure 2 is the graph of an 8×4 -wing chaotic attractor when $A = 0.01$ and $N_1 = M_1 = N_2 = M_2 = 1$ and parameter values $a = 10$, $b = 8/3$, $c = 28$, $\beta = 17$, $\gamma = 11.5$ [2].

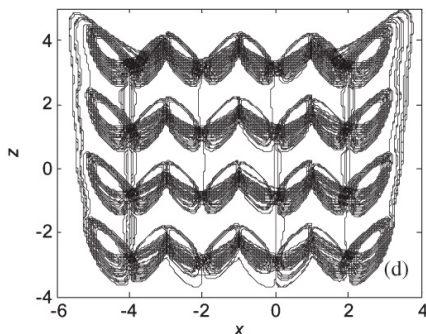


Fig. 2. Grid multiwing butterfly chaotic Lorenz attractor with 32 scrolls.

IV. HEREROCLINIC LOOPS

This method generates grid multiwing chaotic attractors form multipiecewise system. It uses a switching controller to connect heteroclinic orbits (according to the shil'nikov theorem) between linear systems [3].

In Fig. 3 is shown the eigenspaces and heteroclinic orbits of a two wing chaoatic system, where $E^S(P_1)$ (or $E^S(P_2)$) and $E^U(P_1)$ (or an stable eigenline and unstable eigenplane respectively at the equilibria P_1 and P_2 of two fundamental linear systems.

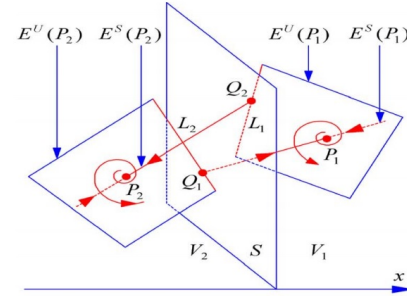


Fig. 3. Eigenspaces and heteroclinic orbits.

To construct a various grid multiwing chaotic attractors, it is necessary to connect all equilibria of the multiwing-PWL system by using an heteroclinic loop. This method [3]calculates the switching planes $S_i(x)$ and $S_j(x)$, the linear subspaces V_{ij} and their corresponding equilibria P_{ij} with the following formula[3]:

$$\begin{aligned} S_i(x) &= \{(x, y, z) | x = 2ix_0\} \\ S_j(x) &= \{(x, y, z) | z = 2jx_0\} \\ V_i &= \{(x, y, z) | (2i-2)x_0 < x < 2ix_0, (2j-2)x_0 < z < 2jx_0\} \end{aligned}$$

where $i, j = 0, \pm 1, \pm 2, \dots$, and their equilibria

$$P_i = \left\{ \left(2i - \frac{|i|}{i} \right) x_0, \left(2i - \frac{|i|}{i} \right) y_0, \left(2j - \frac{|j|}{j} \right) z_0 \right\}$$

where $i = \pm 1, \pm 2, \dots$, and x_0, y_0, z_0 are the....

As an example, from the Lü System

$$\begin{aligned} \dot{x} &= a(y - x) \\ \dot{y} &= -xz + cy \\ \dot{z} &= xy - bz \end{aligned}$$

it is constructed the following multi-PWL system

$$\begin{pmatrix} \dot{x} \\ \dot{y} \\ \dot{z} \end{pmatrix} = \begin{pmatrix} -a & a & 0 \\ -c & c & -T\sqrt{bc} \\ T\sqrt{bc} & T\sqrt{bc} & -b \end{pmatrix} \begin{pmatrix} x \\ y \\ z \end{pmatrix} - u$$

where

$$T = \tanh(Bx) + \sum_{i=1}^M (-1)^i [T_i(x) + T_i(x)]$$

$$u = \begin{pmatrix} T = x_0 \tanh(Bx) + \sum_{i=1}^M x_0 [T_i(x) + T_i(x)] \\ T = y_0 \tanh(Bx) + \sum_{i=1}^M y_0 [T_i(x) + T_i(x)] \\ T = z_0 \tanh(Bx) + \sum_{i=1}^M z_0 [T_i(x) + T_i(x)] \end{pmatrix}$$

Figure 4 shows a multiwing attractor from Lü System for the case $x_0 = 1$, $y_0 = 0.9267$, $z_0 = 1.02$, $M = 3$ and $N = 1$ where it has a grid 8×4 wing butterfly attractor [3].

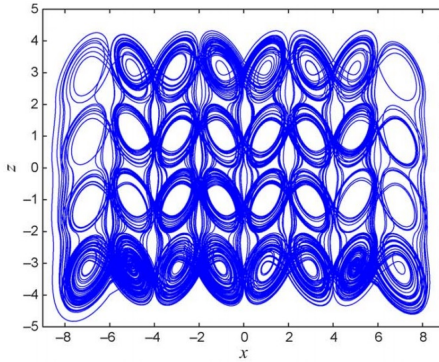


Fig. 4. 8×4 grid wing butterfly chaotic attractor from modified Lü System.

V. CONNECTION OF ATTRACTORS

There exists four-dimensional chaotic systems which due to their symmetry and equations form, produce two wings chaotic attractors disconnected (which depend on the initial conditions). In [4], it is shown a method that connects double wing attractors to form a single attractor just by using a simple linear term which breaks this simetry.

As an example, it is illustrated the four-dimensional system in [4]:

$$\begin{aligned} \dot{x}_1 &= a(x_2 - x_1) + x_2 x_3 x_4, \\ \dot{x}_2 &= b(x_1 + x_2) - x_1 x_3 x_4, \\ \dot{x}_3 &= -cx_3 + x_1 x_2 x_4, \\ \dot{x}_4 &= -dx_4 + x_1 x_2 x_3. \end{aligned} \quad (3)$$

Here $x_i (i = 1, 2, 3, 4)$ are the state variables and a, b, c, d are positive real constants, and for appropiate value of the parameteres the system produces two disconnected attractors with symmetries bewteen $x_1 - x_2$ and $x_3 - x_4$ planes. Due to the third and fourth equations of the System (3) are interchangeable and symmetric, which is the key that this system never produces a four-wing attractor. The strategy is to add a term at that the equation that breaks this symmetries.

By introducing simple linear ex_2 term in the third equation [4]

$$\begin{aligned} \dot{x}_1 &= a(x_2 - x_1) + x_2 x_3 x_4, \\ \dot{x}_2 &= b(x_1 + x_2) - x_1 x_3 x_4, \\ \dot{x}_3 &= -cx_3 + ex_2 + x_1 x_2 x_4, \\ \dot{x}_4 &= -dx_4 + x_1 x_2 x_3. \end{aligned} \quad (4)$$

where e is constant, System (4) breaks the symmetries of the System (3). The System (4) has nine equilibria which are described in [4]. Figure 5 shows the attractor from System 3

before the double two wings attractor are connected; meanwhile Fig. 6 is the four wing single attractor from System (4) (after the system is modified).

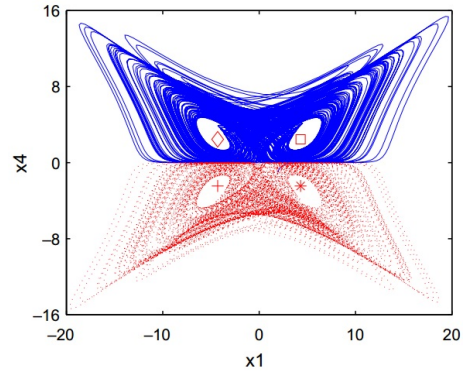


Fig. 5. Four dimensional chaotic system with double two wings disconnected attractors.

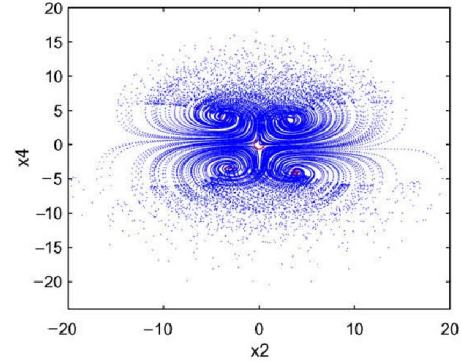


Fig. 6. A single chaotic attractor with four wings.

VI. A SINGLE EQUILIBRIUM POINT

In almost multiwing research work, attractors generated from chaotic systems have wings which oscillate around a nonzero equilibria. In this section, it is shown a four dimensional system which contains four wings but only an equilibrium point [5].

Consider the following simple autonomous system

$$\begin{aligned} \dot{x} &= ax - yz + w, \\ \dot{y} &= xz - by, \\ \dot{z} &= xy - cz + xw, \\ \dot{w} &= -y, \end{aligned}$$

where a, b and c are constants.

$$\begin{aligned} ax - yz + w &= 0, \\ xz - by &= 0, \\ xy - cz + xw &= 0, \\ -y &= 0, \end{aligned}$$

As $y = 0$, it gives as a result that the only equilibrium point is the origen $(0, 0, 0, 0)$.

Figure 7, shows the plane $x - z$ projecton of the four wing attractor formed setting the parameters $a = 8$, $b = 40$ and $c = 14.9$ in [4]. It is easily see that

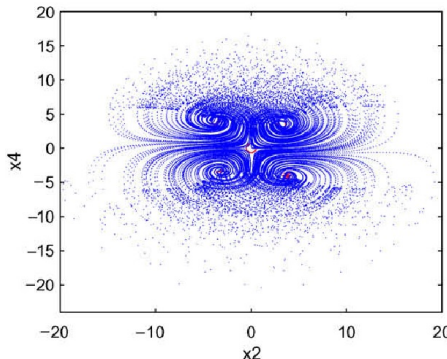


Fig. 7. Phase portrait of the four wing attractor.

VII. CONCLUSION

It has been described some of the mainly methodologies to generate wings from chaotic oscillators. Three methods increase the number of wings by using a piecewise functions. Another method just connects two double wing attractor by using a simple linear term. In alll these methodologies were illustrated examples which the number of equilibria is greater than the number of wings. Nevertheless, it was shown a case where there is only one equilibrium point but four wings. This case is interesting to be analytically studied, like how to calculate the values of the points where the wings are oscillating.

Actually, making low order system attractors with more complex dynamics by increasing the number of wings has been a direction in the study of chaotic systems. It is interesting to find another ways to increase the number in low dimensional chatoic systems, like the using of forced systems and/or delayed systems.

REFERENCES

- [1] Simin Yu, Wallace K.S. Tang, Jinhu Lü and Guarong Chen, *Generating 2n-wing attractors from Lorenz-like systems*, Int. J. Circ. Theor. Appl., DOI: 10.1002/cta.558, 2008.
- [2] Yun Huang, Peng Zhang, Weifeng Zhao, *Novel Grid Multiwing Butterfly Chaotic Attractors and ther Circuit Design*, IEEE Transaction on Circuits and Systems (62), 2015.
- [3] Simin, Yu, Jinhu Lü, Guanrong Chen, Xinghuo Yu, *Generating Grid Multiwing Chaotic Attractors by Constructing Heteroclinic Loops Into Switching Systems*, IEEE Transactions on Circuits and Systems (58), No. 5, 2011.
- [4] Guoyuan Qi, Barend Jacobus van Wyk, Michaël Antonie van Wyk, *A four-wing attractor a its analysis*, Chaos, Solutions and Fractals (40), 2016-2030, 2009.
- [5] Sara Dadras, Hamid Reza Momeni, Gouyuan Qi, Zhong-lin Wang, *Four-wing hyperchaotic attractor generated form a new 4D system with one equilibrium and its fractional-order form*, Nonlinear Dyn (67), 1161-1173, 2012.

Selective monostability in multi-stable systems: experimental results

R. Sevilla-Escoboza,
R. Jaimes-Reategui,
G. Huerta-Cuellar,
and J.H. Garcia-Lopez
Centro Universitario de los Lagos
Universidad de Guadalajara
47460, Lagos de Moreno, Jalisco, Mexico
Email: ghuertacuellar@gmail.com

A. N. Pisarchik
Centro de Investigaciones en Optica,
Loma del Bosque 115, Lomas del Campestre,
37150 Leon, Guanajuato, Mexico
Center for Biomedical Technology,
Technical University of Madrid,
Campus Montegancedo,
28223 Pozuelo de Alarcon, Madrid, Spain

Abstract—We propose a robust method that allows a periodic or a chaotic multi-stable system to be transformed to a monostable system at an orbit with dominant frequency of any of the coexisting attractors. Our approach implies the selection of a particular attractor by periodic external modulation with frequency close to the dominant frequency in the power spectrum of a desired orbit and simultaneous annihilation of all other coexisting states by positive feedback, both applied to one of the system parameters. The method does not require any preliminary knowledge of the system dynamics and the phase pace structure. The experiments with an erbium-doped fibre laser provide evidence for the robustness of the proposed method in making the system monostable at an orbit with dominant frequency of any preselected attractor [1].

I. INTRODUCTION

Multi-stability is a universal, essentially nonlinear phenomenon that has been found in almost all areas of science and nature from lasers [2] and chemical reactions [3] to climate [4], and brain [5]. Multistability also contributes to the fundamental dynamics of neurons and neuronal networks [6], [7] involving cell differentiation and hysteresis and is compulsory for implementing associative memories, signal processing, pattern recognition and optimization problems [8].

In a real system with multiple coexisting attractors, it is very difficult to keep the trajectory in a particular attractor due to extremely high sensitivity of the multi-stable system to external perturbations or noise. Several feedback and non-feedback control strategies have been developed to direct the system trajectory to a desired attractor. Feedback control [9] and forecast-based control [10] methods allow attractor selection without changing the structure of basins of attraction. Instead, non-feedback control, e.g. in the form of external modulation [11], [12], destroys some of attractors resulting in monostability, but it does not allow in every case the selection of a particular attractor. In practice, the possibility of converting a multi-stable system to a monostable one is very much in demand because this would allow one to avoid any unpredictable switch to another coexisting state that may be caused by environmental fluctuations or increasing internal noise.

As we already mentioned above, due to several limitations, the existing methods for controlling multi-stability are not able to make a system monostable at an attractor with characteristic properties of any one of coexisting states; for example, the method of attractor annihilation by periodic modulation [12] can destabilize only those attractors whose eigenfrequencies are close to the modulation frequency [14]. In this paper, we address the question: Is it possible to design a method capable of eliminating all coexisting orbits except the one with desired properties, i.e. to make the system monostable at an orbit with dominant frequency of any one of the coexisting attractors? Our results give a positive answer to this question. Here we show experimental results in a multi-stable fibre laser with four coexisting periodic orbits.

A. Experiment

The experimental set-up is shown in figure 1. The EDL contains the EDF and two fibre Bragg gratings (FBG1 and FBG2). The EDL is pumped by a laser diode through the polarization controller and the wave-division multiplexer. The EDL output is detected by a photodetector and analysed with an oscilloscope (OSC). The optical isolator avoids an optical feedback from the detector window to the EDL. The signal recorded by the photodetector and amplified enters the diode current controller (DCC) of the diode pump laser. The waveform generators WFG1 and WFG2 produce periodic signals for driving and control, respectively, to be also sent to the DCC.

The OSC traces in figure 2 illustrate the experimental realization of the monostability control in the EDL. First, we apply the positive feedback and then harmonic modulation with frequency $f_c = f_d/i$ ($i = 3, 4, 5, 6$). The control annihilates all attractors and leaves only A_i^* , thus converting the multi-stable laser to monostable. Interestingly, in the experiment, we are able to stabilize orbit A_6^* , whereas orbit A_6 is unstable without the control.

Figure 3 shows the experimental state diagrams for the period-1, period-3, period-4 and period-5 attractors in space of the modulation depth and feedback strength when the control

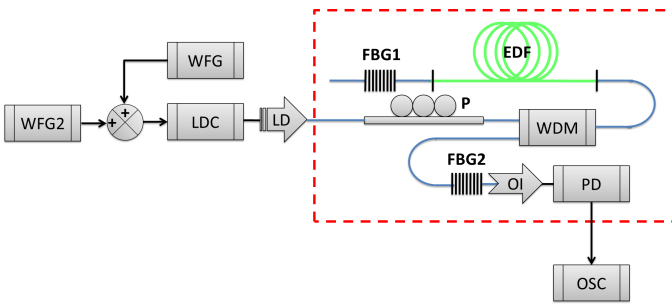


Fig. 1. Experimental set-up. EDF is the erbiumdoped fibre, FBG1 and FBG2 are the fibre Bragg gratings, LD is the pump laser diode, DCC is the diode current controller, PC is the polarization controller, WDM is the wave-division multiplexer, OI is the optical isolator, PD is the photodetector, OSC is the oscilloscope, WFG1 and WFG2 are the waveform generators, and K is the coupling interface.

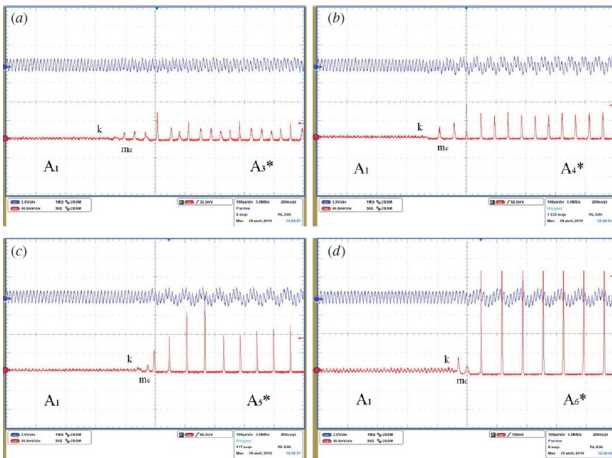


Fig. 2. OSC traces demonstrating transitions from original period-1 to new (a) period-3, (b) period-4, (c) period-5 and (d) period-6 attractors after application of positive feedback with $k = 0.4, 0.8, 0.4, 0.4$ at 400s and harmonic modulation with $f_c = f_i$ ($i = 3, 4, 5, 6$) and $m_c = 0.3, 0.6, 0.6, 0.6$ (180, 360, 360, 360 mVpp) at 480s. The upper trace is the signal applied to the diode pump current and the lower trace is the laser response. $fd = 80$ kHz.

modulation with $f_c = f_i$ is applied. This method works better in practice than in theory [1]. This occurs because small noise, inevitable in experiments, helps in the attractor selection, i.e. in the presence of noise, the system switches to the desired attractor more easily than without noise. The final attractor is globally stable and robust to noise because the system is monostable.

II. CONCLUSION

We have shown experimentally that a multi-stable system can be converted into a monostable one by simply applying an external harmonic modulation. One of the main advantages of our method is its easy implementation for practical applications. Even without preliminary knowledge of the system dynamics, one can select attractors by organizing a positive feedback and tuning the generator frequency. The method can be prominent for technological applications where giant pulses are required or in medicine for designing a pacemaker to stabilize the cardiac rhythm at a desired frequency.

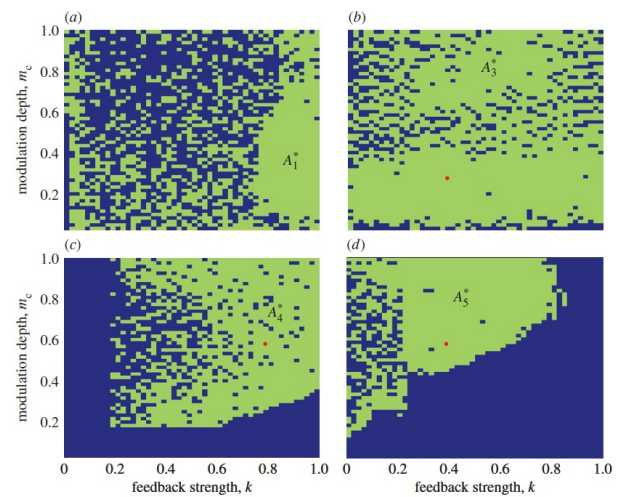


Fig. 3. Experimental state diagrams in (k, m_c) -parameter space for (a) $f_c = f_1$, (b) $f_c = f_3$, (c) $f_c = f_4$ and (d) $f_c = f_5$. Monostability with attractor A_i^* is found in the light and multi-stability in the dark regions. The dark dots in (b-d) indicate the parameters for the time series in figure 2 a-c.

REFERENCES

- [1] R. Sevilla-Escoboza, A. N. Pisarchik, R. Jaimes-Retegui and G. Huerta-Cuellar, Proc. R. Soc. A 471: 20150005. (doi.org/10.1098/rspa.2015.0005)
- [2] Areccchi FT, Meucci R, Puccioni GP, Tredicce J. 1982 Experimental evidence of subharmonic bifurcations, multistability, and turbulence in a Q-switched gas laser. Phys. Rev. Lett. 49, 12171220. (doi:10.1103/PhysRevLett.49.1217)
- [3] Ngonghala CN, Feudel U, Showalter K. 2011 Extreme multistability in a chemical model system. Phys. Rev. E 83, 056206. (doi:10.1103/PhysRevE.83.056206).
- [4] Pisarchik AN, Feudel U. 2014 Control of multistability. Phys. Rep. 540, 167218. (doi:10.1016/j.physrep.2014.02.007).
- [5] Kelso JAS. 2012 Multistability and metastability: understanding dynamic coordination in the brain. Phil. Trans. R. Soc. B 367, 906918. (doi:10.1098/rstb.2011.0351).
- [6] Mincheva M, Craciun G. 2008 Multigraph conditions for multistability. Proc. IEEE 96, 12811291. (doi:10.1109/JPROC.2008.925474).
- [7] Malashchenko T, Shilnikov A, Cymbalyuk G. 2011 Six types of multistability in a neuronal model based on slow calcium current. PLoS ONE 6, e21782. (doi:10.1371/journal.pone.0021782).
- [8] Hopfield JJ. 1984 Neurons with graded response have collective properties like those of twostate neurons. Proc. Natl Acad. Sci. USA 81, 30883092. (doi:10.1073/pnas.81.10.3088)
- [9] Pyragas K. 1992 Continuous control of chaos by self-controlling feedback. Phys. Lett. A 170, 421428. (doi:10.1016/0375-9601(92)90745-8)
- [10] Cornelius SP, Kath WL, Motter AE. 2013 Realistic control of network dynamics. Nat. Commun. 4, 1942. (doi:10.1038/ncomms2939)
- [11] Pisarchik AN, Goswami BK. 2000 Annihilation of one of the coexisting attractors in a bistable system. Phys. Rev. Lett. 84, 14231426. (doi:10.1103/PhysRevLett.84.1423)
- [12] Pisarchik AN. 2001 Controlling the multistability of nonlinear systems with coexisting attractors. Phys. Rev. E 64, 046203. (doi:10.1103/PhysRevE.64.046203)
- [13] Pisarchik AN, Barmenkov YO, Kiryanov AV. 2003 Experimental characterization of the bifurcation structure in an erbium-doped fiber laser with pump modulation. IEEE J. Quantum. Electron. 39, 15671571. (doi:10.1109/JQE.2003.819559)
- [14] Goswami BK, Pisarchik AN. 2008 Controlling multistability by small periodic perturbation. Int. J. Bifur. Chaos 18, 16451673. (doi:10.1142/S0218127408021257)

Deterministic coherence resonance in two unidirectionally coupled Rössler oscillators

R. Jaimes-Reátegui,
 G. Huerta-Cuellar,
 Carlos E. Castañeda,
 R. Chiu-Zarate
 Centro Universitario de los Lagos
 Universidad de Guadalajara
 Enrique Díaz de Leon, Paseos de la Montaña
 Lagos de Moreno, Jalisco 47460, México
 Email: rjaimes@culagos.udg.mx

A. N. Pisarchik
 Computational Systems Biology
 Center for Biomedical Technology
 Technical University of Madrid
 Campus Montegancedo
 28223 Pozuelo de Alarcón,
 Madrid, Spain

Abstract—A small mismatch between natural frequencies of unidirectionally coupled chaotic oscillators can induce coherence resonance in the slave oscillator for a certain coupling strength. This surprising phenomenon looks like “stabilization of chaos by chaos”, i.e., the chaotic driving applied to the chaotic system makes its dynamics more regular when the natural frequency of the slave oscillator is a little different than the natural frequency of the master oscillator. The coherence is characterized with the dominant component in the power spectrum of the slave oscillator, normalized standard deviations of both the peak amplitude and the inter-peak interval, and Lyapunov exponents. The enhanced coherence is associated with increasing negative both the third and the fourth Lyapunov exponents, while the first and second exponents are always positive and zero, respectively abstract goes here.

I. INTRODUCTION

It is of common knowledge that a nonlinear system in the presence of noise can exhibit resonance phenomena such as stochastic [1], [2] or coherence [3] resonance. While the former is seen as an optimal response to external periodic modulation with respect to the noise intensity, the latter manifests itself as increasing regularity in one of the system internal time scales without additional modulation. Coherence resonance was detected first in excitable dynamical systems [3], [4], [5], [6], [7] and then in bistable systems [8], [9], [10]. Examples are typically found in biology in the form of neuron spiking dynamics [11].

In this work, we report on a significantly different case of deterministic coherence resonance. We consider two unidirectionally coupled nonidentical chaotic oscillators, master $\dot{\mathbf{x}}_1 = \mathbf{F}(\mathbf{x}_1, \omega_1)$ and slave $\dot{\mathbf{x}}_2 = \mathbf{F}(\mathbf{x}_2, \omega_2) + \sigma(\mathbf{x}_1 - \mathbf{x}_2)$, where $\mathbf{x}_{1,2}$ are state variables of the master and slave systems, \mathbf{F} is a vector function, and σ is a coupling strength. The oscillators are only distinguished by their natural frequencies ω_1 and ω_2 . Due to nonlinearity, the dominant frequency ω_0 in the chaotic power spectrum of the master oscillator usually does not coincide with its natural frequency. Since the master oscillator acts as a driving force for the slave oscillator, the dominant frequency of the slave oscillator is entrained by the

master oscillator when the coupling is sufficiently strong, thus resulting in phase synchronization [13]. Recently, Pyragiené and Pyragas [14] showed that in the phase synchronization state, the average phase difference $\langle \phi_2 - \phi_1 \rangle$ is negative if the frequency mismatch $\Delta = \omega_2 - \omega_1 < 0$ and positive if $\Delta > 0$. In the former case, the average oscillators’ phases are locked with lag and in the latter case with anticipation.

Here, we will show that a small frequency mismatch not only leads to phase synchronization, but can also improve the performance of chaotic oscillations inducing deterministic coherence resonance in the slave system. This surprising phenomenon looks like “stabilization of chaos by chaos”, i.e., a chaotic system under a chaotic drive behaves more regular, almost periodic. The coherence is maximized with respect to both the frequency mismatch Δ and the coupling strength σ .

A. Coherence enhancement

Let us consider two unidirectionally coupled Rössler oscillators:

$$\begin{aligned} \dot{x}_1 &= -\omega_1 y_1 - z_1, & \dot{x}_2 &= -\omega_2 y_2 - z_2, \\ \dot{y}_1 &= \omega_1 x_1 + a y_1, & \dot{y}_2 &= \omega_2 x_2 + a y_2 + \sigma(y_1 - y_2), \\ \dot{z}_1 &= b + z_1(x_1 - c), & \dot{z}_2 &= b + z_2(x_2 - c). \end{aligned} \quad (1)$$

The master oscillator is chaotic for $a = 0.16$, $b = 0.1$, $c = 8.5$, and $\omega_1 = 1$. The natural frequency of the slave oscillator ω_2 and the coupling strength σ are used as control parameters.

B. Characterization of coherence resonance

In Fig. 1 we illustrate how small mismatch $\Delta = 0.11$ between the natural frequencies of the master and slave oscillators enhances coherence of the slave dynamics for the coupling strength $\sigma = 0.2$. One can see that the dynamics of the slave system is more regular than that of the master oscillator. We should note, that when the natural frequencies coincide ($\Delta = 0$), the chaotic trajectories of the two oscillators are identical.

In Fig. 2 we plot the maximum amplitude S_0 of the slave power spectrum as a function of the two control parameters, ω_2

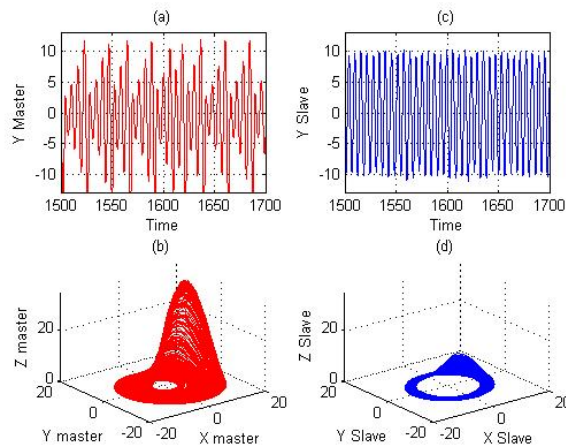


Fig. 1. Color online. Coherence enhancement in coupled chaotic Rössler oscillators Eq. (1) with frequency mismatch $\Delta = 0.11$. Time series of (a) y_1 and (b) y_2 and phase portraits of (c) master and (d) slave oscillators for coupling strength $\sigma = 0.2$.

and σ . Phase synchronization is observed within the Arnold tongue in the vicinity of $\omega_2 = 1$, where the dominant frequency $\omega_0 = 1.05$ of the slave oscillator is entrained by the master oscillator. The red (dark) spot inside this tongue means higher coherence.

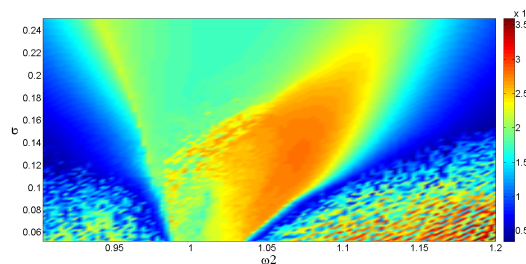


Fig. 2. Color online. Dominant spectral component S_0 at ω_0 in the (ω_2, σ) -parameter space for coupled chaotic oscillators Eq. (1).

Other characteristics of the coherence obtained from the time series of the slave oscillator are shown in Fig. 3. The NSD of both the peak amplitude of y_2 and the IPI minimize when $\omega_2 = 1.11$ for $\sigma = 0.2$. This is the signature of coherence resonance.

II. CONCLUSION

In conclusion, we have demonstrated the existence of deterministic coherence resonance in oscillations of a chaotic system unidirectionally coupled with another, almost identical, chaotic system in the presence of a small mismatch between their natural frequencies. The improved coherence looks like “stabilization of chaos by chaos”. As counterintuitive as it may seem, the two subsystems oscillate at the same dominant frequency but follow a different dynamics; while the master oscillator is chaotic, the slave oscillator is almost periodic. Using a paradigmatic example of Rössler oscillators, we

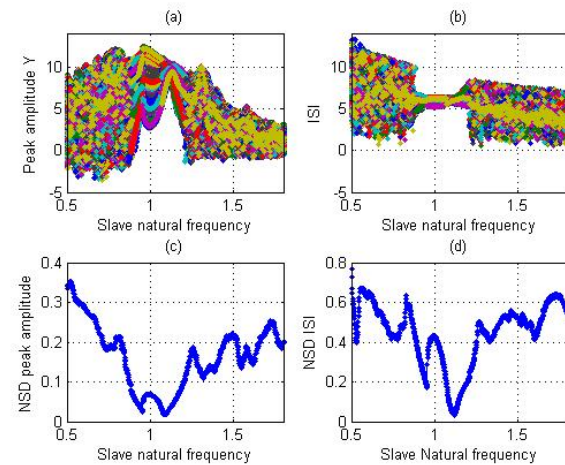


Fig. 3. Color online. Frequency dependences of (a) y_2 peak amplitude, (b) IPI of y_2 , (c) NSD of y_2 peak amplitude, and (d) NSD of IPI for chaotically driven chaotic oscillator Eq. (1). $\sigma = 0.2$.

have found conditions and parameters where this surprising phenomenon occurs. The coherence resonance has been identified with time series and quantitatively characterized by the dominant spectral component, the minima of the normalized standard deviation of both the peak amplitude and the interpeak interval. Therefore, the coherence enhancement occurs due to interaction of chaotic systems, when their phases synchronize and the dominant frequency of the slave oscillator is entrained by the master oscillator.

ACKNOWLEDGMENT

R. J. acknowledges support from CONACYT (Mexico) (project 234594).

REFERENCES

- [1] R. Benzi, A. Sutera, and A. Vulpiani, *J. Phys. A* **14**, 453 (1981).
- [2] L. Gammaitoni, P. Hänggi, P. Jung, and F. Marchesoni, *Rev. Mod. Phys.* **70**, 223 (1998).
- [3] A. S. Pikovsky and J. Kurths, *Phys. Rev. Lett.* **78**, 775 (1997).
- [4] Hu Gang, T. Ditzinger, C. Z. Ning, and H. Haken, *Phys. Rev. Lett.* **71**, 807 (1993).
- [5] A. Neiman, P. I. Saparin, and L. Stone, *Phys. Rev. E* **56**, 270 (1997).
- [6] D. E. Postnov, S. K. Han, T. G. Yim, and O. V. Sosovtseva, *Phys. Rev. E* **59**, 3791(R) (1999).
- [7] G. Giacomelli, M. Giudici, S. Balle, and J. R. Tredicce, *Phys. Rev. Lett.* **84**, 3298 (2000).
- [8] L. S. Tsimring and A. Pikovsky, *Phys. Rev. Lett.* **87**, 250602 (2001).
- [9] K. Panajotov et al., *Phys. Rev. A* **69**, 011801(R) (2004).
- [10] M. Arizala Arteaga et al., *Phys. Rev. Lett.* **99**, 023903 (2007).
- [11] B. Lindner, J. García-Ojalvo, A. Neiman, and L. Schimansky-Geier, *Phys. Rep.* **392**, 321 (2004).
- [12] M. Franaszek and E. Simiu, *Phys. Rev. E* **54**, 1298 (1996).
- [13] M. G. Rosenblum, A. S. Pikovsky, and J. Kurths, *Phys. Rev. Lett.* **76**, 1804 (1996).
- [14] T. Pyragiené and K. Pyragas, *Nonlinear Dyn.* **74**, 297 (2013).

Multiestable structure via chaotic synchronization and preservation of scrolls

E. Jiménez-López
 El Colegio Mexiquense A.C.
 Zinacantepec, Estado de México 51350
 Email: ejimenez@cmq.edu.mx

Abstract—The objective of this study is to show interconnected multi-scroll chaotic systems in master-slave configuration. It focuses in an interesting phenomenon when the master presents different number of scrolls than the slave and how to reach preservation of the number of scrolls in the slave. In particular, the paper introduces and demonstrates the so-called multistability generalized synchronization meaning that a functional relation between the master and the slave subsystems exists.

I. INTRODUCTION

Multistability phenomenon has been presented in different forms in nature, for example the brain presents a multi-stable structure, with this we can have different memories or focus on different activities. The phenomena of nature are therefore inherently non-linear mathematical theory of dynamical systems is used to describe [1]. With this we can describe behaviors, ranging from fixed points, limit cycles, toroids or more complex as chaotic attractors and hyper-chaotic [2], [3]. A characteristic of chaotic attractors is the appearance of a fixed number of scrolls, from there is carried out the characterization of them. However, in recent years it has increased the study of dynamic systems that can generate multiple scrolls [4]. Unidirectionally coupling two different law systems with switching generates a different number of scrolls, dependent on their initial conditions is possible to observe the phenomenon of generalized multistability.

II. MULTISROLL ATTRACTORS BY UNSTABLE DISSIPATIVE SYSTEMS

We consider the class of autonomous systems of linear differential equations given as follows:

$$\dot{x} = Ax + B \quad (1)$$

where $x = [x_1, x_2, x_3]^\top \in R^3$ it is the state vector, $B = [0, 0, \beta_1]^\top \in R^3$ stands for a real vector and $A \in R^{3 \times 3}$ it is a matrix with the following structure:

$$A = \begin{pmatrix} 0 & 1 & 0 \\ 0 & 0 & 1 \\ \alpha_{31} & \alpha_{32} & \alpha_{33} \end{pmatrix} \quad (2)$$

the equilibrium point is located at $\chi^* = (-\beta_1/\alpha_{31}, 0, 0)$, a chaotic attractor is generated with three scrolls to modify values β_1 , according to the following switching law

$$u_3 = \begin{cases} s_3 = \{A, B_3\}, & \text{if } x_1 \geq 0.9; \\ s_2 = \{A, B_2\}, & \text{if } 0.3 \leq x_1 < 0.9; \\ s_1 = \{A, B_1\}, & \text{if } x_1 < 0.3; \end{cases} \quad (3)$$

where $B_1 = (0, 0, 0)^\top$, $B_2 = (0, 0, 0.9)^\top$ and $B_3 = (0, 0, 1.8)^\top$. For the full system u_3 given by Eq.(3), the equilibrium points of the subsystems switched s_1 , s_2 and s_3 they are $\chi_1^* = (0, 0, 0)^\top$, $\chi_2^* = (0, 0, 0.6)^\top$ and $\chi_3^* = (0, 0, 1.2)^\top$, respectively. Similarly, to generate a system ten

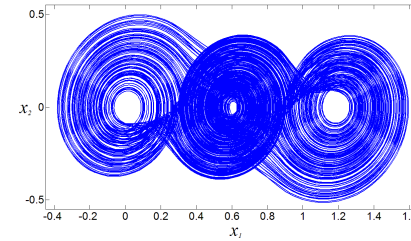


Fig. 1. Projection onto the plane (x_1, x_2) of the chaotic attractor with three scrolls given by Eq.(3).

scroll through a switching system similar to (1), seven subsystems are added as (3)

$$u_{10} = \begin{cases} s_{10} = \{A, B_{10}\}, & \text{if } 6.7 \geq x_1; \\ s_9 = \{A, B_9\}, & \text{if } 5.1 \leq x_1 < 6.7; \\ s_8 = \{A, B_8\}, & \text{if } 4.5 \leq x_1 < 5.1; \\ s_7 = \{A, B_7\}, & \text{if } 3.9 \leq x_1 < 4.5; \\ s_6 = \{A, B_6\}, & \text{if } 3.3 \leq x_1 < 3.9; \\ s_5 = \{A, B_5\}, & \text{if } 2.1 \leq x_1 < 2.7; \\ s_4 = \{A, B_4\}, & \text{if } 1.5 \leq x_1 < 2.1; \\ s_3 = \{A, B_3\}, & \text{if } 0.9 \leq x_1 < 1.5; \\ s_2 = \{A, B_2\}, & \text{if } 0.3 \leq x_1 < 0.9; \\ s_1 = \{A, B_1\}, & \text{if } x_1 < 0.3; \end{cases} \quad (4)$$

where B_1 , B_2 y B_3 they are as above, $B_4 = (0, 0, 2.7)^\top$, $B_5 = (0, 0, 3.6)^\top$, $B_6 = (0, 0, 4.5)^\top$, $B_7 = (0, 0, 5.4)^\top$, $B_8 = (0, 0, 6.3)^\top$, $B_9 = (0, 0, 7.2)^\top$ and $B_{10} = (0, 0, 8.1)^\top$. The equilibrium points are $\chi_4^* = (0, 0, 1.8)$, $\chi_5^* = (0, 0, 2.4)$, $\chi_6^* = (0, 0, 3)$, $\chi_7^* = (0, 0, 3.6)$, $\chi_8^* = (0, 0, 4.2)$, $\chi_9^* = (0, 0, 4.8)$, and $\chi_{10}^* = (0, 0, 5.4)$, respectively.

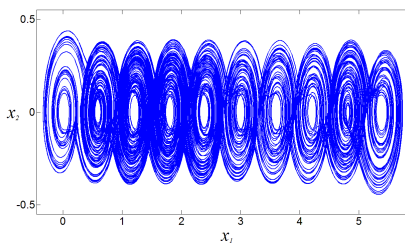


Fig. 2. Ten scrolls chaotic attractor.

III. RESULTS

The synchronization phenomenon is observed between a coupled pair of dissipative and unstable systems with different numbers of scrolls and their detection approach it is through the auxiliary system [5]. Fig. 3.

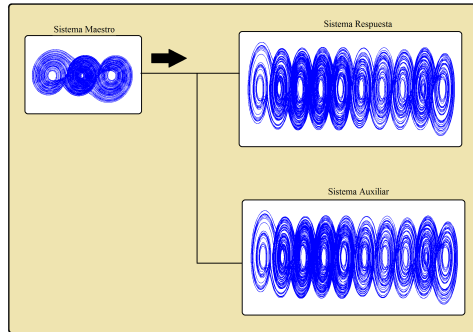


Fig. 3. Form of coupling.

The coupling system is explicitly written as follows:

Master system

$$\begin{aligned}\dot{x}_1^M &= x_2^M, \\ \dot{x}_2^M &= x_3^M, \\ \dot{x}_3^M &= \alpha_{31}x_1^M - \alpha_{32}x_2^M - \alpha_{33}x_3^M + u^M.\end{aligned}\quad (5)$$

Slave system

$$\begin{aligned}\dot{x}_1^R &= x_2^R, \\ \dot{x}_2^R &= x_3^R + C(x_2^M - x_2^R), \\ \dot{x}_3^R &= \alpha_{31}x_1^R - \alpha_{32}x_2^R - \alpha_{33}x_3^R + u^R.\end{aligned}\quad (6)$$

The synchrony between systems with different numbers of scrolls, leads to the preservation of scrolls but in a different position of the slave attractor depending on the initial conditions of the master system. This leads us to mention the following theorem. Observed in Fig. 4.

Theorem Let $G_m = \{S_1^m, S_2^m, \dots, S_{\#S_m}^m\}$ and $G_s = \{S_1^s, S_2^s, \dots, S_{\#S_s}^s\}$ be the sets conformed by the control signals u^m and u^s , respectively. For a given system in the form of (6) presents multistability if $G_m \subset G_s$ and the number of multiple basins of attraction is $\#S_s - \#S_m + 1$.

The slave system has multistability, a large number of scrolls that when connecting to the master system with a smaller number of scrolls, the scrolls are preserved master system.

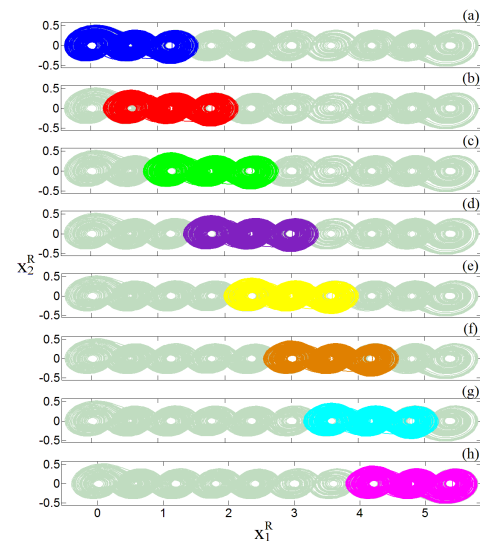


Fig. 4. Multiple chaotic attractors coexist in the plane (x_1, x_2) .

The position of the scrolls appear depending on the initial conditions of the master system, which simulates a control signal which determines the position of the scrolls in the slave system. Fig. 5.

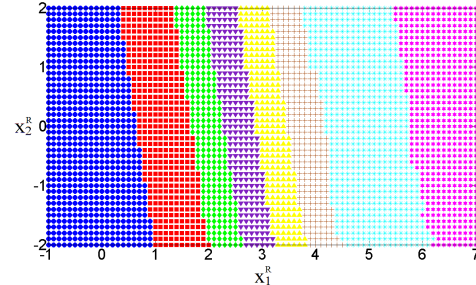


Fig. 5. Eight basins of attraction on to plane (x_1, x_2) , given by the couple system (3) and (4)

IV. CONCLUSION

This paper has evaluated a mechanism for building multi-stable structures generalized in a couple of unidirectionally coupled systems. In particular, the existence of multiple attractors is demonstrated as a result of coupling two systems exhibiting different number of scrolls. Se mostró que el número de scrolls en el sistema maestro se preserva en el espacio de fase del sistema esclavo que tiene un número más grande de scrolls, con ello se observó el fenómeno de multiestabilidad.

ACKNOWLEDGMENT

E.J.L. acknowledge the Colegio Mexiquense A.C. during the realization of this work. The IPICYT for the hospitality during his stay in DMAp-IPICYT.

REFERENCES

- [1] Jiménez-López, E., Salas, J. G., Ontañón-García, L. J., Campos-Cantón, E., and Pisarchik, A. N. *Generalized multistable structure via chaotic synchronization and preservation of scrolls*. Journal of the Franklin Institute, 350(10), 2853–2866, (2013).
- [2] E. Campos-Cantón, R. Femat, J.G. Barajas-Ramirez, and I. Campos-Cantón, *A multivibrator circuit based on chaos generation*, Int. J. Bif. and Chaos, 22, 1250011, (2012).
- [3] D. Angelis, J. E. Ferrell, Jr., and E. D. Sontag, *Detection of multistability, bifurcations, and hysteresis in a large class of biological positive-feedback systems*, PNAS, 101, 1822 – 1827, (2004).
- [4] E. Campos-Cantón, J.G. Barajas-Ramirez, G. Solis-Perales and R. Femat, *Multiscroll Attractors by Switching Systems*, Chaos, **20**, 013116 (2010).
- [5] H. D. I. Abarbanel, N. F. Rulkov, and M. M. Sushchik. *Generalized synchronization of chaos: the auxiliary system approach*. Phys. Rev. E 53, 4528 – 4535, (1996).

The participation ratio as a signature of chaos in an interacting radiation-atoms system

S. Lerma-Hernández
 and B. López-del-Carpio
 Facultad de Física
 Universidad Veracruzana
 Circuito Aguirre Beltrán s/n, Xalapa
 Veracruz, México, C.P. 91000

M. A. Bastarrachea-Magnani,
 J. Chávez-Carlos
 and J. G. Hirsch
 Instituto de Ciencias Nucleares
 Universidad Nacional Autónoma de México
 Apdo. Postal 70-543, México D. F., C.P. 04510

Abstract—Quantum chaos deals with those quantum systems whose classical version shows extreme sensitivity to initial conditions. In the present contribution we report results for a very well known system in quantum optics, the so called Dicke model, which describes a set of two-level atoms interacting with a single mode of the electromagnetic field. The classical version of this model presents chaos for certain values of the interaction strength and large enough energy. A clear correlation between the classical Lyapunov exponent and a quantum measure (the participation ratio of coherent states respect to the Hamiltonian eigenstates) is exhibited for different points in the phase space.

I. INTRODUCTION

Quantum chaos is in the core of a fundamental problem of the quantum theory: the appearance of the classical world from the more fundamental quantum description. Since the beginning of the quantum theory, it was noticed that the discrete energy spectrum of the bound states could be linked to the classical action trough the Einstein-Brillouin-Keller conditions [1]. However these conditions are not applicable to the case of non-integrable classical systems. Furthermore, the classical sensitivity to initial conditions can not be simply extended to the quantum domain because the evolution in quantum mechanics is described by an unitary transformation which, by definition, leaves invariant the internal product of two arbitrary initial states. The connection between the classical and quantum description of certain systems can be established trough the propagator

$$\langle x' | e^{-i\hat{H}t/\hbar} | x \rangle = \int_x^{x'} \mathcal{D}[x(t)] e^{iS(x,x',t)/\hbar},$$

where the Hamiltonian operator is $\hat{H} = \hat{P}^2/(2m) + V(\hat{x})$, and $S(x, x', t) = \int_0^t L(x, \dot{x}, t') dt'$ is the action with $L = mx^2/2 - V(x)$. The symbol $\int_x^{x'} \mathcal{D}[x(t)]$ is a shorthand notation for $\lim_{n \rightarrow \infty} (m/(2\pi i \hbar \tau))^{n/2} \int dx_1 \dots dx_n$, indicating an integration over all the possible trajectories connecting the initial and final points x and x' respectively. The semi-classical approximation is obtained by evaluating the previous integral by means of the stationary phase approximation [2]

$$\langle x' | e^{-i\hat{H}t/\hbar} | x \rangle = \left(\frac{1}{2\pi i \hbar} \right) |D_{xx'}|^{1/2} \exp \left[\frac{i}{\hbar} S_{cl}(x, x', t) \right],$$

where $S_{cl}(x, x', t)$ is the classical action evaluated in the classical trajectory that comes from the minimal action principle $\delta S = 0$, which defines a classical system

$$\frac{d}{dt} \frac{\partial L(x, \dot{x})}{\partial \dot{x}} = \frac{\partial L(x, \dot{x})}{\partial x}.$$

The previous ideas can be extended to more general quantum systems as it is briefly discussed in the following.

A. The Dicke model

The model we study, the Dicke model, describes the interaction between a system of \mathcal{N} two level atoms and a sole bosonic mode of the photonic field [4]. The Hamiltonian has three terms: one associated to the monochromatic quantized radiation field of energy and frequency ω_0 , a second one for the two levels atoms with an energy separation given by ω , and a last one which describes the interaction between them, the strength of this interaction is quantified by γ . With $\hbar = 1$, it reads

$$H_D = \omega a^\dagger a + \omega_0 J_z + \frac{\gamma}{\sqrt{\mathcal{N}}} (a + a^\dagger) (J_+ + J_-). \quad (1)$$

The operators a and a^\dagger annihilate and create photons respectively and close the so called Heisenberg algebra $[a, a^\dagger] = 1$, whereas the operators J_+ and J_- excites and desexcites the atoms and, together J_z , form the algebra of the $SU(2)$ group.

A classical Hamiltonian can be obtained by following the procedure outlined above for the propagator, but using coherent states [3], which are defined as

$$|\alpha\rangle = e^{-|\alpha|^2/2} e^{\alpha a^\dagger} |0\rangle, \quad |z\rangle = \frac{1}{(1+|z|^2)^j} e^{z J_+} |j, -j\rangle. \quad (2)$$

for the bosonic and atomic sector (with $j = \mathcal{N}/2$) respectively. The classical Hamiltonian that is obtained is given by

$$h_{cl}(p, q, \tilde{j}_z, \phi) = \frac{\langle \alpha, z | H_D | \alpha, z \rangle}{j} = \quad (3)$$

$$= \omega_0 \tilde{j}_z + \frac{\omega}{2} (q^2 + p^2) + 2\gamma \sqrt{1 - \tilde{j}_z^2} q \cos \phi. \quad (4)$$

where the canonical classical variables are linked to the parameters of the quantum coherent states trough $\alpha = \sqrt{\frac{i}{2}}(q + ip)$ and $z = \tan(\theta/2)e^{i\phi}$ with $\tilde{j}_z = (j_z/j) = -\cos \theta$ and

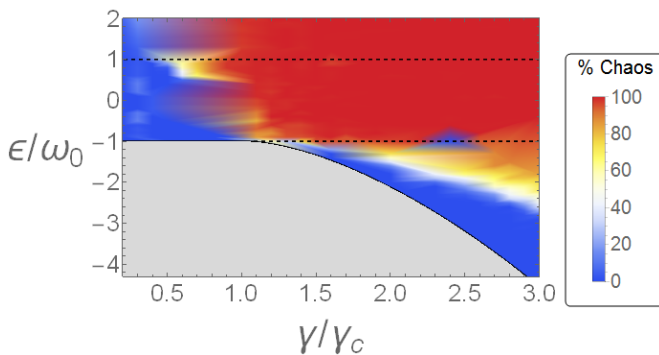


Fig. 1. Percentage of chaos in the classical energy surface as a function of coupling and energy ($\epsilon \equiv E/j$) for a system in resonance $\omega = \omega_o$.

$\phi = \arctan(j_y/j_x)$, where θ and ϕ are spherical angular variables of a classical vector $\vec{j} = (j_x, j_y, j_z)$ with $|\vec{j}| = j$.

B. Classical and quantum results

We perform a comparative study of the previous classical Hamiltonian and its respective quantum version (see [5], [6] for more details). For the classical model we calculate the Poincaré sections and the maximal Lyapunov exponent for different initial conditions, for given parameter values and given energy surfaces. For the same set of Hamiltonian's parameters and the same energy, we study the spread of coherent states in the basis of eigenstates of the Hamiltonian operator using the so called Participation Ratio, which is defined as

$$P_R = \frac{1}{\sum_k |\langle \phi_k | \Psi \rangle|^4}, \quad (5)$$

where $|\phi_k\rangle$ is the basis of eigenstates and $|\Psi\rangle$ the state of interest (coherent states in our study). When $P_R = 1$ it means the state $|\Psi\rangle$ is identical to one of the states of the basis, and it is considered as having maximum localization. On the other hand, if every state of the basis equally contributes to the state, P_R takes its maximum value and is related to maximum delocalization in the given basis.

In Fig. 1 we present a global view of the appearance of chaos in the classical model for the case of resonance $\omega = \omega_o$. The figure shows the phase space percentage, for a given energy, covered by chaotic trajectories. The horizontal axis represents the value of the coupling strength between the field and the atoms. This strength is shown in units of the critical value $\gamma_c = \sqrt{\omega\omega_0}/2$, which signals the transition between the normal phase (where the minimal energy is $E = -\omega_o J$) and the so-called superradiant phase where the minimal energy decreases monotonically as a function of the coupling and the corresponding configuration has a finite number of photons and excited atoms. From the figure is clear that chaos is present for every coupling except in the region close to the non interacting case. Excepting the latter interval, chaos is present for large enough excitation energies. In the region above but close to the critical value γ_c , chaos appears even in the region of low excitation energy. In Fig. 2 we present

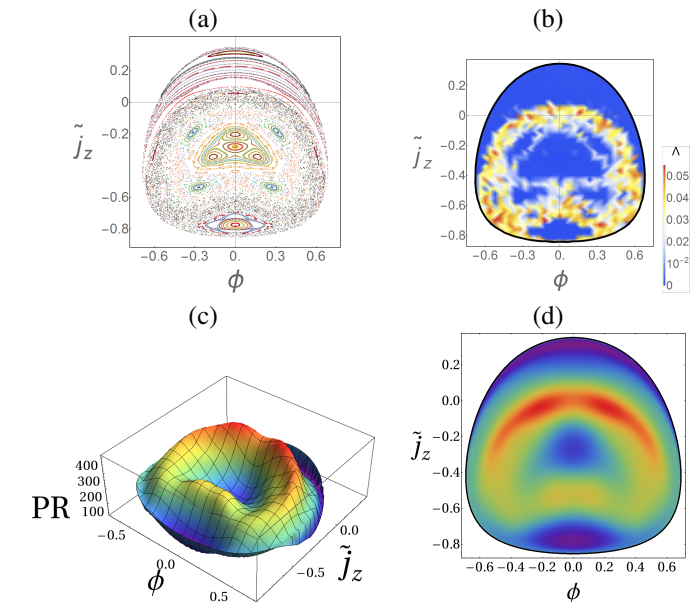


Fig. 2. Classical and quantum results for the same system as previous figure, $\omega = \omega_o = 1$, but for a particular coupling ($\gamma = 2\gamma_c$) and energy ($\bar{E}/(\omega_o J) = -1.4$), with mixed classical phase space. (a) Poincaré sections, (b) Lyapunov exponent for different initial conditions. (c) and (d) Participation Ratio for coherent states with parameters in the same energy surface as the classical results, in 3D and density plots respectively.

results for the particular case of $\gamma = 2\gamma_c$ and for an energy with mixed (regular and chaotic) dynamics. In the top row classical results are shown, Poincaré sections at the left and the corresponding Lyapunov exponents at the right. In the bottom row the Participation Ratio of quantum coherent states with parameters defined in the same energy surface as the classical results is shown in a 3D plot (left) and a density plot (right). A clear correspondence between the classical and quantum results is observed.

II. CONCLUSION

We found a close correspondence between the appearance of chaos in the classical version of the Dicke model and the Participation Ratio of coherent quantum states respect to the basis of Hamiltonian eigenstates. The Participation Ratio of the coherent states has a direct connection with the evolution of the states which, in turn, is determined by the spread of the states in the energy eigenbasis. The Participation Ratio allows to characterize chaos and regularity directly from the quantum theory without resorting to classical definitions.

REFERENCES

- [1] J.B.Keller, *Ann. Phys.* **4** 180, 1958.
- [2] H-J. Stöckmann, *Quantum chaos*, 1st ed. Cambridge, England: Cambridge University Press, 2000.
- [3] M. Stone, K-S. Park and A. Garg, *J. Math. Phys.* **41**, 8025, 2000; A.D. Ribeiro, M.A.M. de Aguiar and A.F.R. de Toledo Piza, *J. Phys. A: Math. Gen.* **39**, 3085, 2006.
- [4] R.H. Dicke, *Phys. Rev.* **93**, 99, 1954.
- [5] M. A. Bastarrachea-Magnani, S. Lerma-Hernández, and J. G. Hirsch, *Phys. Rev. A* **89**, 032102, 2014.
- [6] M. A. Bastarrachea-Magnani, B. López-del-Carpio, J. Chávez-Carlos, S. Lerma-Hernández and J. G. Hirsch, arXiv:1509.05918, 2015.

Polynomial Trajectories To Provoke Chaos and Bifurcations

Jorge A. López-Renteria
 Department of Physics and Mathematics
 Iberoamerican University
 Mexico, D.F., CP 01219
 Email: jalr_82@hotmail.com

Abstract—The aim of this work is to show the use of polynomials trajectories in the design a linear feedback state controls to obtain chaos behavior in piecewise linear control systems as well to make a nonlinear affine system undergoing the Hopf bifurcation. The considered trajectories are rays of polynomials and the Hurwitz connecting-curve.

I. INTRODUCTION

The use of polynomials in the analysis of the solutions behavior of dynamical systems is a very studied topic in different science fields due to they provide the dynamics of a system by mean of their roots. Even there exists another methods for the analysis, for example, Lyapunov functions used to determinate stability [1], it is essential the use of the polynomials to exhibit the spectrum of the system and so the internal dynamics can be determined. Particularly, in control theory there exist a lot of techniques to determinate the stability of a control system that involves the design of a suitable control law to achieve it [3]-[5]. This approach can be addressed to obtain any different and required dynamics like chaotic behavior or bifurcations. Recently, in [2] a polynomial approach has been used to generate a family of multi-scroll attractors in a control linear systems called *unstable dissipative systems* (UDS's), whose description will be given in the next section. With similar ideas, a linear feedback control is designed to make a nonlinear affine system undergoes the Hopf bifurcation and it is controlled as well [7]. This work is based on these results to unify and exhibit the technique of the design of controllers in question. The rest of the manuscript is organized as follows: In section II, the maximal interval of robust dynamics of a rays of polynomials is given and its is implemented in the design of a multi-saturated control that induces and preserves dynamics of chaotic behavior. In section III, the Hurwitz connecting curve of polynomials is used to assign continuously poles in order to provoke and control the Hopf bifurcation.

II. RAYS AND CHAOS

Before anything, the class of systems that undergoes chaotic behavior to deal in this work are the well known unstable dissipative systems, which are defined as follows.

Definition 1 (Campos-Canton *et al.*, 2012 [6]). *Consider the system $\dot{x} = Ax$, where $A \in \mathbb{R}^3$ has eigenvalues λ_i , $i = 1, 2, 3$ such that $\sum_{i=1}^3 \lambda_i < 0$. Then the system is said to be an UDS*

of type I (UDS-I) if one of its eigenvalues is negative real and the other two are complex conjugate with positive real part; and it is said to be of type II (UDS-II) if one of its eigenvalues is positive real and the other two are complex conjugate with negative real part.

A. System Description I

The aim is to design a monoparametric family of 3D-control systems

$$\dot{x} = A(k)x + bu, \quad (1)$$

where $x, b \in \mathbb{R}^3$ and $A(k)$ is a (3×3) -real matrix depending on the parameter $k \in \mathbb{R}$, given by

$$A(k) = \begin{bmatrix} 0 & 1 & 0 \\ 0 & 0 & 1 \\ -A_3(k) & -A_2(k) & -A_1(k) \end{bmatrix}, \quad (2)$$

where $A_l(k) = -a_l - k c_l$, with a_l, c_l given constants. The system will be governed by a switching law

$$u = \begin{cases} u_1 & \text{in } \mathcal{D}_{x_1^*}; \\ \vdots & \\ u_j & \text{in } \mathcal{D}_{x_j^*}; \\ \vdots & \\ u_r & \text{in } \mathcal{D}_{x_r^*}. \end{cases} \quad (3)$$

that generate multi-scroll attractors for $k = 0$, with u_i on a domain $\mathcal{D}_i \subset \mathbb{R}^3$, $i = 1, 2, \dots, r$, with $\cap_{i=1}^r \mathcal{D}_i = \emptyset$ and $\cup_{i=1}^r \mathcal{D}_i = \mathbb{R}^3$. For a specific equilibria set x_1^*, \dots, x_r^* in any convenient place in \mathbb{R}^3 . Thus each x_i^* determines its respective $u_i = B^{-1}A(k)x_i^*$. In resume, the idea is that with the saturated control (3) we can generate multi- scroll attractors for $k = 0$ and then perturb the parameter k to find an interval in which the system (1) keeps its chaotic behavior.

B. The maximal robust dynamics interval

In this section, only the maximal robust dynamical interval will be computed. Every result is given in the general case of \mathbb{R}^n and then they are applied in the case of interest, \mathbb{R}^3 . It is well known that characteristic polynomial of the n -dimensional system (1) is $\mathcal{P}(t, k) = p_0(t) + kp_1(t)$, where $p_0(t) = t^n + a_1t^{n-1} + \dots + a_n$ is the characteristic polynomial for $k = 0$ and $p_1(t) = c_nt^n + c_{n-1}t^{n-1} + \dots + c_1$. If the system is of type UDS-I for $k = 0$, we can perturb the variable k around zero

obtain the maximal UDS-interval (\underline{k}, \bar{k}) . Let \mathbb{C}^- denotes the open left half complex plane, \mathbb{C}^+ is the right half open plane, and $i\mathbb{R}$ the imaginary axis. In order to establish a result for a family of polynomials $\mathcal{P}(t, k) = p_0(t) + kp_1(t)$ for which $p_0(t)$ has n_1 roots in \mathbb{C}^- and $n - n_1$ roots in \mathbb{C}^+ for all k in the maximal robust dynamics interval, (k_{\min}^-, k_{\max}^+) , let us to considerate the following evaluations in the imaginary axis. Namely, it is not hard to see that $p_0(-i\omega) = P(\omega^2) - i\omega Q(\omega^2)$ and $p_1(i\omega) = p(\omega^2) + i\omega q(\omega^2)$, and then $\mathcal{P}(i\omega, k)p_0(-i\omega) = G(\omega) + kF(\omega) + ik\omega H(\omega)$, where

$$\begin{aligned} F(\omega) &= p(\omega^2)P(\omega^2) + \omega^2q(\omega^2)Q(\omega^2), \\ G(\omega) &= P^2(\omega^2) + \omega^2Q^2(\omega^2), \\ H(\omega) &= q(\omega^2)P(\omega^2) - p(\omega^2)Q(\omega^2). \end{aligned}$$

Now, let us to denote as $R(f) = \{\xi \in \mathbb{C} | f(\xi) = 0\}$ to the zeroes set of $f(t)$. Let $R(f)_{\mathbb{R}^+}$ be the set of positive real elements of $R(f)$ and now we define the sets

$$\begin{aligned} K^+ &= \{F(\omega_l) : \omega_l \in R(H)_{\mathbb{R}^+} \cup \{0\}, F(\omega_l) > 0\} \\ K^- &= \{F(\omega_l) : \omega_l \in R(H)_{\mathbb{R}^+} \cup \{0\}, F(\omega_l) < 0\} \end{aligned}$$

Then, with the aforementioned we give the following result that generalizes the maximal stability interval given in [8].

Theorem 1 (Aguirre-Hernandez *et al.*, 2015 [2]). *Consider the polynomial family $\mathcal{P}(t, k) = p_0(t) + kp_1(t)$, where $p_0(t)$ is a n -degree polynomial with n_1 roots in \mathbb{C}^- and $n - n_1$ roots in \mathbb{C}^+ . Suppose the $n > \deg p_1(t)$ and let $F(\omega)$, $G(\omega)$ and $H(\omega)$ be the polynomials defined above. Then $\mathcal{P}(t, k)$ has n_1 roots in \mathbb{C}^- and $n - n_1$ roots in \mathbb{C}^+ for all $k \in (k_{\min}^-, k_{\max}^+)$, where*

$$k_{\min}^- = \max \left\{ -\frac{G(\omega_l)}{F(\omega_l)} : F(\omega_l) \in K^+ \right\} \quad (4)$$

$$k_{\max}^+ = \min \left\{ -\frac{G(\omega_l)}{F(\omega_l)} : F(\omega_l) \in K^- \right\} \quad (5)$$

C. Generation of multi-scroll chaotic systems

In order to generate multi-scroll attractors, additionally to the maximal structural stability interval it is necessary to find the maximal dissipativity interval for the ray of polynomials $\mathcal{P}(t, k)$.

Lemma 1 (Dissipativity Interval). *The sum of the roots of the polynomial family $\mathcal{P}(t, k) = (t^n + a_1t^{n-1} + \dots + a_{n-1}t + a_n) + k(c_1t^{n-1} + \dots + c_{n-1}t + c_n)$ is negative if and only if $k > -\frac{a_1}{c_1}$.*

Finally, the intersection of these both intervals arises the maximal interval of the UDS's and the following theorem is held.

Theorem 2. *If the 3D-control system (1) is an UDS that undergoes chaotic behavior with the saturated control (3) for $k = 0$, then the maximal UDS interval around zero to generate chaos is given by $(\underline{k}, \bar{k}) = K \cap D$, where $K = (k_{\min}^-, k_{\max}^+)$ and $D = \{k \in \mathbb{R} | k > -\frac{a_1}{c_1}\}$.*

The following example illustrates the technique.

Example 1 (See [2]). *Consider the control system (1) with*

$$A(k) = \begin{bmatrix} 0 & 1 & 0 \\ 0 & 0 & 1 \\ -30 & -4 & -1 + \frac{1}{2}k \end{bmatrix} \text{ and } b = \begin{bmatrix} 0.15 \\ 0.3 \\ 0.4 \end{bmatrix}, \quad (6)$$

which eigenvalues set for $k = 0$ is $\{-3, 1 \pm 3i\}$, and then it is UDS-I. Figure 1 shows that the system undergoes a four-scroll attractor generated with the control law

$$u = \begin{cases} 3 & \text{for } 0.375 < x_1; \\ 2 & \text{for } 0.225 \leq x_1 \leq 0.375; \\ 1 & \text{for } 0.075 \leq x_1 \leq 0.225; \\ 0 & \text{for } x_1 \leq 0.075. \end{cases} \quad (7)$$

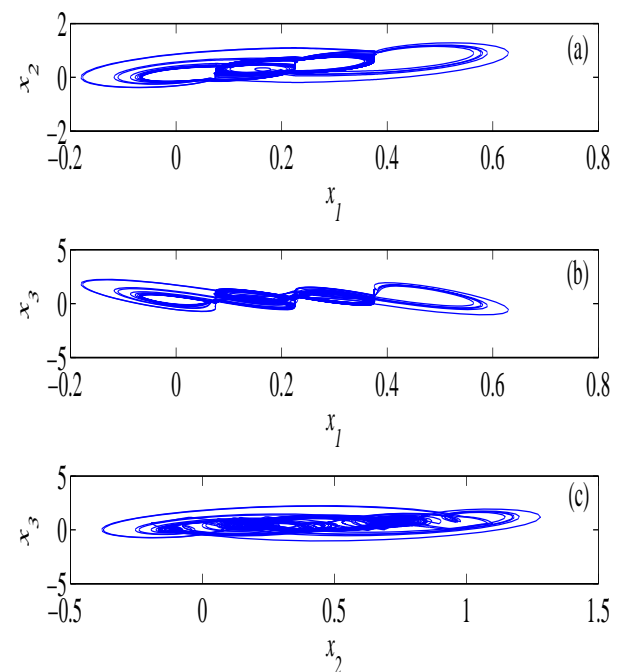


Fig. 1. Projections of the attractor for $k = 0$ onto the planes: (a) (x_1, x_2) ; (b) (x_1, x_3) ; and (c) (x_2, x_3) .

The characteristic polynomial of the open loop system is $\mathcal{P}(t, k) = (t^3 + t^2 + 4t + 30) - kt^2$. Therefore,

$$\begin{aligned} F(\omega) &= \frac{1}{2}\omega^2(30 - \omega^2), \\ G(\omega) &= \omega^6 - 7\omega^4 - 44\omega^2 + 900, \\ H(\omega) &= -\frac{1}{2}\omega^2(4 - \omega^2). \end{aligned}$$

Consequently, the maximum interval of hyperbolicity is described by $k_{\min}^- = -\frac{G(2)}{F(2)} = -\frac{676}{52} = -13$ and $k_{\max}^+ = +\infty$. Now, since $a_1 + kc_1 = 1 - \frac{1}{2}k$, then the dissipativity interval is $S = (-\infty, 2)$. Therefore the maximal UDS-I interval is

$(\underline{k}, \bar{k}) = (-13, 2)$. For $k = -1$, figure 2 shows the projections of the attractor, where

$$b = \begin{bmatrix} 0.3 \\ 0.25 \\ 0.4 \end{bmatrix}$$

and the control signal can be given as follows:

$$u = \begin{cases} 3, & \text{for } 0.75 < x_1; \\ 2, & \text{for } 0.45 < x_1 \leq 0.75; \\ 1, & \text{for } 0.15 < x_1 \leq 0.45; \\ 0, & \text{for } x_1 \leq 0.15. \end{cases}$$

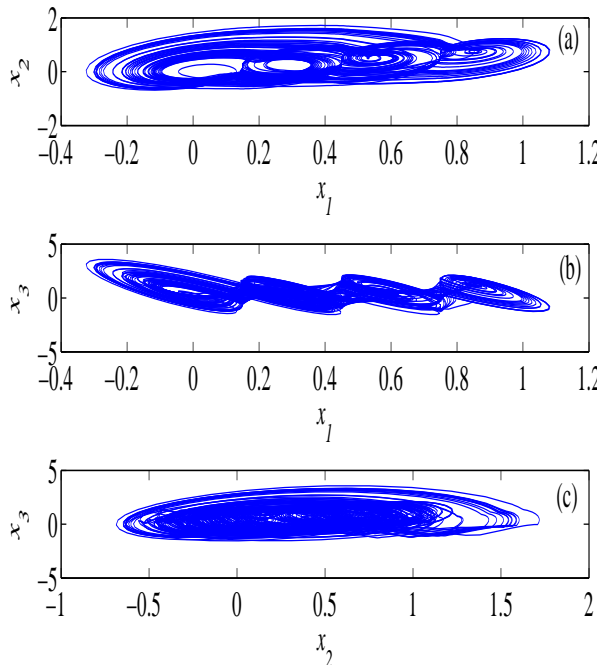


Fig. 2. Projections of the attractor for $k = -1$ onto the planes: (a) (x_1, x_2) ; (b) (x_1, x_3) ; and (c) (x_2, x_3) .

III. THE CONNECTING-CURVE AND THE HOPF BIFURCATION

A. The Hopf bifurcation in the plane

Consider the following non linear system

$$\dot{x} = F(x, \mu) \quad (8)$$

with $x = (x_1, x_2)$, $F = (x, \mu)$ is a smooth vector field and $\mu \in [\epsilon_1, \epsilon_2]$. Suppose that x_0 is an equilibrium point such that $F_x(x_0) = A(\mu)$ has eigenvalues $\lambda_{1,2}(\mu) = \alpha(\mu) \pm \beta(\mu)$. The following two-dimension version theorems of the Hopf bifurcation [1].

Theorem 3. Consider the nonlinear system (8) and suppose that for a suitable value μ_0 the following conditions are satisfied:

- 1) $d = \frac{d\alpha(\mu)}{d\mu}|_{\mu=\mu_0} \neq 0$ (transversality condition),
- 2) $l_1 \neq 0$, (genericity condition),

where l_1 is the first Lyapunov coefficient. Then a unique circle limit bifurcates from the equilibrium x_0 into $\mu > 0$ if $l_1 d < 0$ or $\mu < 0$ if $l_1 d > 0$.

Thus, the equilibrium point x_0 is stable for $\mu < 0$ (resp. $\mu > 0$) and unstable for $\mu > 0$ (resp. $\mu < 0$) if $d > 0$ (resp. $d < 0$) whilst the periodic solutions are unstable (resp. stable) if the equilibrium point is stable (resp. unstable) on the side of μ_0 where the periodic solutions exist. Respect to the first Lyapunov coefficient, if $l_1 < 0$ then the periodic solutions are stable while they are unstable if $l_1 > 0$. There exists an expression to calculate the first Lyapunov coefficient when for that such suitable μ_0 the system has a simple pair of purely imaginary eigenvalues $\lambda_{1,2}(\mu_0) = \pm i\omega_0$, $\omega_0 > 0$.

Theorem 4. Consider the system

$$\dot{x} = Jx + F(x) \quad (9)$$

with $J = \begin{pmatrix} 0 & -\omega_0 \\ \omega_0 & 0 \end{pmatrix}$, $F(x) = \begin{pmatrix} F_1(x) \\ F_2(x) \end{pmatrix}$, $F(x_0) = 0$ and $DF(x_0) = 0$. Then

$$l_1 = \frac{1}{16\omega_0}(R_1 + \omega_0 R_2), \quad (10)$$

where

$$\begin{aligned} R_1 &= F_{1x_1x_2}(F_{1x_1x_1} + F_{1x_2x_2}) - F_{2x_1x_2}(F_{2x_1x_1} + F_{2x_2x_2}) \\ &\quad - F_{1x_1x_1}F_{2x_1x_1} + F_{1x_2x_2}F_{2x_2x_2}, \\ R_2 &= F_{1x_1x_1x_1} + F_{1x_1x_2x_2} + F_{2x_1x_1x_2} + F_{2x_2x_2x_2} \end{aligned}$$

If we are able to control the sign of d and l_1 , then it is said that we are *controlling the Hopf bifurcation*.

B. System Description II

Consider the non linear affine system

$$\dot{x} = f(x) + g(x)u \quad (11)$$

where $x^T = (x_1, x_2) \in \mathbb{R}^2$, $f = (f_1, f_2)^T$ and $g = (g_1, g_2)^T$ are smooth enough vector fields in x , and $u(\cdot)^T$ is the scalar linear state feedback control, which takes values on $I \subset \mathbb{R}$. Let us to consider the following hypothesis:

- H1) $x = x_0$ is a point such that $f(x_0) = 0$ and $g(x_0) = b = \begin{pmatrix} 0 \\ 1 \end{pmatrix}$.
- H2) The Jacobian matrix $A = Df(x)|_{x=x_0}$ has eigenvalues $\lambda, \bar{\lambda} = \rho \pm i\sigma$, $\sigma > 0$, expressed in the form

$$\begin{pmatrix} 0 & 1 \\ -a_1 & -a_2 \end{pmatrix}$$

with characteristic polynomial $p_A(t) = t^2 + a_2t + a_1$, where $a_1 = |\lambda|^2$ and $a_2 = -2Re(\lambda)$.

Without loss of generality we suppose that $x_0 = 0$. By computing the taylors series around the origin of the system (11) we obtain

$$\begin{aligned}\dot{x} &= Ax + F_2(x) + F_3(x) + \dots \\ &\quad + (b + Mx + G_2(x) + \dots)u,\end{aligned}\tag{12}$$

where $M \in \mathbb{R}^{n \times n}$, $F_2(x)$ and $G_2(x)$ are quadratic terms, and $F_3(x)$ is a cubic terms function vector. The objective is to design a *linear feedback control* that provokes Hopf bifurcation in the system (11) and allows to control the sign of d and l_1 .

C. Provoking the Hopf bifurcation

Let $p(t) = t^2 + p_2t + p_1$ and $q(t) = t^2 + q_2t + q_1$ be real polynomials with roots $\zeta, \bar{\zeta} = \alpha \pm i\beta$ and $z, \bar{z} = \gamma \pm i\eta$, respectively, such that $\alpha\gamma < 0$ and $\beta, \eta > 0$. Then the curve

$$p(t, s) = t^2 + \delta_2(s)t + \delta_1(s)\tag{13}$$

where $\delta_2(s) = -2\text{Re}[s(z-\zeta)+\zeta]$ and $\delta_1(s) = |s(z-\zeta)+\zeta|^2$, is a *real curve* with $p(t, 0) = p(t)$ and $p(t, 1) = q(t)$. If $p(t)$ and $q(t)$ are Hurwitz stable, then $p(t, s)$ represents de *Hurwitz connecting-curve* [1]. Next, define the change of variable $\mu = s - s^*$ to get

$$P(t, \mu) = t^2 + \Delta_2(\mu)t + \Delta_1(\mu)\tag{14}$$

where $\Delta_1(\mu) = |(\mu + s^*)(z - \zeta) + \zeta|^2$, $\Delta_2(\mu) = -2\text{Re}[(\mu + s^*)(z - \zeta) + \zeta]$ and s^* is the values for which $P(t, \mu)$ has a pair of pure complex eigenvalues $\pm i\omega_0$. Thus, $P(t, -s^*) = p(t)$, $P(t, s_0 - s^*) = p_A(t)$ for some s_0 , $P(t, 0) = p(t, s^*)$ and $P(t, 1 - s^*) = q(t)$. Now, let us to define the linear feedback $u(x, \mu) = -c(\mu)^T x$, where

$$c(\mu)^T = (\Delta_1(\mu) - a_1, \Delta_2(\mu) - a_2),\tag{15}$$

with $c(0)^T = (\omega_0^2 - a_1, -a_2)$. The closed-loop system (12) becomes on

$$\dot{x} = A_c(\mu)x + \tilde{F}_2(x, \mu) + \tilde{F}_3(x, \mu) + \dots\tag{16}$$

where $\tilde{F}_2(x, \mu) = F_2(x) - Mx c(\mu)^T x$, $\tilde{F}_3(x, \mu) = F_3(x) - G_2(x)c(\mu)^T x$, and

$$A_c(\mu) = \begin{pmatrix} 0 & 1 \\ -\Delta_1(\mu) & -\Delta_2(\mu) \end{pmatrix},$$

with $A_c(0) = \begin{pmatrix} 0 & 1 \\ -\omega_0^2 & 0 \end{pmatrix}$. With the before discussion, the following lemma is arisen.

Lemma 2. *The system (11) in closed-loop with the linear control $u(x, \mu) = -c(\mu)^T$ undergoes the Hopf bifurcation around $\mu = 0$.*

D. Controlling the Hopf bifurcation

The following results allows to prove the control of the Hopf bifurcation (see [7]).

Lemma 3. *Consider the closed loop system (16) with the control $u(x, \mu)$ from lemma 2. Then the crossing velocity $d(\mu) = \frac{d[(\mu+s^*)(\gamma-\alpha+\alpha)]}{d\mu}|_{\mu=0} = \gamma - \alpha \neq 0$.*

This result is based on the fact that $\alpha\gamma < 0$. Moreover, notice that $d(\mu)$ does not depends on β and η , thus one might design both of these parameters such that the straight line $(\mu+s^*)[z - \zeta] + \zeta$, which contains to λ , crosses the imaginary axis by a suitable ω_0 for $-s^* = \mu_0 \in [0, 1]$.

Lemma 4. *The first Lyapunov coefficient, $l_1(\omega_0)$, of the system (16) is given by*

$$l_1(\omega_0) = \frac{1}{16} \left(k_1\omega_0^4 + k_2\omega_0^2 + k_3 + \frac{k_4}{\omega_0^2} \right),$$

for $\omega_0 > 0$, where

$$\begin{aligned}k_1 &= g_{1x_2}(f_{1x_2x_2} + 2a_2g_{1x_2} - 2g_{1x_1}) - 3g_{1x_1x_1} \\k_2 &= 4g_{1x_1}g_{2x_1} - (f_{1x_2x_2} + 2a_2g_{1x_2})(f_{2x_2x_2} + 2a_2g_{2x_2}) \\&\quad + g_{2x_2}(2g_{2x_2} - 2a_1g_{2x_2} - f_{2x_2x_2}) + g_{1x_2}(f_{1x_1x_1} + 2a_1g_{1x_1}) \\&\quad - (f_{1x_1x_2} + 2a_2g_{1x_1} + a_1g_{1x_2})(f_{1x_2x_2} + 2a_2g_{1x_2} - 2g_{1x_1}) \\&\quad + f_{1x_1x_2x_2} + f_{2x_2x_2x_2} + a_2(2g_{1x_1x_2} + 3g_{2x_2x_2}) \\&\quad - 2g_{2x_1x_2} + a_1g_{1x_2x_2} \\k_3 &= -(f_{1x_1x_1} + 2a_1g_{1x_1})(f_{1x_1x_2} + a_2g_{1x_1} + a_1g_{1x_2}) \\&\quad - g_{2x_2}(f_{2x_1x_1} + 2a_1g_{2x_1}) \\&\quad + (f_{2x_2x_2} + 2a_2g_{2x_2} - 2g_{2x_1})(f_{2x_1x_2} + a_2g_{2x_1} + a_1g_{2x_2}) \\&\quad - 2g_{1x_1}(f_{2x_1x_1} + 2a_1g_{2x_1}) - 2g_{2x_1}(f_{1x_1x_1} + 2a_1g_{1x_1}) \\&\quad + f_{1x_1x_1x_1} + f_{2x_1x_1x_2} + a_2g_{2x_1x_1} + a_1(3a_1g_{1x_1x_1} + 2g_{2x_1x_2}) \\k_4 &= (f_{1x_1x_1} + 2a_1g_{1x_1})(f_{2x_1x_1} + 2a_1g_{2x_1}) \\&\quad + (f_{2x_1x_1} + 2a_1g_{2x_1})(f_{2x_1x_2} + a_2g_{2x_1} + a_1g_{2x_2}).\end{aligned}\tag{17}$$

Finally, the main theorem of this section is held.

Theorem 5 (Lopez-Renteria *et al.*, 2015 [7]). *Consider the system (11) under hypothesis H1) and H2). Then the linear control $u(x, \mu) = -c(\mu)^T x$ from lemma 2 is a feedback control that controls the Hopf bifurcation if the polynomial $\tilde{l}(y) = k_1y^3 + k_2y^2 + k_3y + k_4$ has at least one real positive root, where k_j are given by equations in (17).*

As before, the following lemma illustrates the main result.

Example 2 (See [7]). *Consider the system*

$$\begin{pmatrix} \dot{x}_1 \\ \dot{x}_2 \end{pmatrix} = f(x_1, x_2) + g(x_1, x_2)u,\tag{18}$$

with $f(x_1, x_2) = \begin{pmatrix} x_2 \\ \mu_1 + \mu_2x_1 + \xi x_1x_2 \end{pmatrix}$ and $g(x_1, x_2) = \begin{pmatrix} 0 \\ x_1^2 \end{pmatrix}$, $f(p) = 0$ for $p = (-\frac{\mu_1}{\mu_2}, 0)^T$, $\mu_2 \neq 0$. Now, the Jacobian

$$A = Df(p) = \begin{pmatrix} 0 & 1 \\ \mu_2 & -\xi\frac{\mu_1}{\mu_2} \end{pmatrix}$$

has as characteristic polynomial $p_A(t) = t^2 + \xi \frac{\mu_1}{\mu_2} t - \mu_2$, with roots $\lambda_{1,2} = \rho + i\sigma$, with $\rho = -\frac{1}{2}\xi \frac{\mu_1}{\mu_2}$ and $\sigma = \frac{1}{2}\sqrt{\xi^2 \frac{\mu_1^2}{\mu_2^2} + 4\mu_2}$. Thus we shall get complex eigenvalues if $\xi^2 \frac{\mu_1^2}{\mu_2^2} + 4\mu_2 < 0$.

Set the change of coordinates $y = P^{-1}(x-p)$, $y = (y_1, y_2)$, where $P = \frac{\mu_2^2}{\mu_1^2} I$ to leave the system (18) as

$$\begin{aligned} \dot{y} &= \tilde{A}y + \frac{1}{2}y^T \left(\frac{\mu_1^2}{\mu_2^2} D^2 f(p) \right) y \\ &\quad + [\tilde{b} + Dg(p)y + \frac{1}{2}y^T \left(\frac{\mu_1^2}{\mu_2^2} D^2 g(p) \right) y]u, \end{aligned} \quad (19)$$

with $\tilde{A} = A$ and $\tilde{b} = \begin{pmatrix} 0 \\ 1 \end{pmatrix}$. Thus, the system (19) satisfies the hypothesis **H1**) and **H2**). By closing the loop with the control $u(\mu) = -c(\mu)^T y$ the system undergoes the Hopf bifurcation and the first Lyapunov coefficient is given by

$$l_1(\omega_0) = \frac{1}{16} \left(-2\xi \frac{\mu_1^3}{\mu_2^3} - 4\xi \frac{\mu_1^3}{\mu_2^2} \frac{1}{\omega_0^2} \right).$$

Note that $l_1(\bar{\omega}_0) = 0$ for $\bar{\omega}_0 = \pm\sqrt{-2\mu_2}$. We are just interested on $\omega_0 > 0$. Thus, by choosing $\mu_1 = \xi = 1$ and $\mu_2 = -1$. It yields $\lambda = \rho + i\sigma = \frac{1}{2} + i\frac{\sqrt{3}}{2}$ and $\bar{\omega}_0 = \sqrt{2}$. Therefore, $l_1(\omega_0) < 0$ for $0 < \omega_0 < \sqrt{2}$; while $l_1(\omega_0) > 0$ for $\omega_0 > \sqrt{2}$.

STABLE PERIODIC ORBIT. Choose $\omega_0 = \sigma = \frac{\sqrt{3}}{2}$ and since $\alpha = \rho$ and $\gamma = -\rho$, then $\beta = \eta = \sigma$. Therefore, the crossing velocity is $d = -2 < 0$. Thus, the system (18) is written as

$$\dot{x}_1 = x_2 \quad (20)$$

$$\dot{x}_2 = 1 - x_1 + x_1 x_2 + x_1^2 u(x, \mu), \quad (21)$$

where $u(x, \mu) = -[(\mu^2 - \frac{1}{4})(x_1 - 1) + (2\mu + 1)x_2]$. Moreover $l_1(\frac{\sqrt{3}}{2}) = -\frac{5}{24} < 0$, thereby a periodic orbit will appear at the side of $\mu < 0$ (fig. 3).

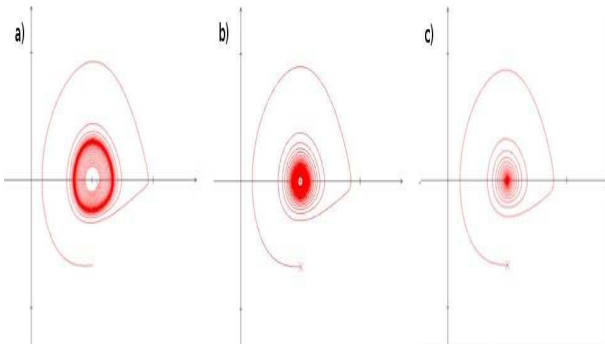


Fig. 3. Appearing of a stable periodic orbit: a) $\mu = -0.02$; b) $\mu = 0$; c) $\mu = 0.02$.

UNSTABLE PERIODIC ORBIT. Now, consider the system

$$\dot{x} = -f(x) - g(x)u, \quad (22)$$

with $f(x)$ and $g(x)$ the vector fields of the system (18). Stable periodic orbits of the system (22) represents unstable periodic

orbits of the system (18). For $\omega_0 = 2$ we claim that the system (18) has an unstable periodic orbit via the system (22). For $\alpha = \rho$ and $\gamma = -\rho$, take $\beta = \sigma = \frac{\sqrt{3}}{2}$ and $\eta = 4 - \frac{\sqrt{3}}{2}$ to obtain the feedback $u(x, \mu) = -[(\mu^2 + (4 - \sqrt{3})\mu + 2)^2 - 1](x_1 - 1) + (2\mu + 1)x_2]$. Moreover $l_1(\omega_0) = l_1(2) = \frac{1}{16} > 0$, then there must emerge a stable periodic orbit of the system (22) at the side $\mu > 0$. This stable orbit (fig. 4) represents an unstable orbit of the system (18).

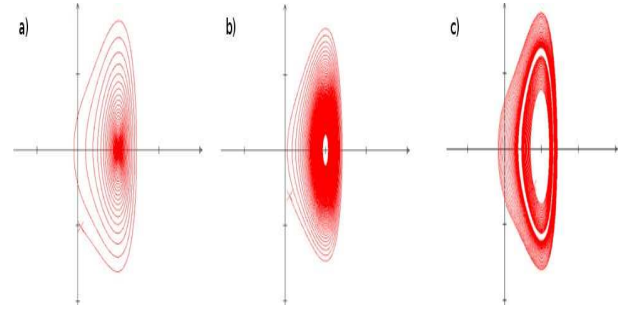


Fig. 4. Appearing of an unstable periodic orbit: a) $\mu = -0.04$; b) $\mu = 0$; c) $\mu = 0.01$.

IV. CONCLUSION

Techniques involving polynomial families have been given in order to obtain chaotic behavior as well make a non-linear system undergoing the Hopf bifurcation from a control point of view. As it is shown, these techniques of control design can be extended and unified to obtain any desired dynamics.

ACKNOWLEDGMENT

Author wants to thank to CONACYT by the postdoctoral grant number 290941-UIA.

REFERENCES

- [1] Kuznetsov, Yuri A.: Elements of Applied Bifurcation Theory. Springer-Verlag, New York, N.Y. (2004)
- [2] Aguirre-Hernández, B., Campos-Cantón, E., López-Rentería, J.A., Díaz González, E.C.: A polynomial approach for generating a monoparametric family of chaotic attractors via switched linear systems. Chaos, Solitons & Fractals. 71, 100–106 (2015)
- [3] Aguirre, B., Ibarra, B., Suárez, R.: Sufficient algebraic conditions for stability of cones of polynomials. Systems & Control Letters. 46, 255–263 (2002)
- [4] Aguirre, B., Suárez, R.: Algebraic test for the Hurwitz stability of a given segment of polynomials. Boletín de la Sociedad Matemática Mexicana. 3(12), 261–275 (2006)
- [5] Bhattacharyya, S.P., Chapellat, H., Keel, L.H.: Robust control: The parametric approach. Prentice Hall (1995)
- [6] Campos-Cantón, E., Femat, R., Chen G.: Attractors generated from switching unstable dissipative systems, Chaos. 22, 033121 (2012). doi: 10.1063/1.4742338
- [7] López-Rentería, J.A., Aguirre-Hernández, B., Verdúzco, F.: Control of the Hopf bifurcation by a linear feedback control. International Journal of Bifurcation and Chaos (2015). doi:10.1142/S0218127415500066
- [8] López-Rentería, J.A., Aguirre-Hernández, B., Verdúzco F.: The Boundary Crossing Theorem and the Maximal Stability Interval. Mathematical Problems in Engineering (2011). doi:10.1155/2011/123403.
- [9] López-Rentería, J.A., Aguirre-Hernández, B., Verdúzco F.: On Hurwitz and Schur Connecting-Curves and Dense Trajectories. AIP Conf. Proc. (2011). doi:10.1063/1.3663511.

Electronic Implementation of Chaotic Systems

J.M. Muñoz-Pacheco

Facultad de Ciencias de la Electrónica,
 Benemérita Universidad Autónoma de Puebla, Puebla, MEXICO
 *Email: jesusm.pacheco@correo.buap.mx

Abstract—In this paper the nonlinear effects in the electronic design of a simple chaos generator are analyzed. A Verilog-A model emulating a nonlinear capacitor is used. The nonlinear model of capacitor is based on a varactor, which includes the charge-dependence with the voltage. By using the H-Spice simulator, the sensitivity of the chaos generation in the simple chaotic oscillator as a function of the varactor is studied.

Index Terms—Chaos, Verilog-A, Nonlinear Capacitor.

I. INTRODUCTION

From circuit theory point of view, any mixed-signal and analog circuit block containing semiconductor devices is nonlinear. Nonlinear circuits can evolve in a chaotic regime. In the last two decades, circuit implementation of several chaotic systems has been of increasing interest, specially by their applications in engineering [1]-[5]. A tendency is to design chaotic oscillators with a reduced form factor, i.e., the number of circuit elements is minimized. Piper and Sprott [2] proposed a simple chaotic circuit composed by four resistors, three capacitors and two opamps only.

It is well known that chaotic behavior is extremely sensitive to small variations of its initial conditions and parameters. The former conducts to multiple trajectories in time domain, but all converge to the same chaotic attractor in phase space domain. The latter can lead to different dynamical behaviors in both domains or even to lose chaotic behavior [3]-[5]. In literature, the designs of chaotic oscillators are classified as custom-made designs due to the system's parameters were tuned for a specific application, and any deviation of these, has important issues such as multiple re-design cycles or to cancell the chaotic regime [1]-[5]. In this manner, it is mandatory to analize about the tolerances that may cause fault conditions in chaotic oscillators.

This work presents a tolerance analysis of the system's parameters in the chaotic oscillator given in [2]. Verilog-A is applied to model the nonlinear analog behaviors focused in the second order effects of capacitors that incorporates a nonlinear model based on a varactor. In this manner, a voltage swept to find the tolerances for the chaotic oscillator as a funtion of the maximun capacitance change from nominal and the voltage change for maximum capacitance is performed by using H-SPICE circuit simulator.

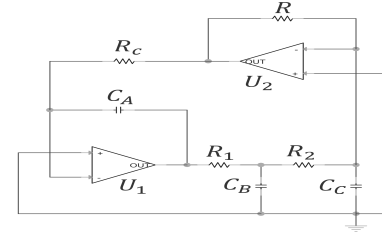


Figure 1. Opamp-based circuit synthesis of (1).

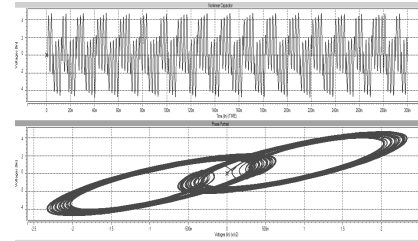


Figure 2. Transient response and two-scroll chaotic attractor of (1).

II. AN SPROTT'S CHAOTIC OSCILLATOR

Piper and Sprott proposed a simple chaotic oscillator given as follows [2]:

$$\begin{aligned}\dot{x} &= y, \\ \dot{y} &= z, \\ \dot{z} &= -Cx - By - Az + C\text{sgn}(x).\end{aligned}\quad (1)$$

System (1) can be considered as a piecewise linear system with three linear regions. The function *signum*, in the inner region, connects the two outer regions by

$$\text{sgn}(x) - x \approx x/\epsilon, \quad |x| < \epsilon. \quad (2)$$

Therefore, chaotic system in (1) is rewritten as

$$\begin{aligned}\dot{x} &= y, \\ \dot{y} &= z, \\ \dot{z} &= (C/\epsilon)x - By - Az.\end{aligned}\quad (3)$$

The resulting electronic circuit is shown in Fig. 1 [2]. One active integrator and a passive second order integrator are used in this reduced circuit contrary to only active integrators. By setting $R_1 = R_2 = 47\text{k}\Omega$, $R \approx 28\text{k}\Omega$, $R_c = 1\text{M}\Omega$, $C_A = 1\text{nF}$, $C_B = 10\text{nF}$, $C_C = 20\text{nF}$, it is obtained the chaotic attractor shown in Fig. 2. From circuit design point of view, A , B , and C depend on the linear passive elements only.

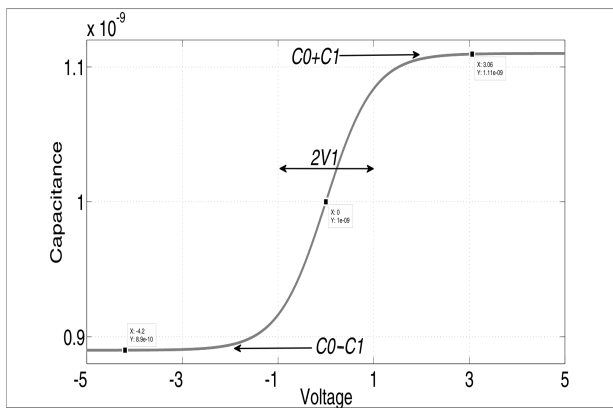


Figure 3. Capacitance exhibited by the capacitor C_A of Fig. 1 under the nonlinear capacitance C_1 .

III. SECOND ORDER EFFECTS OF CAPACITORS

Any deviation of the system's parameters of chaotic oscillators can lead to different dynamical behaviors such as, limit cycle, fixed point, n -period attractor and chaotic attractor, for instance. At system level, the parameters values depend on the rounding error of the numerical integration algorithm and host computer. Nevertheless, at circuit level, second order effects of circuit elements can modify that value.

A. Maximum capacitance change from nominal

This case focus on determining the interval where the chaotic behavior remains unaltered under variations of the nominal capacitances C_A , C_B and C_C . The effect of this nonlinear capacitance is to add an offset in the curve of capacitance as shown in Fig. 3.

The results are summarized in Table I. As a result, it is observed that C_A and C_B are the dominant capacitors for the chaotic behavior of the chaotic oscillator in Fig. 1. Those capacitors only can be varied in 10% from its nominal value. Whereas C_C admits variations up to 35% from its nominal value. A circuit designer could relax the design criteria for this integrator.

B. Voltage change for maximum capacitance

On the other hand, a second case is related to the changes in the nonlinear voltage V_1 . The effect of this nonlinear voltage is to increase or reduce the slope of the curve of the capacitance as shown in Fig. 4. From Table I, V_{1min} and V_{1max} are the minimum and maximum nonlinear voltages respectively. It is observed that V_{1min} is the dominant voltage, i.e., when the slope increases the chaotic behavior disappears. Otherwise, V_{1max} has no influences in the chaotic behavior as expected

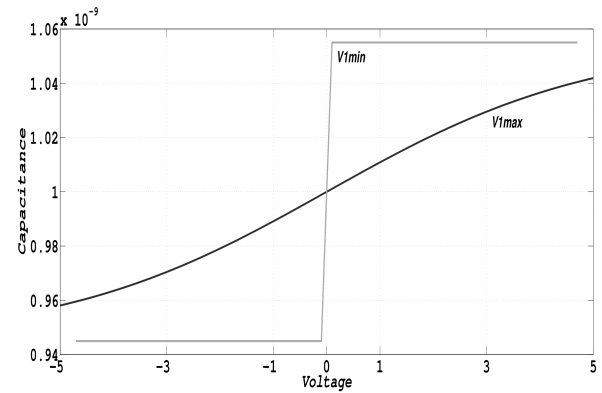


Figure 4. Capacitance exhibited by the capacitor C_A of Fig. 1 under the nonlinear voltage V_1 .

since the slope is minimum and the nonlinear model is similar to a linear capacitor. Furthermore, contrary to previous case, C_C is the dominant capacitor.

IV. CONCLUSIONS

The fault conditions of a simple chaotic system reported in [2] has been determined by using a varactor. In particular, the maximum capacitance change from nominal and the voltage change for maximum capacitance have been analyzed. Those results are crucial to known the fault conditions as a function of the tolerances of the passive elements. Note that for values outside the tolerances provided in Table I, the chaotic circuit does not generate a chaotic attractor. This paper could open new topics about sensitivity analysis and design verification.

ACKNOWLEDGMENT

This scientific research has been partially supported by VIEP-BUAP through “2015 VIEP projects”

REFERENCES

- [1] L. Jinhu and G. Chen, *Generating multiscroll chaotic attractors: theories, methods and applications*, International Journal of Bifurcation and Chaos, 2006.
- [2] J. R. Piper and J. C. Sprott, *Simple autonomous chaotic circuits*, Circuits and Systems II: Express Briefs, IEEE Transactions on, 2010.
- [3] S. Faraji, M.S. Tavazoei, *The effect of fractionality nature in differences between computer simulation and experimental results of a chaotic circuit*, Central European Journal of Physics, Vol. 11, No. 6, pp. 836-844, 2013.
- [4] C. Sánchez-López, et al., *On the trade-off between the number of scrolls and the operating frequency of the chaotic attractors*, IEEE International Symposium on Circuits and Systems, pp. 2950-2953, 2011.
- [5] J.M. Muñoz-Pacheco, et al., *Frequency limitations in generating multi-scroll chaotic attractors using CFOAs*, International Journal of Electronics, Vol. 101, No. 11, pp. 1559-1569, 2014.

Capacitor	C_0	C_1	V_{1min}	V_{1max}
C_A	1nF	110pF	6.7mV	5V
C_B	10nF	1nF	3.3mV	5V
C_C	20nF	7nF	200mV	5V

Table I

MAXIMUM TOLERANCES FOR CAPACITORS AS A FUNCTION OF C_1 AND V_1 .

Bio-inspired chaotic systems and their application

L.J. Ontañón-García
 Coordinación Académica Región Altiplano Oeste
 Universidad Autónoma de San Luis Potosí
 Salinas de Hidalgo, San Luis Potosí, México
 Email: luis.ontanon@uaslp.mx
 Telephone: +52(496) 963-0446

Abstract—The properties of chaotic systems can be widely extended to multiple applications in science, for example in the study of biological systems in nature. Such systems are characterized for their rich and complex behavior which is often confused or forced to be periodic to ease their study. For example the bio-inspired dynamical systems which represent the behavior of some difficult to reproduce biological systems, as the neurons and cells in the body. If coupling methods are adjusted to this type of systems in order to synchronize them, then they can be further implemented on almost any area of science for similar engineering purposes.

I. INTRODUCTION

Since the mid 21 century the study of biological systems has become a commonly recurrent area. Scientists from multiple disciplines have began to focus efforts in the development and characterization of different biological phenomena. The motivations are several although the primordial idea is to have a summarized mathematical model that describes the behavior of difficult to reproduce situations in nature. In this way such models take the conceptualization and experimentation of different new techniques at the reach of more hands in order to attend difficult problems in humanity. For example, in the treatment and prevention of different worldwide diseases such as the AIDS virus, the diabetes mellitus, several cardiac diseases as arrhythmias or heart attacks [1], [2].

II. MATHEMATICAL MODELS OF BIO-INSPIRED SYSTEMS

The boom of the study of biological systems through mathematical dynamical systems emerged after the Hodgkin-Huxley model of the axon of the giant squid [3], which was developed using a voltage-clamp technique to measure the current and membrane potential of the axon. After this two important models were developed, first in the simplification designed by FitzHugh [4] of the Hodgkin-Huxley model. And secondly the Hindmarsh-Rose model [5], which not only described the behavior of the neuron but also the interaction with some parameters that allow different behaviors as their values change, such as periodic and continuous spiking activity which has also been reported experimentally in ex vivo neurons [6]. Due to their easy implementation this mathematical models of the neuron worked as a new tendency in the study of several biological systems.

For example the behavior of the beta cells located in the pancreatic area. This cells are responsible for the releasing of the insulin hormone to the blood stream in the glucose

homeostasis. One model that describes this behavior properly is the one developed by Pernarowski [7], in which one single beta cell located in some cluster is represented by a three state differential equation. Their solution over time can be appreciated in Figure 1. The state u represents the membrane potential, ω a channel activation for the voltage-gated potassium channel, and c the concentrations of calcium which regulates the Bursting Electrical Activity (BEA) that the cell presents.

One of the main features of this model is that it can represent three commonly experimentally observed behaviors of the beta cell by the variation of their parameters similar as the Hindmarsh-Rose model. The behaviors are: an active phase, inactive phase and continuous spiking as described in [8]. The later two are associated with not operational behaviors that can be the result of the isolation of the cells from the cluster as Smolen et al explained in their work [9].

A. Synchronization

This comes out as a major result in biological systems, since the couplings among the clusters of cells can lead to synchronization and therefore the forcing of inactive cells to behave as active cells in the insulin production and secretion [8]. Beta cells are known to be arranged in clusters in the Langerhans islets coupling between themselves in a bidirectional way, as it can be appreciated in the illustration of the Figure 2. Each cell connects via gap junctions by the secretion of different chemical substances or by electric impulses generated by the membrane potential in the closest neighbors. In order to generate a functional synchronization algorithm one can take

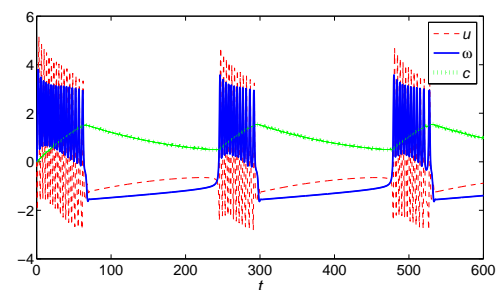


Fig. 1. Time series of the states of the mathematical model of the beta cell [7].

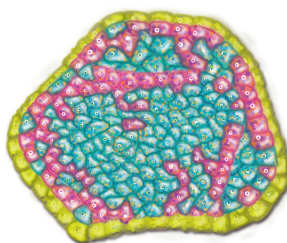


Fig. 2. Langerhans islet illustration depicting the clusters of beta cells in blue.

advantage of the Poincaré planes in order to detect specific behaviors in the cells. An example of this is depicted in Figure 3, where a Poincaré plane (marked in blue dash line) is being located in order to detect the change of the membrane potential from negative to positive values in a single active beta cell. The information marked in red asterisks gives us precise time events from which forcing signals can be generated in order to couple two or more inactive cells to synchronize with an active cell.

This concept of synchronization techniques that have been applied to dynamical systems considering different forms of couplings, can be extended to several applications in biology, such as the integrate and fire behavior in the neurons which describe brief periods of synchronization among the neurons [10]. Or even different type of systems in other areas of science, systems which in general present difficult to analyze behaviors as the chaotic systems present.

B. Chaotic dynamics in bio-inspired systems

Another important characteristic of biological systems is their complex behavior observed in experimental data. The beta cell is a clear example of this since its experimental behavior is far from being periodic presenting a completely chaotic membrane potential [11]. Although there have been some reports on which chaotic behaviors can be obtained from the mathematical models by the variation of some parameters, this models haven't represent totally the natural chaotic behavior of biological systems.

III. CONCLUSION

Precise mathematical models of a bio-inspired system are important from different points of view. First, to develop mathematical models that resemble more closely to the real biological systems in nature. After this models scientist can develop methods and techniques that help biologist with a costless analysis in the study of diseases as the diabetes, epilepsy or cardiac failure. Due to the complexity of bio-inspired systems, the synchronization analysis that result from this type of systems will be helpful even in some areas of science in which the coupling may appear impossible due to the complexity of the systems, for example the ones with nonlinear dynamics and chaotic behavior. Or even in greater number of systems as in the network synchronization in neural

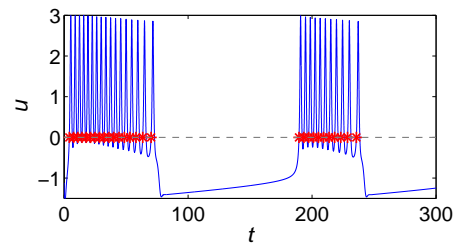


Fig. 3. Poincaré plane detecting the crossing events of the membrane potential of the model of a beta cell.

networks. Finally, since bio-inspired dynamical systems can be represented by electronic implementations with analog devices(for example the Op-Amp), this could result in a more feasible manner to probe the methods and techniques which involve this systems in a more real and tangible way [12].

ACKNOWLEDGMENT

L.J.O.G. acknowledges the financial support through the following projects PRODEP/DSA/103.5/15/6988, and C15-FAI-04-80.80. Also to G.D. Mariana Olvera Astorga for the illustration of the Langerhans islet.

REFERENCES

- [1] Haefer, J. W., *Modeling Biological Systems: Principles and Applications*, Springer Science & Business Media. 2005.
- [2] Bellouquid, A., & Delitala, M., *Mathematical Modeling of Complex Biological Systems*. Birkhäuser Boston. 2006.
- [3] Hodgkin, A. L. & Huxley, A. F., *The dual effect of membrane potential on sodium conductance in the giant axon of Loligo*. Journal of Physiology, volume 116, pages 497-506, 1952.
- [4] FitzHugh, R., *Impulses and physiological states in theoretical models of nerve membrane*. Biophysical Journal, volume 1, pages 445–466, 1961.
- [5] Hindmarsh, J. L. & Rose, R. M., *A model of neuronal bursting using three coupled first order differential equations*. Proceedings of the Royal Society of London B: Biological Sciences, volume 221.1222, pp. 87–102. 1984.
- [6] Gerstner, W., & Kistler, W. M., *Spiking neuron models: Single neurons, populations, plasticity*. Cambridge university press. 2002.
- [7] Pernarowski, M., *Fast and slow subsystems for a continuum model of bursting activity in the pancreatic islet*. SIAM J. Appl. Math., volume 58, pages 1667 - 1687, 1998.
- [8] Ontañón-García, L. J., & Campos-Cantón, E., *Discrete Coupling and Synchronization in the Insulin Release in the Mathematical Model of the Cells*. Discrete dynamics in Nature and Society, 2013.
- [9] Smolen, P., Rinzel, J., & Sherman, A., *Why pancreatic islets burst but single beta cells do not. The heterogeneity hypothesis*. Biophysical journal, 64(6), pp. 1668. 1993.
- [10] Brunel, N., & Hakim, V. *Fast global oscillations in networks of integrate-and-fire neurons with low firing rates*. Neural computation, 11(7), 1621-1671. 1999.
- [11] Sherman, A., Rinzel, J., & Keizer, J., *Emergence of organized bursting in clusters of pancreatic beta-cells by channel sharing*. Biophysical journal, 54(3), 411. 1988.
- [12] Ontañón-García. L.J, Campos-Cantón, E. & Campos-Cantón, I., *Electronic implementation of a pancreatic beta cell*. Memorias del XVI Congreso Latinoamericano de Control Automático, CLCA 2014, Octubre 14-17, 2014. Cancún, Quintana Roo, México.

Simulation model of renal arterial tree growth in 3D

Francisco C. Ordaz-Salazar

Universidad Politécnica de

San Luis Potosí,

Dpto. Ingeniería en Telemática

San Luis Potosí, S.L.P., México 78360

Email: francisco.ordaz@upsdp.edu.mx

Ricardo Femat

Instituto Potosino de Investigación

Científica y Tecnológica

División de Matemáticas Aplicadas,

San Luis Potosí, S.L.P., México, 78216

Email: rfem@ipicyt.edu.mx

Aurora Espinoza-Valdez

Universidad de Guadalajara

Dpto. Ciencias Computacionales

Guadalajara, México,

Email: aurora.espinoza@cucei.udg.mx

Abstract—The kidney is a complex organ due to its anatomical structure and physiology. The model that it is considered is focus on the anatomical structure of renal arterial tree. There are two facts that are the motivation of this work. The first is that it is known that some variations in the anatomical structure are related to some congenital anomalies and diseases, the second is related to an actual trend which refers to regeneration of biological organs. The identification of congenital anomalies, diseases and the regenerative therapeutic interventions will draw on the basic understanding of normal embryonic developmental of the kidney and its final anatomical structure. In previous works we proposed a renal vascular branching model based on angiogenesis and its two processes of growth, sprouting and splitting. With this model it was obtained some characteristics that were compared with characteristics of real kidney, like fractal dimension and length of branches, finally this model was drawn in 2D. The propose is to get a 3D model and consider another characteristics like thickness of the vessels. In this workshop we present some advances in that direction.

I. INTRODUCTION

The kidney is vital for life because is in charge of many functions: excretory functions, modulates fluid volume, blood pressure, red cell count and bone density, thereby acting as a central regulator of homeostasis. The normal kidney morphogenesis is crucial for the interpretation of congenital anomaly and diseases. In humans, nephron formation is a fetal event with final nephron number set before birth. It exists evidence that humans after birth do not have capacity to form new nephrons and a clear inverse relationship between nephron number and renal disease [1].

Development of vascular tree is programmed genetically and controlled by local determinants [2]. In the development of vascular tree intervene two mechanisms, vasculogenesis and angiogenesis. The initial process in the vascular growth is related to vasculogenesis. The formation of new blood vessels from pre-existing vessels is related to angiogenesis. Angiogenesis has two processes of growth, sprouting and splitting [3].

II. THE MODEL

The model of renal branching that was proposed by Aurora Espinoza et.al. [3] is based on angiogenesis. As mentioned earlier, angiogenesis has two processes of growth, sprouting and splitting. In the process of sprouting angiogenesis endothelial cells activate and branch out from a existing vessel. In

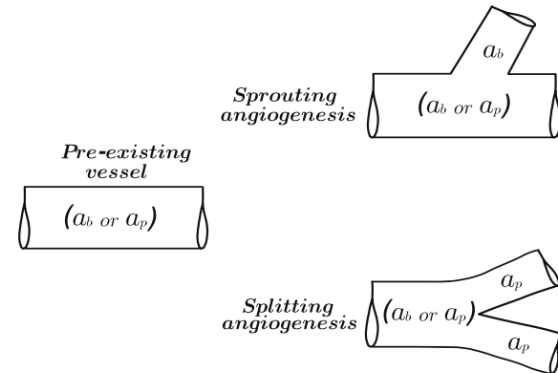


Fig. 1. Above sprouting angiogenesis and below splitting angiogenesis; taken from [3]

the process of splitting angiogenesis we get two new vessels by the division of an existing blood vessel. The processes sprouting and splitting angiogenesis generates a branching tree structure [3]. The Figure 1 shows these processes which were explained in [3]. For modeling purposes it is considered two types of branching growth, sprouting angiogenesis a_b and splitting angiogenesis a_p .

The proposed model of the renal arterial tree is represented by a mathematical binary graph in which every point of growth is a node and the edge is the segment of vessel which are labeled with its physical properties like type of branching growth, coefficient growth factors C_{gf} and thickness [3]. In the case of sprouting angiogenesis exists documentation about the dependence of length and thickness vessels of C_{gf} [4] and for experimental data consider [5]. The idea is that based on these local properties, local rules and stochastic process generates every level of branching in the binary tree. The model consider nine levels of the binary tree according to the levels reported in a renal arterial tree.

The function to get length of vessels when consider sprouting angiogenesis, according to [4] is:

$$l_e = 0.00878C_{gf}^3 - 0.51326C_{gf}^2 + 8.52128C_{gf} + 81.12064 \quad (1)$$

this equation is a function of l_e vs. C_{gf} , where l_e is a dimensionless length value. According to experimental data obtained by [5] and based on equation 1 Nordsletten et.al

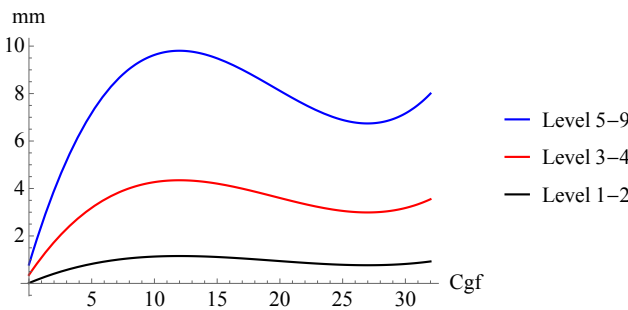


Fig. 2. Length of the new vessel formed by sprouting angiogenesis according to level of branch based on experimental data [5].

derived the next functions for different levels of branches. For levels 1 and 2 the length is between [0.793 mm, 10.306 mm] modeled by:

$$l = 0.207078952l_e - 16.00545171, \quad (2)$$

for level 3 and 4 the length is between [0.357 mm, 4.569 mm]:

$$l = 0.091686802l_e - 7.08072507, \quad (3)$$

and for levels from 5 to 9 the length is between [0.014 mm, 1.217 mm]:

$$l = 0.0261869l_e - 2.110307516, \quad (4)$$

In the same way that length was derived some functions for diameter according to different levels of branch and C_{gf} value are defined. The function to get diameter of vessels when consider sprouting angiogenesis, according to [3] is for C_{gf} ≤ 15:

$$d_e = 0.0050715C_{gf}^2 + 0.0641459C_{gf} + 3.9232 \quad (5)$$

otherwise:

$$d_e = 0.008C_{gf}^2 - 0.46C_{gf} + 11.06 \quad (6)$$

and according to levels by [3] we get the next functions that shows in figure 3. For level 1 and 2 and C_{gf} ≤ 15

$$d = (21.274d_e + 81.004)0.001, \quad (7)$$

otherwise:

$$d = (-37.294d_e + 341.983)0.001, \quad (8)$$

For levels 3 and 4 and C_{gf} ≤ 15

$$d = (16.367d_e + 11.573)0.001, \quad (9)$$

otherwise:

$$d = (-28.692d_e + 212.36)0.001, \quad (10)$$

For levels 5 to 9 C_{gf} ≤ 15

$$d = (10.4455d_e - 8.9097)0.001, \quad (11)$$

otherwise:

$$d = (-18.311d_e + 119.232)0.001. \quad (12)$$

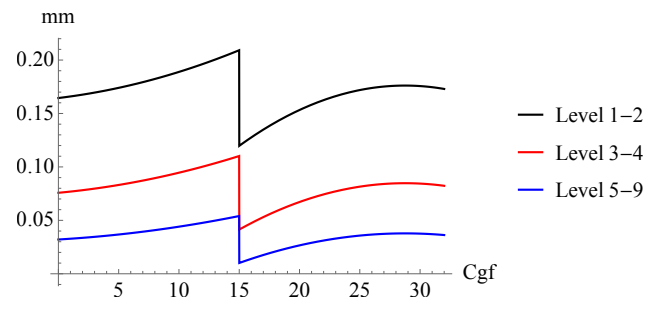


Fig. 3. Width of the new vessel formed by sprouting angiogenesis according to level of branch based on experimental data [5].

A. Algorithm

The algorithm is defined in this way [3].

- 1) The type of branching growth a_b or a_p is determined in a stochastic process. This process requires to defines the probability of a_b , P_{ab} and its complement the probability of a_p , P_{ap} . The selection of type of branching growth en every step is random in function of these probabilities.
- 2) In the same way the value C_{fg} is determined in every step by function of distribution of uniform probabilities between the interval [0, 35] ng/mL.
- 3) The number of levels of branches is 9; then the number of branches is 2⁹.
- 4) If the development of a new branch is a_b then:
 - a) C_{fg} is generated according to step 2. Then l_e is obtained by equation 1 and d_e by equation 5 or 6.
 - b) l is obtained by equation 2, 3 or 4 according to level of branching.
 - c) d is obtained by corresponding equation from 7 to 12. This is a new part of the algorithm considered in [3].
 - d) verify that the diameter of new vessel is minor than its parent vessel
 - e) the diameter of the other vessel is equal to its parent vessel
 - f) the angle of sprouting vessel is in the interval +, − [60°, 80°]
- 5) If the development of a new branch is a_p then:
 - a) The length of the new vessels are generated with a reduction factor of the parent vessel's length
 - b) The diameter of new vessel is the half of the parent vessel
 - c) The angle between the new vessels is 75°
- 6) Repeat these steps until get 9 levels of branching.

III. PREVIOUS RESULTS

In the first simulation consider only the length and construct trees in 2D. Some examples of trees with different probabilities of P_{ab} , P_{ap} are shown in figure 4. Another result is the comparative of the mean of 5000 trees generated and the experimental results by Nordsletten, this result is shown in figure 5.

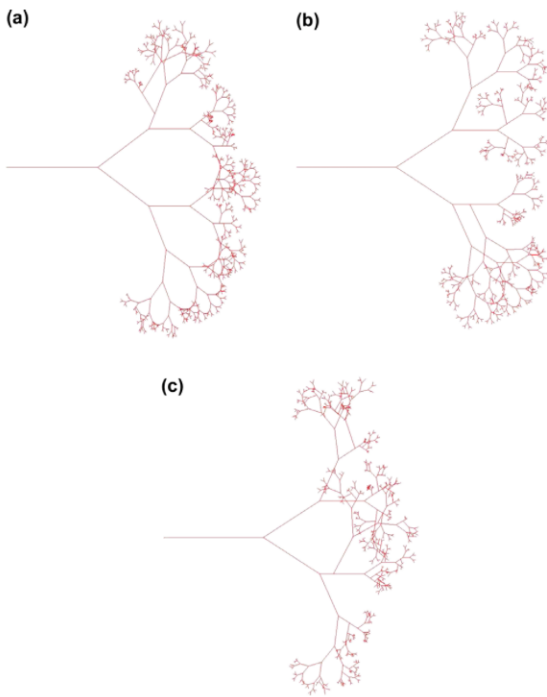


Fig. 4. Examples generated with probabilities of $P_{ab} = 0.2, 0.3, 0.5$ respectively for a), b) and c); taken from [3]

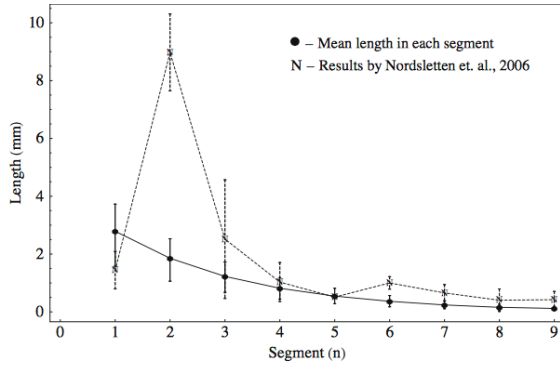


Fig. 5. Comparisons with the mean of 5000 trees generated an the experimental results by Nordsletten ; taken from [3]

IV. SIMULATION IN 3D

In the 3D model we consider the diameter of the vessels and the vessels are considered like vectors in 3D. For simulate the model it was selected the Mathematica® Software by Wolfram company, because is a high level language and consider the paradigm of functional programming. These characteristics have the advantage that the language contain many designed functions and the paradigm of programming permit construct complicated programs with short codes.

The first step in the design of simulation is construct the principal functions that generate the tree. The principal functions are types of growth. Then for splitting angiogenesis a_p its was defined a functions in which the parameters are the factor of reduction for new vessels (F_p), the angle between new

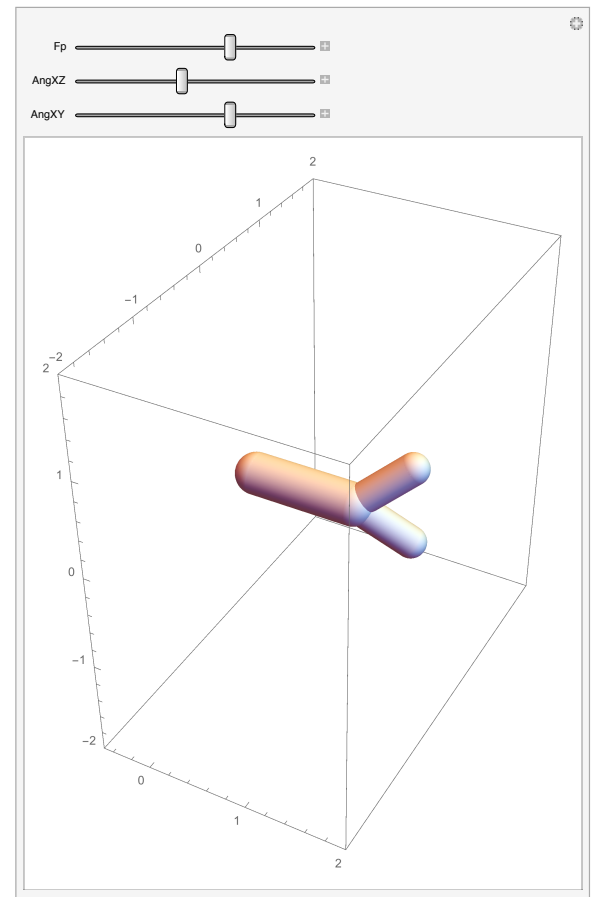


Fig. 6. In this interface it is shown the function for simulate the splitting angiogenesis growth and control the parameters: reduction factor, angle between new vessels and angle to plane XY.

vessels ($AngXZ$) and the angle to the plane XY ($AngXY$). In figure 6 we shows the simulation of this function.

For sprouting angiogenesis it was defined a function in which the parameter are the point of sprouting (F_b), the length of the new vessel (F_{db}), the angle of the new vessel to the parent vessel ($AngXZ$), and the angle to the plane XY ($AngXY$). In figure 7 we shows the simulation of this function.

The principal functions are used based on the defined algorithm to construct some simulations. An example with $P_{ab} = 0.1$ is shown in figure 8.

V. CONCLUSION

Based on some basic rules related to angiogenesis growth we can construct models of renal arterial tree which can helps to understand the mechanism involved in some congenital anomalies and diseases and in the reconstruction of the kidneys. There exist many challenges because the generated models do not converge to the morphology of the real kidney then is important capture another variables that permit to have seemed the real organ.

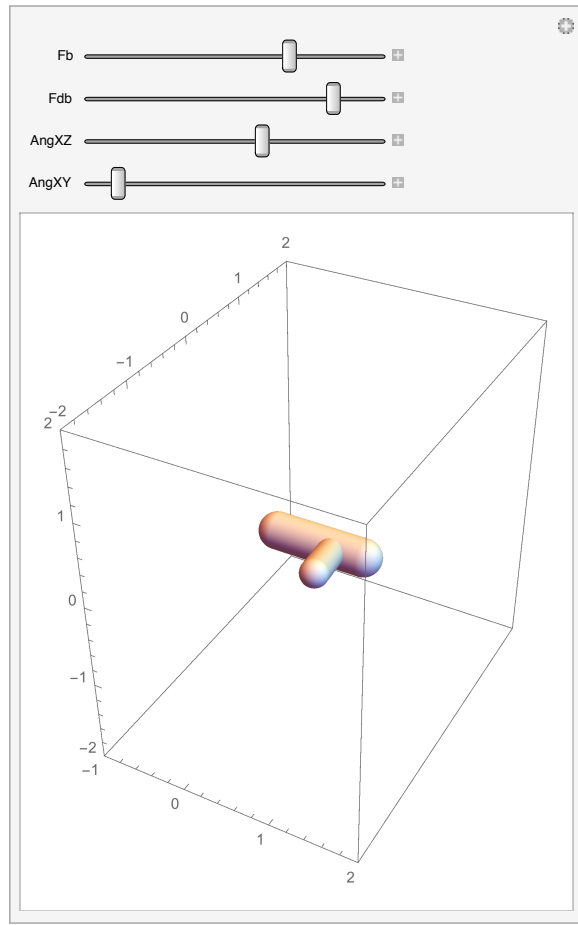


Fig. 7. In this interface it is shown the function for simulate the sprouting angiogenesis growth and control the parameters: point of sprouting, length of the new vessel, angle between new vessel and parent vessel and, angle to plane XY.

ACKNOWLEDGMENT

Francisco Ordaz thanks to Laboratorio para Biodinámica y Sistemas Alineales, División de Matemáticas Aplicadas, IPICYT for the opportunity to collaborate in this work. This research was partially supported by CONACyT under research grant 35022.

REFERENCES

- [1] M. H. Little, *Kidney Development, Disease, Repair and Regeneration*, 1st. ed. Oxford, UK: Academic Press, 2016.
- [2] R. J. Tomake, *Assembly of the Vasculature and its Regulation*, Birkhäuser, Berlin, 2001.
- [3] Aurora Espinoza-Valdez, Ricardo Femat, Francisco C. Ordaz-Salazar, *A model for renal arterial branching based on graph theory*, Mathematical Biosciences, Vol. 225, pp. 36-43, Pensilvania, USA: Elsevier, May 2010.
- [4] M. N. Nakatsu, C. A. Sainson, S. Pérez-del-Pulgar, J. N. Aoto, M. Aitkenhead, K. L. Taylor, P. M. Carpenter, C. W. Chistopher, *VEGF121 and VEGF165 regulate blood vessel diameter through vascular endothelial growth factor receptor 2 in an in vitro angiogenesis model*, Lab. Investigat. 83, 2003.
- [5] D. A. Nordsletten, S. Blackett, M. D. Bentley, E. L. Ritman, N. P. Smith, *Structural morphology of renal vasculature*, Am. J. Physiol. Heart Circ. Physiol. 291, 2006.

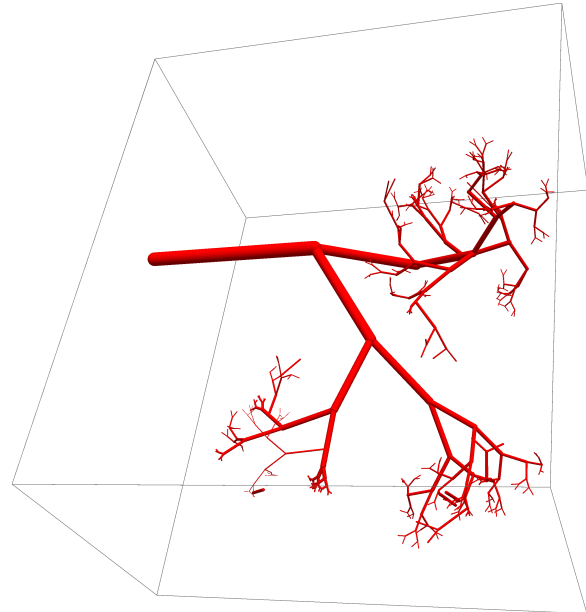


Fig. 8. This a simulation of arterial renal tree with $P_{ab} = 0.1$

Brain regions organization in epileptic seizure

G. Solís Perales

Depto. de Electrónica, CUCEI,
Universidad de Guadalajara

Av. Revolución, 1500, Guadalajara, Jal.

Email: gualberto.solis@cucei.udg.mx

A. Espinosa, H. Vélez, R. Romo

Depto. de Ciencias Computacionales
CUCEI,

Universidad de Guadalajara

A. A. González-Garrido

Instituto de Neurociencias
CUCBA,

Universidad de Guadalajara

Av. Revolución, 1500, Guadalajara, Jal. Francisco de Quevedo, 180, Guadalajara, Jal.

Abstract—The dynamic underlying the interactions between different brain regions during epileptic seizures in temporal lobe epileptic patients is described in this contribution. From the electroencephalograms a sequence of matrices that estimates direct interactions between brain regions are obtained using the Partial Direct Coherence (PDC). These matrices were interpreted as graphs and the eigenvalues of the matrices were used to evaluate EEG connectivity in epileptic patients. Basically the eigenvalues provides information on the time evolution of the connectivity in interictal and ictal periods, where the electrical relationships between some brain regions decreased or virtually disappeared. This can be seen as a reorganization dynamics of the brain regions before during and after an epileptic seizure. Therefore, the EEG data analysis using signal processing techniques and graph theory could help to improve our understanding of the cerebral electrophysiological dynamics during epileptic seizures.

I. INTRODUCTION

Epileptic seizure is one of the major brain disorders worldwide [1]. It is a chronic condition caused by neurological disorders and characterized by repeated seizures due to disturbances of the brain cells that may eventually result in cognitive and neurobiological consequences [2]. A great percentage of patients are treated with drugs, however, the rest of the patients are drug-resistant and their best treatment option is surgery [3]. Therefore, the precise localization of the epileptogenic zone and the understanding of the underlying network connections are very important in planning a surgical procedure [4]. In this sense, there are several recent efforts to make sense of brain connectivity using graph theory in electroencephalogram (EEG) signals [5], [6], [7], but particularly applying graph method to the study of the cerebral electrical activity in epileptic patients including electrocorticography (ECOG) [8], [9], intracerebral [10], [11] and scalp EEG recordings [12], mainly focusing on ictal activity (e.g. seizures). Seizures are the result of abnormal excessive or synchronous neuronal activity in the brain [13], and can be classified as focal (or partial) and generalized. Focal seizures are conceptualized as originating at some point within networks that are limited to one hemisphere, while generalized seizures are conceptualized as originating at some point within bilaterally-distributed networks [14], [15]. Seizures associated with the medial or lateral temporal lobe are the most common type, so temporal lobe epilepsy (TLE) is the best-known and probably the most common form of localization-related epilepsy in adults. In brief, seizures in

focal epilepsy seem to arise more from abnormal epileptogenic networks than from focally-isolated sources. Epilepsy is characterized not only by recurrent seizures but also includes interictal discharges. As discharges may be localized sufficiently distant from the electrodes where ictal discharges are expected to occur, it is possible to detect seizures even in the absence of accompanying scalp-recorded abnormal EEG activity [16]. Ictal activity can thus be determined by using cross-correlation and coherence between scalp electrodes. By this means, propagation of the crisis can be inferred and the brain regions more heavily involved in the seizure can be deduced. Significant support for local and inter-regional connectivity disruptions in TLE has come from studies using graph theoretical analysis as a way to characterize the organizational properties of brain networks [17], [18], [19], [20]. In fact, graph theory based analysis has been considered as providing a unique framework to quantify whole-brain network topology [21], [22]. However, the understanding of how functional connectivity relates to brain structure in TLE is still far from be reached (see [23] for comprehensive review). In this sense, we aimed to study pre-surgical TLE patients using auto-regressive modeling and graph theory to further understand the evolution of the connectivity in patients with epilepsy in an interictal and ictal periods. The electrical activity between brain regions is measured by means of electrodes in the extended International 10-20 System. The interpretation of the information about the electrical interconnections between brain regions in the interictal and ictal intervals is strongly supported in the analysis of the structural changes of a graph which describes the interconnections.

II. METHODS AND MEDICAL DATA

The procedure used to analyze the degree of variability between different brain regions basically includes a sequence of connectivity matrices that define the interaction between brain regions during EEG recording. With the connectivity studies the idea is to find the connectivity variability between an interictal and ictal periods. In order to evaluate the time evolution of the connectivity between brain regions, the EEG recordings of 6 epileptic patients were analyzed. From the EEG recordings a sequence of connectivity matrices is generated each time and then this matrices contains the information of the electrical relationship between brain regions and this matrices are analyzed to find out information

on the time evolution of the brain regions connectivity in interictal and ictal periods.

Six scalp EEG recordings from epileptic adults suffering from TLE (aged 16 to 51) were analyzed. The considered signals are obtained from 6 patients diagnosed with temporal lobe epilepsy, at the University Hospital (CHU) from Nancy, France. Each patient gave his informed consent and the study was approved by the ethics committee of the hospital. The EEGs were recorded using a Micromed System with electrodes placed on the scalp according to the extended International 10-20 System (see Figure 1), with a common reference at FPz, and the notch filter set at 50 Hz. Sampling frequency was 256 Hz. However, based on clinical experience, only 12 channels (6 for the left hemisphere: F7, T3, T5, O1, FT9, P9; and 6 for the right hemisphere: F8, T4, T6, O2, FT10, P10) were selected by the neurologists as the most representative of TLE [24].

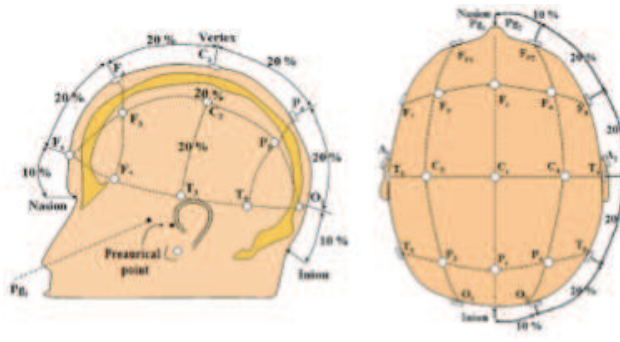


Fig. 1. The International 10-20 System for placement of electrodes.

A. Pre-processing EEG signals

Since EEG signals are usually contaminated by artifacts and noise, two previous steps are performed. The first is to apply a filter to remove the very low frequency artifacts (baseline shifts, slow ocular movements) by means of a high-pass filter with cut-off frequency of 1Hz. The second step is to remove artefacts (ocular, high frequency muscle and ECG artefacts) and noise, based on blind source separation (BSS), supervised classification and wavelet denoising. This methodology successfully rejected artefacts and noise, while preserving almost all the cerebral activity (for more detail, see [25]). All EEG recordings were uniformly adjusted and they contained 500 sec of time divided into two periods: 350 sec before (interictal) and 150 sec (ictal), after seizure onset. All recordings were reviewed by two neurophysiologists who in agreement indicated the onset and the end of each seizure at 350 sec (+/-20 sec), with an average duration of approximately 50 sec. The time period between 330 sec and 370 sec represented then the occurrence of the seizure.

B. Brain connectivity model

The EEG changes associated with epileptic activity are analyzed departing from a sequence of matrices constructed from an auto-regressive (AR) model, estimated from EEG recordings [24]. Since AR model is used in stationary processes, a 20 sec sliding window with a 0.5 sec sliding step were used [25], [26]. Thus, the 500 sec records used in this study contain 990 windows. The mathematical expression of the AR model is:

$$\mathbf{x}(t) = \sum_{k=1}^p \mathbf{A}(k) \mathbf{x}(t-k) + \mathbf{e}(t). \quad (1)$$

with $\mathbf{A}(k)$ as the AR coefficients matrix, $\mathbf{x}(t-k)$ the time-delayed values vector, p the model order and $\mathbf{e}(t)$ the error vector. The $\mathbf{A}(k)$ coefficients were estimated solving the Yule-Walkers equations [27] using the Levinson-Durbin's algorithm [28] and p was calculated using the Akaike's Information Criterion (AIC) [29]. A classic tool used in EEG signal-processing is the Cross-Power Spectral Density (CPSD), which represents the distribution of power between two signals given by $\sigma_{x,y}(f)$ (electrode x and y , where $x, y = 1, \dots, 6$) as a function of frequency (0.532 Hz). Thus, a symmetric matrix CPSD $\in \mathbb{R}^{6 \times 6}$ in each 20 sec sliding window for each hemisphere is computed. At the same time and sliding window, the Partial Directed Coherence (PDC) [30] is calculated in order to estimate direct causal relationships between every pair of electrodes, the PDC is defined as:

$$\pi_{xy}(f) = \frac{\bar{a}_{xy}(f)}{\sqrt{\bar{a}_y^H(f)\bar{a}_y(f)}} \quad (2)$$

where $\bar{a}_{xy}(f)$ is the x, y -th element, \bar{a}_y a vector column of $\bar{\mathbf{A}}(f)$ and H denotes the Hermitian. Once the PDC is calculated in the sliding window, the values $\pi_{x,y}(f)$ are averaged in frequency ($\bar{\pi}_{x,y}(f)$). Thus, a matrix PDC is constructed where $PDC_{x,y} = 1$ if $\bar{\pi}_{x,y} > \bar{\pi}_{y,x}$, otherwise $PDC_{x,y} = 0$ (the elements on the diagonal matrix are set at zero). Therefore, we obtain a *mask* containing directivity information estimated by the PDC. In the same way than for the PDC, it is possible to construct a matrix CPSD as $CPSD_{x,y} = 1$ if $\pi_{x,y} > \bar{\pi}_{x,y}$, where $\bar{\pi}_{y,x}$ is the mean in the sliding window (the elements on the diagonal matrix are also set at zero). This *mask* contains the notion of power (most significant channels). Finally, the elements of a new matrix M are calculated as follow: $M_{x,y}(t) = PDC_{x,y}CPSD_{x,y}$. The sequence of matrices obtained through this procedure are not symmetrical, evolve in time at a rate of 0.5 sec, and contain only the information of the most highly energy-charged channels (previously defined by experts), and the notion of the directivity. At this point, the matrices given by M are interpreted as connectivity matrices in graphs. From graph theory an analysis is performed to obtain some representative metrics, as connectivity degree and spectral ratios. Based on the graphs, this paper studies the connectivity evolution between electrodes according to a continuous assessment over

a period of time with the EEG data.

C. Brain connectivity analysis

As it was stated before, graph theory-based analysis has been used to study different models of neural networks, anatomical connectivity, and functional connectivity based on fMRI [31], [32], MEG [33] and EEG [34]. (For a detailed review, see [35]) Due to connectivity in the brain can be perceived as the interconnection between brain regions by means of anatomical extensions, such regions define a complex network that shares numerous characteristics with many other physiological and biological networks, and it seems that they can all be analyzed using methods of complex networks and graph theory [36]. One of the major advantages of the analysis of complex networks is that it is possible to quantify the brain networks based on a reduced number of easily-determined but highly-meaningful biological measures, and so can be used clinically in epileptic patients (for an extensive review, see [37]).

The following definitions are needed for completeness [38]. A graph G is defined as an ordered triple $(V(G), E(G), \psi_G)$ consisting of a non-empty set $V(G)$ of vertices which for this study are the electrodes, a set of edges $E(G)$ which are the interconnections, given by the electrical interactions, $V(G)$, and an incidence function ψ_G that associates each edge with an unordered pair of (not necessarily distinct) vertices of G . $\psi_G : E(G) \rightarrow W(G)$ where $W(G)$ is the set of pairs of vertices defined as $W(G) = \{\{u, v\} | u, v \in V(G)\}$ so that if $e \in E(G)$, $\psi_G(e) = \{u, v\}$, then this means that $e \in E(G)$ joins u and v .

In this application the graph vertex represents an electrode, thus the electrode has electrical interactions with other electrodes. The total number of electrodes interacting with another electrode is known as the degree of the electrode. A useful representation of a graph G which describes these interactions is the Laplacian matrix $L = (l_{x,y})$ given by [39].

$$l_{ij} = \begin{cases} d_i & \text{if } i = j \\ -1 & \text{if } i \neq j \text{ and } (i, j) \in E \\ 0 & \text{otherwise} \end{cases}$$

From the matrix M , we obtain the Laplacian matrix which comprises all the topological properties of the graph. The analytical tool used to analyze the behavior of the graph are eigenvalues of the Laplacian matrix. Which provides information on the topological structure of the graph. There are two possible cases, when the Laplacian matrix L has eigenvalues $0 = \lambda_1 \leq \lambda_2 \leq \dots \leq \lambda_6$ which represent a graph with 6 nodes where possibly some of them could not be connected and therefore there is a subgraph with k connected nodes and $6 - k$ isolated nodes. On the other hand, the second case is defined when the Laplacian matrix is block diagonal, thus, in such a case the entire network is divided into at least two subgraphs and the eigenvalues can be given as $0 = \lambda_1^i \leq \lambda_2^i \leq \dots \leq \lambda_{k_i}^i$ where i stands for

the number of subgraphs, k_i for the size of each subgraph, and $\sum_i k_i = 6$, in this case there coexists isolated subgraphs. The first eigenvalue different from zero λ_1^i (in any of the cases described above) provides information on the algebraic connectivity of the underlying graph G (a measure of the connectivity graph). Thus the ratio, $\lambda_1^i / \lambda_{k_i}^i$, is an index which characterizes the connectivity of the graph or subgraph. Therefore, the ratio provides information of the connectivity between electrodes; the advantage of this ratio is that, if the index is 1 then the nodes in the graph are connected all to all.

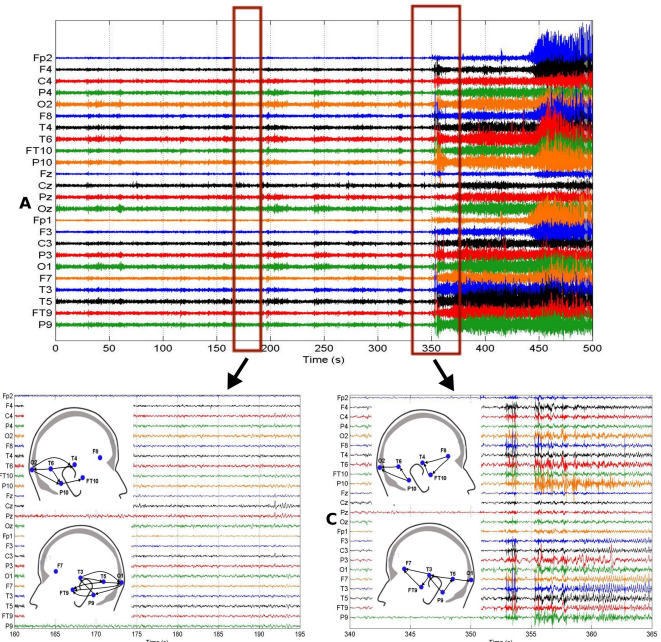


Fig. 2. EEG recording of Patient 1 (A). Inter ictal window (B) and ictal window (C), where the graphs represents the connections between of the electrodes at the time 176.5s and 353s.

III. RESULTS DESCRIPTION

It has been reported that complex network theory provides a tool which helps to determine the epileptogenic zones [36]; however, that process has been performed using electrocorticograms, which is an aggressive technique. It has also been reported that this method makes it possible to obtain information on the interactions between the brain regions where the degree of connectivity of several nodes decreases during a seizure [40]. Our principal interest was to find information that underlies the connectivity of the electrodes of patients with epilepsy in interictal and ictal periods; i.e., how the interconnections between electrodes, or brain regions, change in terms of the electrical signals emitted before and during a seizure.

Since the dimension of the matrices M is 6×6 then there are 6 eigenvalues (the number of relevant electrodes) in the

spectral ratio, the numerical results are provided in Table I, for 6 patients. From the analysis the goal is to determine the changes in the electrical activity by means of the changes in the structural characteristics of the network in inter ictal and ictal periods.

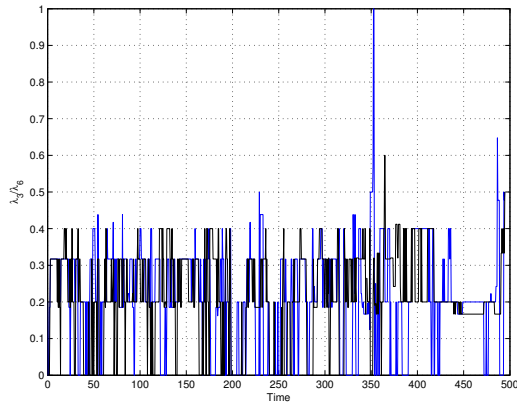


Fig. 3. Time evolution of the eigenratio $\lambda_l^i / \lambda_{k_i}^i = 1$ the blue and black lines represent the rates in the right and left hemisphere respectively.

For patient 1, Figure 2(A) illustrates the time EEG recording for the two hemispheres and two windows were defined to compare the network characteristics in inter ictal and ictal windows. Then, in (B) the graphs obtained describe the connections between electrodes in the left and right hemisphere and in $t = 176.5$ sec. In (C) the graphs for the left and right hemispheres at $t = 353$ sec. are illustrated, this corresponds to the ictal window. Note that in the right hemisphere two subgraphs are generated this phenomenon does not occur in the left hemisphere (Right patient). On the other hand, the rate $\lambda_l^i / \lambda_{k_i}^i = 1$ implies that each electrode is connected or is interacting with other two electrodes but only in the right hemisphere and in the ictal window at $t = 353$ sec. Figure 3(B) shows the eigenratio at the same time in the right hemisphere, this means that all the electrodes have the same number of connections. The estimated rate provides information on the evolution of the electrical activity between the brain regions analyzed and seems to indicate that during seizures some regions are disconnected while others increase their electrical activity. Briefly, this could indicate that at least one region of the brain reduces its electrical activity while the other regions increase the electrical activity in the sense that the subgraph is an all to all connected network, this is that the connected nodes have electrical activity with all the nodes in the subgraph. Table I shows the analysis for all 6 patients based on determining the time at which the seizure occurred. Here the connectivity of the graph given by the eigenratio means that there exists multiplicity of the eigenvalues of the matrix L, which implies that the nodes that remain connected have the same degree at that time instant.

TABLE I
 EIGENRATIO FOR 6 PATIENTS.

Patient	Time	$\lambda_l^i / \lambda_{k_i}^i$
1	177	0.5/0.4
	353	1/0.01
2	176	0.2/0.4
	352	1/1
3	176	0.25/0.19
	352	1/1
4	174	0.2/0.2
	344.5	0.2/1
5	170	0.02/0.2
	343	1/0.4
6	174.5	0.01/0.17
	354	0.4/1

IV. CONCLUSION

The present study described and evaluated the behavior of connectivity between different nodes or regions in the brain during epileptic seizures. Graph analysis allowed us to demonstrate that the degree of connectivity among different brain regions changed during epileptic seizures. Also, we were able to gather useful information which suggests that while certain regions tended to disconnect, others remained equally connected, as seems to be indicated by the rate. These results agree with previous evidence suggesting that seizures seem to arise from abnormal and complex disruptive changes in extended brain neural networks, but also provide evidence of the relative usefulness of different measures usually considered part of graph analysis. Recently, it was reported that during certain types of epileptic seizures (e.g. absence seizures) time-course analysis revealed that the activity across several components of the neural network tended to increase just before or just after seizure onset [41]. In fact, studies with neuroimaging tools based on Magnetic Resonance methods have reported a decreased resting-state functional connectivity in the medial prefrontal cortex, the angular gyrus, and the inferior parietal lobule in patients with childhood absence epilepsy (CAE) [42]. Moreover, several studies have evidenced a significant change in the interaction between the thalamus and the cortex in CAE in the baseline or resting state, probably depicting alterations in the normal relationships with connected brain networks [43], [44] and then predicted the potential appearance of abnormal changes in neural connectivity during ictal or interictal events. TLE has been conceived as a network disease involving both structural and functional changes in temporal and related brain areas [45], [46], [47] and has been evaluated using graph methods that focus on improving accuracy in surgical planning. In patients with TLE, EEG studies using graph methods have been performed with several aims, such as employing a quantitative approach to further characterize the complex neural dynamics involved, and to predict epileptogenic focus lateralization [48], post-surgical outcomes using the Wada

test (the intra-arterial amobarbital procedure) as a reversible model for the effect of lesions on brain network topology [49], and seizure onset [50], among others (see Haneef and Chiang, in press, for an extensive review) [51].

node and others is practically null or insignificant while the event is occurring. In 6 clinical cases it was possible to verify how the evolution of the connectivity increased during seizures. Therefore, two main conclusions can be elucidated: a) during epileptic seizures, electrical connectivity between some brain regions decreases or disappears; and, b) the use of a signal-processing technique such as PDC and graph theory can be useful in evaluating the evolution of electrophysiological changes during seizures. However, despite our best efforts and those of other authors, our current ability to understand the brain dynamics associated with epilepsy remains limited. In light of this, the methods of graph analysis appear to be a valuable tool that should be further explored in the near future.

REFERENCES

- [1] Engel, J., Seizures and Epilepsy, 2ed, Oxford University Press, (2012)
- [2] Kotagal, P., Lüders, H., The Epilepsies: Etiologies and Prevention. Elsevier, (1998)
- [3] Organization, W.H., Atlas: epilepsy care in the world (2005)
- [4] Bartolomei, F., Chauvel, P., Wendling, F.: Epileptogenicity of brain structures in human temporal lobe epilepsy: a quantified study from intracerebral eeg. *Brain* 131(7), 18181830 (2008)
- [5] Reijneveld, J.C., Ponten, S.C., Berendse, H.W., Stam, C.J.: The application of graph theoretical analysis to complex networks in the brain. *Clinical Neurophysiology* 118(11), 23172331 (2007)
- [6] Stam, C.: Characterization of anatomical and functional connectivity in the brain: a complex networks perspective. *International Journal of Psychophysiology* 77(3), 186194 (2010)
- [7] He, Y., Evans, A.: Graph theoretical modeling of brain connectivity. *Current opinion in neurology* 23(4), 341350 (2010)
- [8] Van Dellen, E., Douw, L., Baayen, J.C., Heimans, J.J., Ponten, S.C., Vandertop, W.P., Velis, D.N., Stam, C.J., Reijneveld, J.C.: Long-term effects of temporal lobe epilepsy on local neural networks: a graph theoretical analysis of corticography recordings. *PLoS One* 4(11), 8081 (2009)
- [9] Wilke, C., Worrell, G., He, B.: Graph analysis of epileptogenic networks in human partial epilepsy. *Epilepsia* 52(1), 8493 (2011)
- [10] Bartolomei, F., Bettus, G., Stam, C., Guye, M.: Interictal network properties in mesial temporal lobe epilepsy: a graph theoretical study from intracerebral recordings. *Clinical Neurophysiology* 124(12), 23452353 (2013)
- [11] Ponten, S., Bartolomei, F., Stam, C.: Small-world networks and epilepsy: graph theoretical analysis of intracerebrally recorded mesial temporal lobe seizures. *Clinical neurophysiology* 118(4), 918927 (2007)
- [12] Clemens, B., Puskas, S., Besenyi, M., Spisak, T., Oppositus, G., Hollody, K., Fogarasi, A., Fekete, I., Emri, M.: Neurophysiology of juvenile myoclonic epilepsy: Eeg-based network and graph analysis of the interictal and immediate preictal states. *Epilepsy research* 106(3), 357369 (2013)
- [13] Fisher, R.S., Boas, W.v.E., Blume, W., Elger, C., Genton, P., Lee, P., Engel, J.: Epileptic seizures and epilepsy: definitions proposed by the international league against epilepsy (ilae) and the international bureau for epilepsy (ibe). *Epilepsia* 46(4), 470472 (2005)
- [14] Berg, A.T., Scheffer, I.E.: New concepts in classification of the epilepsies: entering the 21st century. *Epilepsia* 52(6), 10581062 (2011)
- [15] Trevelyan, A.J., Muldoon, S.F., Merricks, E.M., Racca, C., Staley, K.J.: The role of inhibition in epileptic networks. *Journal of Clinical Neurophysiology* 32(3), 227234 (2015)
- [16] Sato, S., Kufta, C., Ito, B., Rose, D., Theodore, W., Porter, R., et al.: Electroencephalographic studies of simple partial seizures with subdural electrode recordings. *Neurology* 39(4), 527527 (1989)
- [17] Burns, S.P., Santaniello, S., Yaffe, R.B., Jouny, C.C., Crone, N.E., Bergey, G.K., Anderson, W.S., Sarma, S.V.: Network dynamics of the brain and influence of the epileptic seizure onset zone. *Proceedings of the National Academy of Sciences* 111(49), 53215330 (2014)
- [18] Doucet, G.E., Rider, R., Taylor, N., Skidmore, C., Sharan, A., Sperling, M., Tracy, J.I.: Presurgery resting-state local graph-theory measures predict neurocognitive outcomes after brain surgery in temporal lobe epilepsy. *Epilepsia* 56(4), 517526 (2015)
- [19] Haneef, Z., Chiang, S., Yeh, H.J., Engel, J., Stern, J.M.: Functional connectivity homogeneity correlates with duration of temporal lobe epilepsy. *Epilepsy and Behavior* (2015)
- [20] Vecchio, F., Miraglia, F., Curcio, G., Della Marca, G., Vollono, C., Mazzucchi, E., Bramanti, P., Rossini, P.M.: Cortical connectivity in fronto-temporal focal epilepsy from eeg analysis: A study via graph theory. *Clinical Neurophysiology* 126(6), 11081116 (2015)
- [21] Bassett, D.S., Gazzaniga, M.S.: Understanding complexity in the human brain. *Trends in cognitive sciences* 15(5), 200209 (2011)
- [22] Bullmore, E., Sporns, O.: Complex brain networks: graph theoretical analysis of structural and functional systems. *Nature Reviews Neuroscience* 10(3), 186198 (2009)
- [23] Caciagli, L., Bernhardt, B.C., Hong, S.-J., Bernasconi, A., Bernasconi, N.: Functional network alterations and their structural substrate in drug-resistant epilepsy. *Frontiers in neuroscience* 8 (2014)
- [24] Velez-Perez, H., Romo-Vazquez, R., Ranta, R., Louis-Dorr, V., Maillard, L.: Eeg preprocessing for synchronization estimation and epilepsy lateralization. In: *Engineering in Medicine and Biology Society, EMBC, 2011 Annual International Conference of the IEEE*, pp. 50285031 (2011). IEEE
- [25] Romo-Vazquez, R., Velez-Perez, H., Ranta, R., Louis-Dorr, V., Maquin, D., Maillard, L.: Blind source separation, wavelet denoising and discriminant analysis for eeg artefacts and noise cancelling. *Biomedical Signal Processing and Control* 7(4), 389400 (2012)
- [26] Velez-Perez, H.: Localisation et caractérisation du déroulement de la crise dépèlpsie temporelle. PhD thesis, Institut National Polytechnique de Lorraine-INPL (2010)
- [27] Anderson, C.W., Stoltz, E., Shamsunder, S., et al.: Multivariate autoregressive models for classification of spontaneous electroencephalographic signals during mental tasks. *Biomedical Engineering, IEEE Transactions on* 45(3), 277286 (1998)
- [28] Durbin, J.: The fitting of time-series models. *Revue de l'Institut International de Statistique*, 233244 (1960)
- [29] Akaike, H.: A new look at the statistical model identification. *Automatic Control, IEEE Transactions on* 19(6), 716723 (1974)
- [30] Baccala, L.A., Sameshima, K.: Partial directed coherence: a new concept in neural structure determination. *Biological cybernetics* 84(6), 463474 (2001)
- [31] Salvador, R., Suckling, J., Coleman, M.R., Pickard, J.D., Menon, D., Bullmore, E.: Neurophysiological architecture of functional magnetic resonance images of human brain. *Cerebral cortex* 15(9), 13321342 (2005)
- [32] Achard, S., Salvador, R., Whitcher, B., Suckling, J., Bullmore, E.: A resilient, low-frequency, small-world human brain functional network with highly connected association cortical hubs. *The Journal of neuroscience* 26(1), 6372 (2006)
- [33] Stam, C.J.: Functional connectivity patterns of human magnetoencephalographic recordings: a small-world network? *Neuroscience letters* 355(1), 2528 (2004)
- [34] Sporns, O., Tononi, G., Edelman, G.M.: Connectivity and complexity: the relationship between neuroanatomy and brain dynamics. *Neural Networks* 13(8), 909922 (2000)
- [35] Stam, C.J., Reijneveld, J.C.: Graph theoretical analysis of complex networks in the brain. *Nonlinear biomedical physics* 1(1), 3 (2007)
- [36] Ortega, G.J., Sola, R.G., Pastor, J.: Complex network analysis of human ecog data. *Neuroscience letters* 447(2), 129133 (2008)
- [37] Chiang, S., Haneef, Z.: Graph theory findings in the pathophysiology of temporal lobe epilepsy. *Clinical Neurophysiology* 125(7), 12951305 (2014)
- [38] Diestel, R.: Graph theory, ser. Graduate Texts in Mathematics. Springer-Verlag, Heidelberg 173 (2005)
- [39] Chung, F.R.: Spectral Graph Theory vol. 92. American Mathematical Soc., ??? (1997)
- [40] Kramer, M.A., Kolaczyk, E.D., Kirsch, H.E.: Emergent network topology at seizure onset in humans. *Epilepsy research* 79(2), 173186 (2008)

- [41] Carney, P.W., Jackson, G.D.: Insights into the mechanisms of absence seizure generation provided by eeg with functional mri. *Frontiers in neurology* 5 (2014)
 - [42] Luo, C., Li, Q., Lai, Y., Xia, Y., Qin, Y., Liao, W., Li, S., Zhou, D., Yao, D., Gong, Q.: Altered functional connectivity in default mode network in absence epilepsy: a resting-state fmri study. *Human brain mapping* 32(3), 438449 (2011)
 - [43] Bai, X., Guo, J., Killory, B., Vestal, M., Berman, R., Negishi, M., Danielson, N., Novotny, E., Constable, R., Blumenfeld, H.: Resting functional connectivity between the hemispheres in childhood absence epilepsy. *Neurology* 76(23), 19601967 (2011)
 - [44] Masterton, R.A., Carney, P.W., Jackson, G.D.: Cortical and thalamic resting-state functional connectivity is altered in childhood absence epilepsy. *Epilepsy research* 99(3), 327334 (2012)
 - [45] Bonilha, L., Rorden, C., Halford, J.J., Eckert, M., Appenzeller, S., Cendes, F., Li, L.M.: Asymmetrical extra-hippocampal grey matter loss related to hippocampal atrophy in patients with medial temporal lobe epilepsy. *Journal of Neurology, Neurosurgery and Psychiatry* 78(3), 286294 (2007)
 - [46] Engel Jr, J., Thompson, P.M., Stern, J.M., Staba, R.J., Bragin, A., Mody, I.: Connectomics and epilepsy. *Current opinion in neurology* 26(2), 186 (2013)
 - [47] Spencer, S.S.: Neural networks in human epilepsy: evidence of and implications for treatment. *Epilepsia* 43(3), 219227 (2002)
 - [48] Quraan, M.A., McCormick, C., Cohn, M., Valiante, T.A., McAndrews, M.P.: Altered resting state brain dynamics in temporal lobe epilepsy can be observed in spectral power, functional connectivity and graph theory metrics. *PloS one* 8(7), 68609 (2013)
 - [49] Douw, L., Van Dellen, E., Baayen, J.C., Klein, M., Velis, D.N., Alpherts, W.C., Heimans, J.J., Reijneveld, J.C., Stam, C.J.: The lesioned brain: still a small-world? *Frontiers in human neuroscience* 4 (2010)
 - [50] Bialonski, S., Lehnertz, K.: Assortative mixing in functional brain networks during epileptic seizures. *Chaos: An Interdisciplinary Journal of Nonlinear Science* 23(3), 033139 (2013)
 - [51] Haneef, Z., Chiang, S.: Clinical correlates of graph theory findings in temporal lobe epilepsy. *Seizure* 23(10), 809818 (2014)
- H. Kopka and P. W. Daly, *A Guide to L^TE_X*, 3rd ed. Harlow, England: Addison-Wesley, 1999.

Integrated Multi-Scroll Chaotic Systems

Esteban Tlelo-Cuautle

INAOE

Luis Enrique Erro No.1. Tonantzintla, Puebla. 72840 Mexico

E-mail: etlelo@inaoep.mx

Abstract—Multi-scroll chaotic oscillators have been implemented by using different kinds of discrete electronic devices, micro-controllers and field-programmable gate arrays. However, as modern engineering applications require wireless, wearable and low power consumption designs, then this work revises the implementation of chaotic systems using integrated circuit (IC) technology. Simulation results are shown for generating 7-scrolls using IC technology of $0.35 \mu\text{m}$, and experimental results for generating 5-scrolls using IC technology of $0.5 \mu\text{m}$.

I. INTRODUCTION

In electronics, the first realizations of chaotic oscillators started by using discrete active devices [1], mainly operational amplifiers (opamps) and current-feedback opamps (CFOAs). Those chaos generators showed the well-known double-scroll attractor, whose unpredictability is low compared to multi-scroll ones [2]. That way, nowadays researchers cope with the challenge of implementing multi-scroll chaotic attractors with high values of their maximum Lyapunov exponent (MLE). However, not all of them are suitable for designing ICs as the ones based on piecewise-linear (PWL) functions. For instance, a review on the electronic design of chaotic oscillators using discrete devices and IC technology is given in [1], where it is highlighted that PWL-function-based oscillators are preferred because of their relatively simple mathematical description, dynamical analysis and circuit implementation.

II. RECENT INVESTIGATIONS ON GENERATING MULTI-SCROLL CHAOTIC ATTRACTORS

The authors in [3] showed a family of attractors based on a class of unstable dissipative systems of type affine linear systems. Although the electronic implementation is not discussed, the challenge is realizing as many scrolls as possible and with high MLE values. It is quite clear that electronic devices cannot allow generating infinite number of scrolls. In particular, traditional opamps have low frequency response and requires high voltage supply levels, as ± 18 volts. Other similar devices are the CFOAs, which were used in [4] for generating 3-D grid multi-scroll chaotic attractors by using staircase nonlinear functions. Although CFOAs offer higher bandwidth than the opamps, both have the frequency limitations discussed in [5], where the maximum frequency is around hundreds of kHz, and where one can appreciate the difficulty of generating 10-scrolls attractors.

On the side of IC realizations, the authors in [6] introduced a novel chaotic oscillator based on cross-coupled inverter rings, which topology is suitable for area-efficient implementation

on a complementary metal-oxide-semiconductor (CMOS) IC. Numerical simulation based on PWL approximation predicted the generation of positive spikes having approximately constant periodicity but highly variable cycle amplitude.

Unpredictability can be augmented by implementing chaotic systems with more than one MLE, as done in [7], where an hyperchaotic multi-scroll PWL system in R4 is binarized to generate a pseudo-random sequence which encrypt a grayscale image via symmetric-key algorithm. The conclusion highlights that the encryption quality is evaluated depending on the variation of the number of scrolls, which can be easily implemented by using field-programmable gate arrays (FPGAs), and much better by using IC technology, which requieres pretty low power consumption. Unpredictability can also be augmented by realizing multi-scrolls attractors in more directions, as shown in [8], which are also suitable for IC realizations.

III. INTEGRATED CHAOS GENERATORS

As mentioned in [1], the first integrated chaos generators were introduced in the 90s showing 2-scrolls. The majority of realizations were based on Chua's circuit, which can be modified to generate multi-scroll chaotic attractors. For example, the first IC realization generating 5-scrolls and using a variant of Chua's circuit with PWL functions was introduced in [9]. The most relevant issue was the implementation of a saw-tooth-like nonlinear function, which was designed by using floating gate MOS (FGMOS) transistors. The fabricated IC is shown in Fig. 1, and the experimental result showing 5-scrolls is given in Fig. 2.

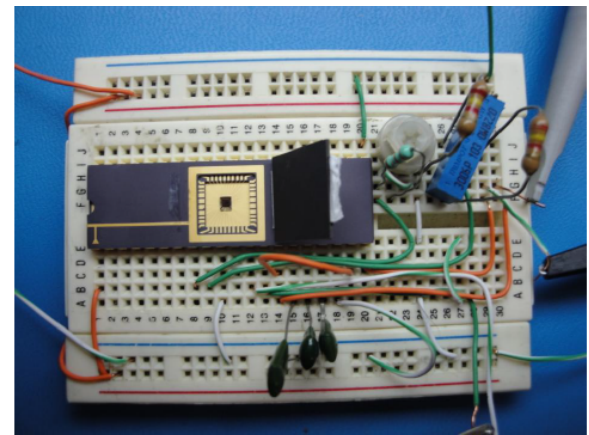


Fig. 1. IC connected to generate 3 and 5-scrolls attractors.

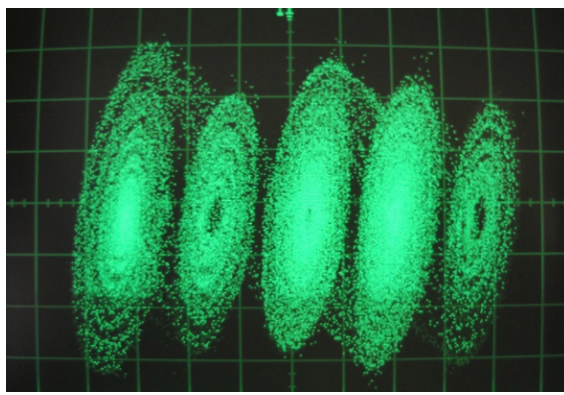


Fig. 2. Experimental observation of 5-scrolls generated by an IC using technology of $0.5 \mu\text{m}$.

Generating multi-scroll chaotic attractors and working at high frequency can be solved by using FPGAs, as shown in [10], where two 6-scrolls chaotic attractors were synchronized to implement a secure communication system to transmit grey scale images. The experiment showed that by using 2-scrolls attractors, the unpredictability of the information in the channel is low compared to using 6-scrolls attractors. It lead the authors concluding that using attractors with more scrolls and with high MLE values is better to diminish the correlation between the channel and the transmitted/received image. Further, to provide solutions in the world of wireless, wearable and low power consumption applications, the challenge is the implementation of ICs. On this direction, using IC technology of $0.35 \mu\text{m}$, 7-scrolls attractors have been generated as shown in Fig. 3, where the voltage ranges are within ± 0.55 volts, which is quite low compared to using opamps. This integrated chaotic attractor has been optimized to provide high unpredictability and it will be fabricated in 2016 and then tested in a secure communication system.

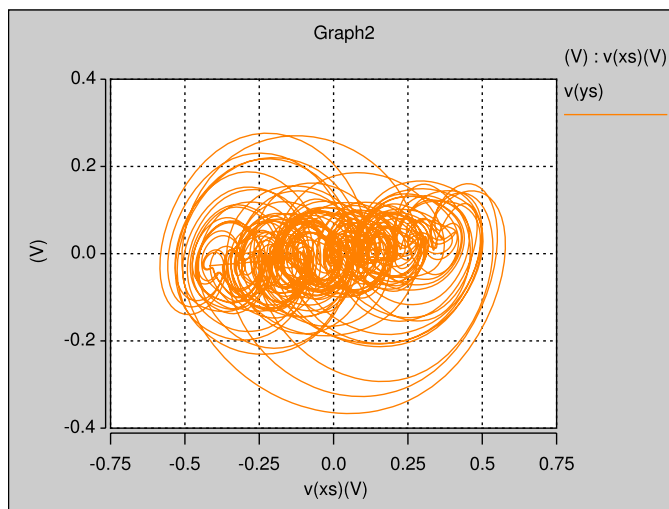


Fig. 3. Simulation of 7-scrolls generated by an IC using technology of $0.35 \mu\text{m}$.

IV. CONCLUSION

Integrated chaos generators are suitable to be fabricated in modern IC technologies. They can further be used in electronic applications to provide solutions in the world of wireless and wearable products.

REFERENCES

- [1] R. Trejo-Guerra, E. Tlelo-Cuautle, V. H. Carbajal-Gómez, and G. Rodríguez-Gómez, "A survey on the integrated design of chaotic oscillators," *Applied Mathematics and Computation*, vol. 219, no. 10, pp. 5113–5122, 2013.
- [2] V. H. Carbajal-Gómez, E. Tlelo-Cuautle, and F. V. Fernández, "Application of computational intelligence techniques to maximize unpredictability in multiscroll chaotic oscillators," in *Computational Intelligence in Analog and Mixed-Signal (AMS) and Radio-Frequency (RF) Circuit Design*. Springer, 2015, pp. 59–81.
- [3] B. Aguirre-Hernández, E. Campos-Cantón, J. López-Rentería, and E. D. González, "A polynomial approach for generating a monoparametric family of chaotic attractors via switched linear systems," *Chaos, Solitons & Fractals*, vol. 71, pp. 100–106, 2015.
- [4] X. Wu and Y. He, "A systematic design method for 3-d grid multiscroll chaotic attractors and its circuit implementation employing cfoas," *International Journal of Bifurcation and Chaos*, vol. 25, no. 03, p. 1550041, 2015.
- [5] J. Muñoz-Pacheco, E. Tlelo-Cuautle, I. Toxqui-Toxqui, C. Sánchez-López, and R. Trejo-Guerra, "Frequency limitations in generating multi-scroll chaotic attractors using cfoas," *International Journal of Electronics*, vol. 101, no. 11, pp. 1559–1569, 2014.
- [6] L. Minati, "Experimental implementation of networked chaotic oscillators based on cross-coupled inverter rings in a cmos integrated circuit," *Journal of Circuits, Systems and Computers*, vol. 24, no. 09, p. 1550144, 2015.
- [7] M. García-Martínez, L. Ontañón-García, E. Campos-Cantón, and S. Čelikovský, "Hyperchaotic encryption based on multi-scroll piecewise linear systems," *Applied Mathematics and Computation*, vol. 270, pp. 413–424, 2015.
- [8] J. M. Muñoz-Pacheco, E. Zambrano-Serrano, O. Félix-Beltrán, L. C. Gómez-Pavón, and A. Luis-Ramos, "Synchronization of pwl function-based 2d and 3d multi-scroll chaotic systems," *Nonlinear Dynamics*, vol. 70, no. 2, pp. 1633–1643, 2012.
- [9] R. Trejo-Guerra, E. Tlelo-Cuautle, J. Jiménez-Fuentes, C. Sánchez-López, J. Muñoz-Pacheco, G. Espinosa-Flores-Verdad, and J. Rocha-Pérez, "Integrated circuit generating 3-and 5-scroll attractors," *Communications in Nonlinear Science and Numerical Simulation*, vol. 17, no. 11, pp. 4328–4335, 2012.
- [10] E. Tlelo-Cuautle, V. Carbajal-Gómez, P. Obeso-Rodelo, J. Rangel-Magdaleno, and J. Nez-Prez, "Fpga realization of a chaotic communication system applied to image processing," *Nonlinear Dynamics*, vol. 82, no. 4, pp. 1879–1892, 2015. [Online]. Available: <http://dx.doi.org/10.1007/s11071-015-2284-x>

Sensorial stimulation effects on a neural dynamic systems

Luis M. Torres-Treviño
 Facultad de Ingeniería Mecánica y Eléctrica
 Universidad Autónoma de Nuevo León
 S/N Ciudad Universitaria, 66451
 San Nicolás de los Garza, N.L., México
 Email: luis.torrestv@uanl.edu.mx

Abstract—In this work, a behavior of a dynamic neural system is presented. This neural system can be stimulated by two forms, using a signal generated by a single neuron that uses a Gaussian function that depends on two parameters: (i) Center of mass and (ii) Width of the bell, the form of the Gaussian function. Changing these parameters, different forms of oscillations inclusive chaotic can be generated. Second input is a external stable signal but can control the behavior of the artificial neural system. This work are preliminary results on artificial dynamic neural systems that can works like a central generator of patterns that is common in living forms.

I. INTRODUCTION

Natural neural systems has a dynamic performance, inclusive has been shown that there are chaos in these systems [1], [2]. An artificial neural system can be build using a model of a neural circuit usually inspired in simplification of real circuit that come from simple animals. However, neural networks is a simplification of real neurons where the architecture is composed of layers of neurons. These connectionist systems can behave in the same way than a real system. Examples of these systems can be found in neural circuits that control the beats of the heart, intestinal movements, diagram for expansion of lugs, posture control, etc.,[3].

When a person is walking, every step is not the same, in a ideal form, the muscles are activated in secuential form considering different intensities in every muscle. When it is necessary to run, several muscles are activated with different signals and intensities. One quality of a dynamic system is robustness because when a perturbation is applied to the system, in most of the times recover the last state. When a person is walking on floor and a obstacle appears, a perturbation exist and most change actual state for a short period of time, avoid the obstacle and then retrieve last walking.

This is a preliminary work of a simple dynamic neural system that can represent the properties of a complex dynamic neural system that has been viewed in real neural circuits. This circuit is stimulated using two inputs, a stable stimulation and another one generated by a single chaotic neuron.

II. A SINGLE CHAOTIC NEURON AS INPUT STIMULUS

A single chaotic neuron can be build using an artificial neuron with a Gaussian activation function [5]. This neuron

has only one input where receives a feedback of the output generated from the activation function (Figure 1).

$$y_k = f_a(x_k, \lambda, cm) = e^{-\frac{1}{\lambda}(x_k - cm)^2} \quad (1)$$

Neuron depends on two parameters to generate from a stable response to a chaotic one. In this work parameters are adjusted for generation of an oscillatory behavior (i.e. $\lambda=0.15$, $cm=0.25$). These parameters can be estimated using Figure 2 as reference to generate a specific behavior, from stable, pseudo and chaotic behavior.

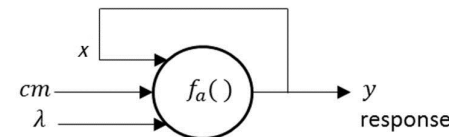


Fig. 1. Configuration of a single chaotic neuron.

III. ARCHITECTURE OF THE DYNAMIC NEURAL SYSTEM

An artificial neural network using two input of signal: Stimulation by an stable and a dynamic signal. The following equation illustrates the complete dynamic neural systems.

$$\begin{aligned} E_{i,j}(k+1) &= e(k) \\ SA_{i,j}(k+1) &= \exp(-1/\lambda)(SA_{i,j}(k)-cm)^2 \\ R_{i,j}(k+1) &= F_{Gauss}[(W1_{i,j} - E_{i,j}) + (W2_{i,j} - SA_{i,j})] \end{aligned} \quad (2)$$

Finally, a single output is calculated using contribution of all neurons:

$$y(k+1) = \frac{\sum_{i=1}^3 \sum_{j=1}^3 R_{i,j}(k) A_{i,j}}{\sum_{i=1}^3 \sum_{j=1}^3 R_{i,j}(k)} \quad (3)$$

IV. PERFORMANCE OF THE DYNAMIC NEURAL SYSTEM.

Two cases will be used to illustrate the performance of this system. A simplification is made using a matrix of size 3x3 where $W1 = [0.1 \ 0.2 \ 0.3; \ 0.6 \ 0.5 \ 0.4; \ 0.7 \ 0.8 \ 0.9]$, $W2 = [0 \ 0.0182 \ 0; \ 0.6814 \ 0 \ 0.2645; \ 0 \ 0.9984 \ 0]$ and $A = [0 \ 0 \ 1; \ 1 \ 0 \ 0; \ 0 \ 1 \ 0]$. Initially $SA_{i,j}(0) = U()$, a random variable with uniform distribution, where $i, j = 1..3$

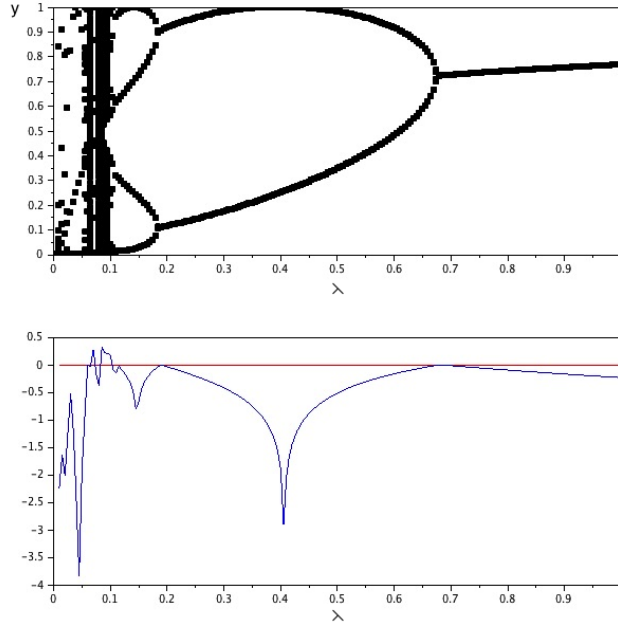


Fig. 2. Bifurcation diagram and Lyapunov estimation of a single chaotic neuron ($cm=0.25$).

In the first case, a stimulus e is set constant to be 0.4, and this is stimulated using a single chaotic neuron with $\lambda=0.15$ and center of mass of 0.25; then the system generate different outputs related with the behavior of the single chaotic neuron, but external stimulus can change the performance without change the parameters of the single chaotic neuron. When there are a perturbation in the system changing state SA , then the output ichange but returns to the original behavoir (Figure 3).

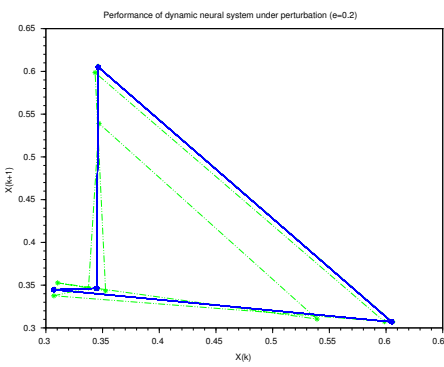


Fig. 3. Performance of the neural system under a perturbation.

When the system is stimulated using the same single chaotic neuron, and three different stimulus is used, then there is a change of the performance of the system that can be better appreciated using a phase graph. In every case the system is disturbed, then returns to the original oscillation. In Figure 4 is shown the performance of the neural system where stimulus

change the attractor of the system. Between every stimulus, a perturbation is appreciated, but the system returns to a quasi periodic oscillation.

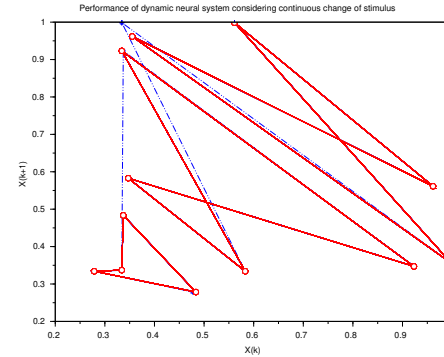


Fig. 4. Performance of the neural system under changes of input stimulus. Three attractors are shown.

V. CONCLUSIONS

It was shown some results of a simple dynamic neural system which behavior change when a stimulus is applied. Attractor of the signal is changed using this stimulus controlling the performance of the system. The dynamic neural system maintains all the properties desirables from a nervous system like auto-organization and robustness. In future work, a mechanism to determine weights and activation matrix will be proposed to generate different behaviors that have potential applications in walking systems, posture control, pumping systems that change its actuation based on stimulations, etc.

REFERENCES

- [1] Pierre Buser, Philippe Faure, Henri Korn, Is there chaos in the brain? I. Concepts of nonlinear dynamics and methods of investigation Comptes Rendus de l'Academie des Sciences - Series III - Sciences de la Vie Volume 324, Issue 9, September 2001, Pages 773-793
- [2] Korn H1, Faure P. Is there chaos in the brain? II. Experimental evidence and related models. C R Biol. 2003 Sep;326(9):787-840.
- [3] Patricia S. Chircrack and Terrence J. Sejnowski The Computational Brain MIT PRESS 1994
- [4] Sajid Iqbal 1, Xizhe Zang, Yanhe Zhu ?, Jie Zhao Bifurcations and chaos in passive dynamic walking: A review Robotics and Autonomous Systems 62 (2014) 889?909
- [5] Luis M. Torres-Trevio, Angel Rodrguez-Lin, Luis Gonzlez-Estrada, and Gustavo Gonzlez-Sanmiguel Single Gaussian Chaotic Neuron: Numerical Study and Implementation in an Embedded System Discrete Dynamics in Nature and Society. Volume 2013 (2013), Article ID 318758 <http://dx.doi.org/10.1155/2013/318758>

Chaotic oscillator derived from a fractional order dynamic system

E. Zambrano-Serrano

Department of Applied Mathematics,

Instituto Potosino de Investigación Científica y Tecnológica,

San Luis Potosí, SLP., México 78216

Email: ernesto.zambrano@ipicyt.edu.mx

Abstract—The nonlinear dynamic behavior of a oscillator described by fractional order differential equations is presented in this paper. Considering the integer version of an unstable dissipative system and the stability theorem of fractional order systems. Then, the transform of a integer-order chaotic system in fractional version to preserve chaotic dynamics when their models become fractional. Numerical simulations coincide with the theoretical analysis.

I. INTRODUCTION

Recently the fractional calculus starts to attract attention of researchers in diverse areas due to the fractional order models increase accuracy results than the corresponding integer-order models [1]-[5]. The fractional order parameter enhance the system performance by increasing one degree of freedom, also the fractional derivative provides an excellent instrument for the description of memory and hereditary properties in several processes [5]. The improvement on the real objects of the fractional order systems are that there are more degrees of freedom in the model and that a memory is included in these systems. The fractional derivatives have been used to describe elegantly some systems; for instance, Fractional calculus has been used in viscoelasticity in order to support an accurate material description only with a few parameters [2], [3]; in control theory the main advantage of fractional order controllers is that the enormous flexibility in improving the control performance and robustness [6], [7]. Recently there has been a tendency to transform integer-order chaotic systems in fractional order versions because of the integer-order versions preserve chaotic behavior when their models become fractional; such as, the fractional Lorenz system [1], the fractional Chen system [8], the fractional Chua's circuit [9] among others. The fractional chaotic systems have some improves over the integer-order systems; the fractional derivatives have complex geometrical interpretation because of their non-local character and high nonlinearity; the power spectrum of fractional order chaotic systems fluctuates complexly increasing the chaotic behavior in frequency domain; and the computational complexity goal is also achieved. Specifically, applications considering fractional order chaotic systems have been improvement, such as a digital cryptography approach, an image encryption method, among others [10], [11].

II. BASIC CONCEPTS

The operator ${}_0D_t^\alpha$, is a combination of differentiation and integration operator commonly used in fractional calculus. In literature, there are different definitions for fractional derivatives [1], [2]. The Caputo definition of the fractional derivative is,

$${}_0D_t^\alpha f(t) = \frac{1}{\Gamma(n-\alpha)} \int_0^t \frac{f^{(n)}(\tau)}{(t-\tau)^{\alpha+1-n}} d\tau, \quad (1)$$

and the Riemann-Liouville definition can be described as

$${}_aD_t^\alpha f(t) = \frac{1}{\Gamma(n-\alpha)} \frac{d^n}{dt^n} \int_a^t (t-\tau)^{n-\alpha-1} f(\tau) d\tau, \quad (2)$$

where $n = \lceil \alpha \rceil$, and Γ is the Gamma function,

$$\Gamma(z) = \int_0^\infty t^{z-1} e^{-t} dt. \quad (3)$$

A. Stability conditions of Fractional-Order Systems.

A general fractional order linear time invariant system is described by

$$\frac{d^\alpha x}{dt^\alpha} = Ax + Bu, \quad (4)$$

where $x \in R^n$ is the state vector, $u \in R$ is a scalar, $A \in R^{n \times n}$ is a linear operator, $B \in R^n$ is a constant vector, and α is the fractional commensurate order. The linear part of the system given by (4) can be rewritten as

$$\frac{d^\alpha x}{dt^\alpha} = Ax, \quad x(0) = x_0, \quad (5)$$

with $0 < \alpha < 1$. The stability analysis of that system can be divided in two conditions as follows [1]:

- *Asymptotically stable*: The system (5) is asymptotically stable if and only if $|\arg(\lambda)| > \frac{\alpha\pi}{2}$ for all eigenvalues (λ) of matrix A . In this case, the solution $x(t)$ tends to 0 like $t^{-\alpha}$.
- *Stable*: The system (5) is stable if and only if $|\arg(\lambda)| \geq \frac{\alpha\pi}{2}$ for all eigenvalues (λ) of matrix A obeying that the critical eigenvalues must satisfy $|\arg(\lambda)| = \frac{\alpha\pi}{2}$ and have geometric multiplicity of one.

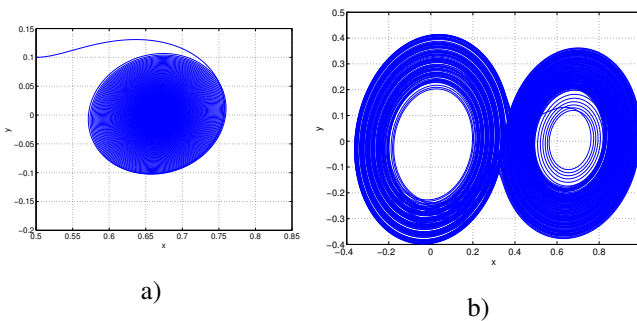


Fig. 1. Projections of the attractors onto the xy -plane.

III. FRACTIONAL ORDER UNSTABLE DISSIPATIVE SYSTEM

A dynamical system is unstable dissipative system (UDS) because it is dissipative in one of its components while unstable in the other two. The UDS is builded with a switching law to obtain a strange attractor. The strange attractor appears as a result of a combination of several unstable one-spiral trajectories [12]. The idea is to find the minimum fractional order where the system keeps chaotic behavior considering the same parameters as the integer-order case. The resulting system is described by

$$\begin{aligned} D^\alpha x &= y, \\ D^\alpha y &= z, \\ D^\alpha z &= -ax - by - cz + f(x), \end{aligned} \quad (6)$$

with

$$f(x) = \begin{cases} \gamma, & \text{if } x \geq 0.35, \\ 0, & \text{otherwise,} \end{cases} \quad (7)$$

being $a = 1.5$, $b = 1$, $c = 1$ and $\gamma = 1$ the system's parameters. Where $\alpha \in (0, 1)$. The system has only two equilibrium points at $O = (0, 0, 0)$ and $E_1 = (0.66, 0, 0)$ which are saddle points of instability index two; therefore, there is a double-scroll attractor given by the system (6) due to its equilibrium points are the same as the integer-order version.

In order to obtain the minimal commensurate order to keep the chaotic behavior of (6), the stability general theorem given in the previous section must be satisfied. As a result, the system (6) displays regular and stable behavior if

$$\alpha < 0.9417, \quad (8)$$

Accordingly, the system does not show chaotic behavior for $\alpha < 0.9417$ as demonstrated in Fig. 1 a) where the projection of the attractor onto the xy -plane for $\alpha = 0.94$ is displayed.

Hence, in order to show that the fractional system can generate chaotic behavior we consider $\alpha \geq 0.95$. Fig. 1 b) shows the projection of the chaotic attractor onto the xy -plane for $\alpha = 0.95$. The chaotic attractor has the same number of equilibria as scrolls. By using the same parameters as integer-order case, we observe that FOUDS generates chaotic behavior with an effective minimum dimension as low as 2.85.

IV. CONCLUSION

A fractional order unstable dissipative system has been introduced and analyzed. Chaotic behavior was observed with different fractional orders as a function of the system's parameters, and the numerical simulations coincide with the theoretical analysis.

Acknowledgments

E. Zambrano-Serrano is a doctoral fellow of CONACYT (Mexico) in the Graduate Program on Control and Dynamical Systems at DMAP-IPICYT.

REFERENCES

- [1] I. Petras, *Fractional-Order Nonlinear Systems Modeling, Analysis and Simulation*. Berlin, Germany: Springer Berlin Heidelberg, 2011.
- [2] I. Podlubny, *Fractional Differential Equations Mathematics in Science and Engineering*. New York, NY, USA: Academic Press, 1999.
- [3] A. Hürkamp, M. Tanaka, and M. Kaliske, "Complex step derivative approximation of consistent tangent operators for viscoelasticity based on fractional calculus," *Nonlinear Dyn.*, vol. 56, no. 5, pp. 1055-1071, Nov. 2015.
- [4] T. J. Freeborn, "A survey of fractional-order circuit models for biology and biomedicine," *IEEE J. Emerg. Sel. Topics Circuits Syst.*, vol. 3, no. 3, pp. 416-424, Sep. 2014.
- [5] A. S. Elwakil, "Fractional-order circuits and systems: An emerging interdisciplinary research area," *IEEE Circuits Syst. Mag.*, vol. 10, no. 4, pp. 40-50, 2010.
- [6] J. S. Tsai, T. Chien, S. Guo, Y. Chang, and L. Shieh, 'State-space self-tunning control for stochastic fractional-order chaotic systems,' *IEEE Trans. Circuits Syst. I*, vol. 54, no. 3, pp. 632-642, Mar. 2007.
- [7] C. Yin, Y. Cheng, Y. Q. Chen, B. Stark, and S. Zhong, "Adaptive fractional-order switching-type control method design for 3D fractional-order nonlinear systems," *Nonlinear Dyn.*, vol. 82, no. 1, pp. 39-52, May. 2010.
- [8] J. G. Lu, and G. Chen, "A note on the fractional order Chen system," *Chaos Solitons Fractals*, vol. 27, pp. 685-688, Feb. 2006.
- [9] D. Cafagna, and G. Grassi, "Fractional-order Chua's circuit: time-domain analysis, bifurcation, chaotic behavior and test for chaos," *Int. J. Bifur. Chaos Appl. Sci. Engrg.*, vol. 18, no. 3, pp. 615-639, Mar. 2008.
- [10] A. Kiani-Ba , K. Fallahib, N. Pariza, and H. Leungb, "A chaotic secure communication scheme using fractional chaotic systems based on an extended fractional Kalman filter," *Commun. Nonlinear Sci. Numer. Simul.*, vol 14, no. 3, pp. 863-879, Mar. 2009.
- [11] P. Muthukumar, P. Balasubramaniam, and K. Ratnavelu, "Fast projective synchronization of fractional order chaotic and reverse chaotic systems with its application to an affine cipher using date of birth (DOB)," *Nonlinear Dyn.*, vol. 80, no. 4, pp. 1883-1897, Jul. 2014.
- [12] E. Campos-Cantón, J. G. Barajas-Ramírez, G. Solis-Perales and R. Femat, "Multiscroll attractors by switching systems," *Chaos*, vol. 20, Mar. 2010